Lab work in photonics

Quantum Photonics

Rooms	**Bell**	**HOM** (GRA)	**NV** (HBT)	**Sat. Abs.**	**Atomic beam**
	N1.3	N1.3	N1.4	S1.29	N1.6

lense.institutoptique.fr | Troisième année | Photonique 3A|M2

Engineer - 3rd year - Palaiseau
Master 2 QLMN
Year 2025-2026

P 1

Entangled photons and Bell's inequality

Please prepare P1 to P10 before the lab session.

Contents

1 Introduction

Quantum theory does not allow one to calculate the outcome of a measurement, but rather the probability of the different possible outcomes. Because of this probabilistic aspect, many physicist, including Einstein, were dubious and thought that quantum mechanics had to be an incomplete theory that was not accounting for the full reality. To illustrate this point, Einstein, Podolski and Rosen presented in 1935 a "gedankenexperiment" (mental experiment) where a measurement on an entangled two-particle state (Bell state or EPR state) lead to a paradox, which the authors interpret as a proof of the incompleteness of the quantum theory [1].

For a Bell state, a measurement of the state of each particle taken individually gives a random outcome, but the results on the two particles are perfectly correlated. In other words, a measurement of the first particle state allows us to predict with certainty the state of the second one. For Einstein, Podolsky

[1] A. Einstein, B. Podolsky et N. Rosen, *Can Quantum-Mechanical Description of Physical Reality Be Considered Complete?*, Physical Review **47**, 777 (1935)

and Rosen, the possibility of predicting the state of the second particle implies that this state exists before the measurement, implying that there is a set of "hidden" variables (in the sense that they are not described by the theory) that determine this state all along the experiment.

For a long time, it has seemed that the debate between an hidden variable interpretation and a purely probabilistic theory was a philosophical discussion. However, in 1964, John Bell [2] showed that there were some cases where the two interpretations were leading to incompatible observations, and that it was possible to settle the debate with an experiment. But it has been necessary to wait 15 more years for the progress in **quantum optics** to implement this experiment with pairs of entangled photons. The first unambiguous results have been obtained at the Institut d'Optique by Alain Aspect, Philippe Grangier and Jean Dalibard [3].

This lab work, inspired by **M. W. Mitchell** and **D. Dehlinger**, aims to produce a two-photons Bell state, and allows you to determine, with your own measurements, which theory can be invalidated.

2 Bell states

2.1 Polarization state of a photon in quantum mechanic

When we measure the polarization of a photon with a vertical analyzer, we refer to the basis formed by the vertical polarization ($|V\rangle$ parallel to the analyzer axis) and the horizontal polarization ($|H\rangle$ orthogonal to the analyzer axis). In this basis, the polarization state is written:

$$|\psi\rangle = c_V|V\rangle + c_H|H\rangle\,. \tag{1.1}$$

The coefficients c_V and c_H are complex number such as $|c_V|^2 + |c_H|^2 = 1$. The measurement of the photon polarization can only gives two outcomes:

- The photon is transmitted by the polariser and its polarization state is projected on $|V\rangle$. Quantum mechanics predicts that the probability of this result is $P_V = |\langle\psi|V\rangle|^2 = |c_V|^2$;
- The photon is blocked by the polariser and its polarization state is projected on $|H\rangle$. The associated probability is $P_H = |\langle\psi|H\rangle|^2 = |c_H|^2$.

P1 Write the polarization state of a photon with a rectilinear polarization, at an angle α from the vertical. What is the probability to measure it in the state $|V\rangle$?

[2] J. S. Bell, *On the Einstein-Podolsky-Rosen paradox*, Physics **1**, 195 (1964)

[3] See for instance : A. Aspect, J. Dalibard et G. Roger, *Experimental Test of Bell's Inequalities Using Time-Varying Analyzers*, Physical Review Letters **49**, 1804 (1982)

P2 Write the polarization state of a photon with a left-circular polarization. What is the probability to measure it in the state $|V\rangle$?

If we choose to measure the polarization state of a photon with a polariser rotated by an angle α from the vertical, the new basis of the polarization state is $\{|V_\alpha\rangle, |H_\alpha\rangle\}$ (figure 1.1).

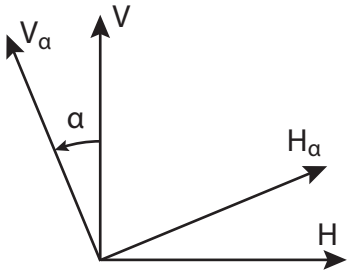

Figure 1.1: The basis of the polarization state $\{|V_\alpha\rangle, |H_\alpha\rangle\}$ is obtained by rotating the basis $\{|V\rangle, |H\rangle\}$ by an angle α.

P3 Consider a photon in the polarization state $|V\rangle$. Write its state in the basis $\{|V_\alpha\rangle, |H_\alpha\rangle\}$. What is the probability P_{V_α} of measuring the polarization V_α?

2.2 Pairs of polarization-entangled photons

During this lab work, you will produce and characterize pairs of polarization-entangled photons. The polarization state of those pairs is a Bell state, written as follow:

$$|\psi\rangle = \frac{1}{\sqrt{2}} \left(|V, V\rangle + |H, H\rangle\right) . \tag{1.2}$$

It is a non separable state, which means that we can not assign a polarization state to each photon individually.

P4 Show that the probability P_V of measuring the photon 1 **or** the photon 2 in the polarization V is 1/2.

P5 What is the probability of measuring the two photons in the same polarization state (V, V or H, H)? What is the probability of measuring the two photons in orthogonal polarization states (V, H or H, V)?

In other words, a polarization measurement on one of the photons gives a random result, but if we measure the polarizations of the two photons of the pair, the results are always **correlated**. More generally, the probability to measure simultaneously the photon 1 in the polarization state V_α and the photon 2 in the polarization state V_β is given by

$$P(V_\alpha, V_\beta) = |\langle V_\alpha, V_\beta|\psi\rangle|^2 \ . \tag{1.3}$$

P6 Show that $P(V_\alpha, V_\beta) = \cos^2(\alpha - \beta)/2$. How does this probability change when the two axis of analysis are rotated by the same angle?

P7 Show that the Bell state has the same form than (1.2) no matter what the basis of analysis is, which implies that:

$$|\psi\rangle = \frac{1}{\sqrt{2}} \left(|V_\alpha, V_\alpha\rangle + |H_\alpha, H_\alpha\rangle\right) \ , \quad \forall\alpha \, . \tag{1.4}$$

This **rotational symmetry** of the polarization state is a crucial property of the Bell state that we will use to reveal the full extent of the correlation between the entangled photons.

2.3 Bell's inequality

For arbitrary orientated analyzers, the degree of correlation between the results of the measurements on the two photons can be quantified by the quantity

$$E(\alpha, \beta) = P(V_\alpha, V_\beta) + P(H_\alpha, H_\beta) - P(V_\alpha, H_\beta) - P(H_\alpha, V_\beta) \, . \tag{1.5}$$

From this quantity, we can define the **Bell parameter** :

$$S(\alpha, \alpha', \beta, \beta') = E(\alpha, \beta) - E(\alpha, \beta') + E(\alpha', \beta) + E(\alpha', \beta') \, . \tag{1.6}$$

It is that parameter that allows one to distinguish between the hidden variable theory and the quantum theory. Indeed, Bell showed that according to the hidden variable theory, S should be lower than 2 no matter the state of the two photons. It is the so-called **Bell inequality**. On the other hand, the quantum theory predicts a value of S strictly greater than 2 for a Bell state, for a certain choice of angles of analysis.

P8 Show that $S = 2\sqrt{2}$ for the set of angles of analysis depicted in figure 1.2. In this configuration, the Bell inequality are maximally violated by quantum mechanics.

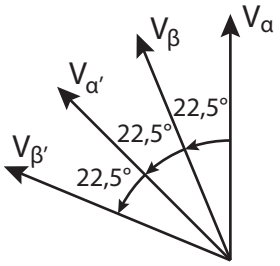

Figure 1.2: This set of angles of analysis maximizes the Bell parameter predicted by quantum mechanic.

3 Experiment : Measurement of Bell's parameter

3.1 GLobal overview of the setup

The source of polarization-entangled photons consists in a laser diode emitting a $405\,\mathrm{nm}$ beam, vertically polarized and focused on two non-linear crystals of BBO. In those crystals, a parametric conversion process turn the $405\,\mathrm{nm}$ photons into a pair of $810\,\mathrm{nm}$ photons. One of the crystal generates pairs of photons with a vertical polarization, and the other one generates a horizontally-polarized pair. The twin photons are emitted symmetrically with respect to the probe beam, inside a cone with an aperture of about $3°$. An half-wave plate working at $405\,\mathrm{nm}$ and a Babinet compensator allows one to adjust the polarization state of the probe beam.

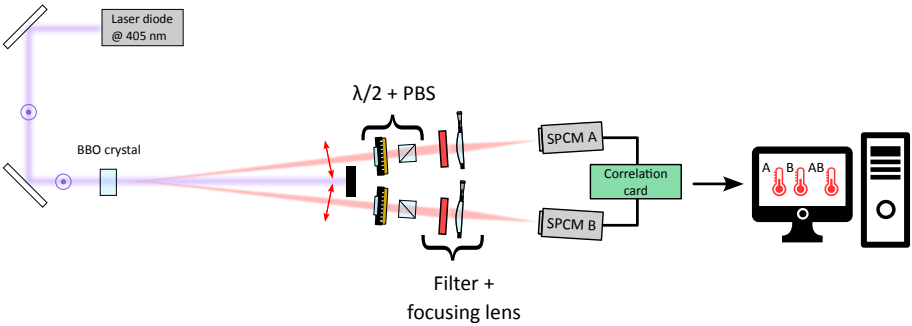

Figure 1.3: Schematic diagram. A BBO crystal pumped by a laser diode creates two beams of correlated, or even polarization-intersecting photons. On each channel, the orientation of the analyzed polarization is adjusted using a half-wave plate. Photons are focused and detected by avalanche photodiodes, whose count and coincidence signals are displayed by the computer.

To collect the infrared photons, we use an avalanche photodiode (APD) on both side of the emission cone. Before entering into the detector, the infrared photons go through a polarization analyzer made of an half-wave plate, a polarization beam splitter (PBS), a lens to focus the beam onto the photodiode, and a interferential filter centered on $810\,\mathrm{nm}$ with a $10\,\mathrm{nm}$ width. A FPGA card is used to count the number of photons detected, as well as the number of coincidences, which correspond to a simultaneous detection on both arms. Those measurement are then displayed by a Labview code.

3.2 Single photon counting modules

The photodetectors are made of silicon avalanche photodiodes used in single photon detection mode. On each arm A and B, the detection of a photon produce a TTL pulse ($0\,\mathrm{V}$ to $5\,\mathrm{V}$) with a temporal width of $25\,\mathrm{ns}$.

Warning ! Those detectors are very, very expensive and would be destroyed by a strong photon flux! Always check that the black tubes and the filters are installed to protect the photodiodes. Wait for the teacher authorization to switch on the detectors, and make sure that the main lights are off and the door is closed.

SW0	SW1	SW2	SW3
1	1	0	0
SW4	SW5	SW6	SW7
1	1	0	1
SW8	SW9	SW10	SW11
1	0	0	1
SW12	SW13	SW14	SW15
0	1	0	1

Table 1.1: Switch positions for operating the Labview VI coincidence rs232.vi.

3.3 Events and coincidences counters

The FPGA card counts the TTL pulses emitted by the detectors (after a conversion from $0\,\mathrm{V}$ to $5\,\mathrm{V}$ to $0\,\mathrm{V}$ to $3{,}3\,\mathrm{V}$), and the number of coincidences between the A and B pulses within an adjustable integration time. To count the coincidences, the FPGA card proceeds as follows: when a pulse arrives on channel A, a time window of adjustable duration is open; if a pulse arrives on channel B before this window is closed, a coincidence is counted. The card send the counting information to the computer via a RS232 link, and the information is displayed by a Labview code. All the connections are already done, and we payed attention to the fact that the cables linking the APD to the coincidence counters have the same length.

Q1 Why do the cables need to have the same length?

$\rightsquigarrow$ Make the following settings:

- Before doing anything else, switch on the FPGA card, then start the Labview program and:
- Switch off every lights and turn the photons counters on.
- Measure the number of dark counts. The lower this number is, the better the detectors are.
- Switch a weak light and check that the number of detected photons stays well below $10^6\,\mathrm{photons/s}$.

3.4 Rate of accidental coincidences

For now, since the light sources are chaotic, the photons arriving in A and B are not correlated, and therefore the potential coincidences that you might detect are accidental. We note n_A and n_B the **counting rate** (average number of photons per second) on channels A and B, n_f the rate of accidental coincidences, and τ, the duration of the coincidence window.

Q2 Show that the rate of accidental coincidence is given by : $n_\mathrm{f} = n_A\, n_B\, \tau$.

The last two switches of the FPGA card, SW16 and SW17, allows one to choose the duration of the coincidence window (see table 2.1). The number given by this table are approximative and need to be re-measured.

SW16	SW17	τ (ns)
off	off	~ 70
on	off	~ 20
off	on	~ 14
on	on	~ 7

Table 1.2: Duration of the coincidence window.

$\rightsquigarrow$ Measure the rate of accidental coincidences for each of the four configurations.

Q3 Calculate the durations of the four coincidence windows using the formula established in question **Q2**.

This measure allows one to check the behavior of the coincidence counters. Call the teacher if the results are way different from the value of table 2.1.

3.5 Pump diode

The pump diode is a $405\,\mathrm{nm}$ laser with about $60\,\mathrm{mW}$ of output power. The light emitted by the diode is linearly polarized. The wearing of security glasses is mandatory!

$\rightsquigarrow$ Make the following settings:

- Press the two buttons to turn on the temperature regulator of the diode. The temperature is already set to obtain the correct wavelength. Don't try to change it.

- Press the two buttons to turn on the current supply of the diode, and set the current at maximum (about $95\,\mathrm{mA}$).
- If they are present on the bench, remove the optical elements mounted before the BBO crystals (half-wave plates at $405\,\mathrm{nm}$ and Babinet compensator) as well as the half-wave plates at $810\,\mathrm{nm}$ and the PBS cubes in front of the detection channels.
- Check the alignement of the beams (they should be already well aligned).

3.6 Parametric conversion

The photon pairs are produced by parametric down conversion in non-linear crystals β-BaB_2O_4 (baryum β-borate, BBO for short). During the non-linear process, a photon of the $405\,\mathrm{nm}$ pump can be converted in a pair of twin $810\,\mathrm{nm}$ photons. The BBO is a negative uniaxial birefringent crystal. We use a type I phase matching, meaning that the twin photons have the same polarization.

The pump beam is orthogonal to the entrance plane of the crystals. The optical axis of the crystals makes an angle of about $29°$ with the pump beam. The optical axis of the first crystal and the axis of the pump are forming a vertical plane, and the $810\,\mathrm{nm}$ twin photons emitted from this crystal are horizontally polarized (see figure 2.3). The optical axis of the second crystal and the axis of the pump are forming a horizontal plane, and the twin photons are emitted with a vertical polarization. In both cases, the twin photons are emitted symmetrically with respect to the pump axis, within a cone of about $3°$ of aperture.

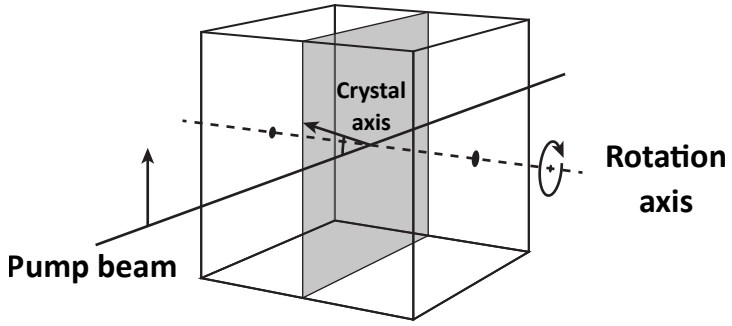

Figure 1.4: The optical axis of the crystal is oriented "vertically" with respect to the pump axis. The other crystal is oriented "horizontally".

Note: The direction of emission of the twin photons varies very quickly with the angle between the crystal axis and the pump axis. To optimize the number

of twin photons arriving onto the detectors, one should carefully set the orientation of the two crystals, using the horizontal and vertical screws of the mount (see figure 2.3).

3.7 Collimation lens

To efficiently detect the pairs, the waist of the pump beam (which is inside the BBO crystals) is imaged onto the APD's sensitive surface. It is a difficult setting because this surface has a diameter of $180\,\mu\mathrm{m}$ only. The lenses have a focal length of $75\,\mathrm{mm}$ and a diameter of $12{,}7\,\mathrm{mm}$. They are mounted $1040\,\mathrm{mm}$ away from the crystal.

Q4 Calculate the position of the image of the waist.

$\rightsquigarrow$ Check that the APD are approximatively at this position.

Q5 What is the magnification? Give an estimation of the diameter of the waist, then check that the size of the sensitive area of the photodiode is not limitating.

3.8 Optimization of the coincidence number

The direction of emission of the twin photons is very sensitive to the orientation of the crystals, which needs to be carefully optimized. The pump beam being vertically polarized, only the crystal whose axis is in a vertical plane can satisfy the phase matching condition for now. Its orientation can be adjusted thanks to the horizontal screw.

$\rightsquigarrow$ Optimize the number of coincidences by tuning the screw.

Q6 Calculate the number of accidental coincidences. Do we need to take it into account?

Q7 Calculate the ratio between the number of coincidences and the number of photons detected on each channel. Comment.

$\rightsquigarrow$ We will now optimize the orientation of the crystal whose axis is in an horizontal plane :

- Put the $405\,\mathrm{nm}$ half-wave plate before the BBO crystals.

- **Carefully identify the own axis of the plate (they do not correspond exactly to the 0 and $90°$ position). A good identification is crucial for the following.**

- Check that the number of coincidences is unchanged if the axis of the plate are horizontal and vertical. Explain why.

- Turn the plate at $45°$ to align the polarization of the pump beam with the horizontal axis.

- Optimize the number of coincidences by touching the vertical screw of the crystals.

3.9 Polarization analyzer

$\rightsquigarrow$ Put the $810\,\mathrm{nm}$ half-wave plates and the PBS cubes on each channel. Together they form a polarization analyzer (see figure 1.5).

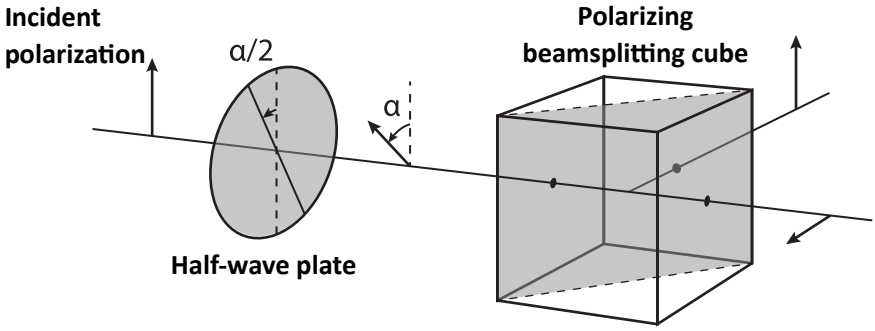

Figure 1.5: The polarization analyzer is made of an half-wave plate (whose orientation is adjustable) and a PBS cube.

Warning : The angle of the analyser is equal to the angle of analysis divided by two. So be careful to distinguish the angle of analysis from the angle of the plate!

Q8 Show that when the plate is vertical, the analyzer transmits the horizontal polarization, and therefore allows to detect the $|H\rangle$ photons. How much do you need to turn the plate to detect $|V\rangle$ photons?

$\rightsquigarrow$ Settings and adjustments:

- Check experimentally that the twin photons are in the state $|H\rangle_1 |H\rangle_2$ if the $405\,\mathrm{nm}$ half wave plate is vertical, and in the state $|V\rangle_1 |V\rangle_2$ if the plate is rotated by $45°$.
- If necessary, turn again the screws of the BBO crystals to have approximatively the same number of coincidences for those two positions of the plate.
- Then set the plate to $22{,}5°$ (try to be very precise) to obtain approximatively the same number of coincidences with the two analyzers in vertical position and the two analyzers in horizontal position (it is impossible to obtain a perfect equality, but try to balance the coincidences as much as you can).

$\rightsquigarrow$ Measure the number of coincidences when the two analyzers are parallel (horizontally or vertically). Measure the number of coincidences when the two analyzers are orthogonal.

$\rightsquigarrow$ Adjust the angle of the half-wave plate to obtain the same rate of coincidence in both situations.

$\rightsquigarrow$ Measure the coincidence rates when the two analyzers are parallel and perpendicular in the diagonal base (at $45°$).

$\rightsquigarrow$ Note the absolutely astonishing result of this measurement!

Q9 What results were you expecting? Compare with the previous measurement.

The previous settings produced a source of photon pairs created in either crystal equiprobably. This is a pair of entangled photons! Now you need to precisely adjust the polarisation state of the pump beam to obtain a Bell state.

3.10 Realization of a Bell state

For now, your twin photons are in the state

$$|\psi\rangle = \frac{1}{\sqrt{2}} \left(|V, V\rangle + e^{i\phi} |H, H\rangle \right) . \tag{1.7}$$

Where ϕ is the phase difference between the twin photons horizontally polarized, and the twin photons vertically polarized. This phase difference is linked to the birefringence of the BBO crystals.

Q10 Calculate the join probability $P(V,V)$ and $P(H,H)$ for the state (1.7). Does it allows you to distinguish the state (1.7) from the Bell state (1.2)?

Q11 Show that $P(V_{45^\circ}, V_{45^\circ}) = (1+\cos(\phi))/4$. What is the difference with the Bell state?

To obtain a Bell state instead of the state (1.7), you need to compensate the dephasing ϕ, by using a Babinet compensator. If the axis of the compensator match the horizontal and the vertical direction, you can translate it orthogonally to the pump axis to linearly vary the dephasing between the two polarisation components (see figure 1.6). For the pump wavelength, this dephasing typically varies by 2π for a translation of about $5\,\mathrm{mm}$.

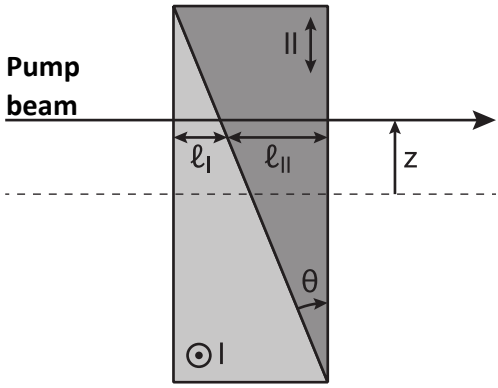

Figure 1.6: The Babinet compensator consist in two pieces of uniaxial birefringent crystal. The pieces are beveled and mounted one against the other, in such a way that the optical axis of the two crystals are orthogonal (and both parallel to the entrance plane). If we note n_1 the refractive index along the optical axis, and n_2 the refractive index along the direction orthogonal to the optical axis, we see that the dephasing $\phi_{\text{B}} = \phi_H - \phi_V$ accumulated between the polarisation components of a beam with a wavelength λ is given by $\lambda\phi_{\text{B}}/2\pi = (n_2\ell_{\text{I}} + n_1\ell_{\text{II}}) - (n_1\ell_{\text{I}} + n_2\ell_{\text{II}}) = 2(n_2 - n_1)\tan(\theta)\, z$.

$\rightsquigarrow$ Mount the compensator on the bench.

$\rightsquigarrow$ Check that the coincidence rate are still equal when the analyzers are parallel horizontally and vertically. If it is not the case, it means that the axis of

the compensator do not match the vertical and horizontal directions, and you need to slightly rotate the compensator.

$\rightsquigarrow$ Put the analyzers at $45°$ on both channels and plot the coincidence rate as a function of the compensator translation over $10\,\mathrm{mm}$ (by step of $0{,}5\,\mathrm{mm}$). Take an integration time of $10\,\mathrm{s}$.

Q12 Does the curve behave as expected? Comment on the contrast.

Q13 What are the points of the curve corresponding to a compensation of the dephasing induced by the crystals?

3.11 Variationt of the join probability

The two theories we want to test (quantum theory and local hidden variable theory) do not predict the same variation of the join probability $P(V_\alpha, V_\beta)$ as a function of the relative angle $\alpha - \beta$. So it is interesting to measure it. Experimentally, we can estimate the probability $P(V_\alpha, V_\beta)$ by setting the analyzers at α and β and calculating the ratio between the coincidence rate and the photon rate on each channel.

Important note: Only complete the measurement below if you have enough time left before the end of the session. Otherwise, go directly to the Bell parameter measurement.

$\rightsquigarrow$ Fix the angle of one of the two analyzers at $0°$ and plot the variation of the coincidence rate as a function of the angle of the second analyzer. During this measurement, check that the photon rate on each channel remains approximatively constant. Re-do the same measurement, but this time set the first angle to $45°$.

Q14 Compare those measurements to the prediction of quantum mechanics (question **P6**).

3.12 Measurement of Bell's parameter

You will now experimentally evaluate the Bell parameter defined by the relation (1.6), and whose value allows you to invalidate the local hidden variable theory. To do so, you will measure the join probabilities $P(V_\alpha, V_\beta)$, $P(H_\alpha, H_\beta)$, $P(V_\alpha, H_\beta)$ and $P(H_\alpha, V_\beta)$ for the following set of angles of analysis: $\{\alpha, \beta\}$, $\{\alpha, \beta'\}$, $\{\alpha', \beta\}$ and $\{\alpha', \beta'\}$ define on figure 1.2. To minimize the uncertainty

of each measurement, one need to maximize the number of coincidences detected, so one needs to count them over a longer duration. Indeed, the fluctuations in the number of coincidences N_c detected over an interval T are linked to the photonic "shot noise", which has a Poisson statistics. This implies that the statistical uncertainty (standard deviation) $\sigma[n_c]$ on the coincidence rate $n_c = \langle N_c \rangle / T$ verifies :

$$\sigma[n_c] = \frac{\sigma(N_c)}{T} = \frac{\sqrt{\langle N_c \rangle}}{T} = \sqrt{\frac{n_c}{T}}\,, \tag{1.8}$$

so that the relative uncertainty

$$\frac{\sigma[n_c]}{n_c} = \frac{1}{\sqrt{\langle N_c \rangle}} = \frac{1}{\sqrt{n_c T}}\,. \tag{1.9}$$

Q15 If you count an average of $100\,\mathrm{coincidences/s}$, what is the standard deviation of the coincidence rate? What is the duration required to divide this standard deviation by 10?

$\rightsquigarrow$ Fill the Excel chart on the computer for each of the 16 measurements. Take an integration time of 10 or $20\,\mathrm{s}$ to have a good precision. The Bell parameter is then automatically calculated.

Q16 What value of the Bell parameter do you obtain and what are the error bars? Does your measurement allow you to invalidate the local hidden variable theory or the quantum theory?

Q17 What result would allow you to invalidate quantum mechanics?

P 2

Two-photon interference : Hong, Ou and Mandel experiment

Contents

1 Introduction

The Hong, Ou and Mandel (HOM) experiment, conducted in 1987 [1], is the first observation of a quantum interference between two photons with no classical explanation (*i.e.* no explanation with a wave description of light). This phenomenon appears when two indistinguishable photons arrive simultaneously at the two input ports of a 50/50 beam splitter. The distribution of the two photons between the two output ports of the beam splitter exhibit a surprising behavior, that can not be explained with a classical theory of light...

1.1 The HOM effect

If a photon arrives on a 50/50 beam splitter, it has 1/2 probability of being transmitted or reflected. When two photons arrive simultaneously on a beam

[1] C. K. Hong, Z. Y. Ou et L. Mandel, *Measurement of subpicosecond time intervals between two photons by interference*, Physical Review Letters **59**, 2044 (1987)

splitter, each one at a different input (a or b), there are four possibilities (see figure 3.1) :

- The photon entered in a goes out in c, and the photon entered in b goes out in d;
- The photon entered in a goes out in d, and the photon entered in b goes out in c;
- Both photons go out in c ;
- Both photons go out in d.

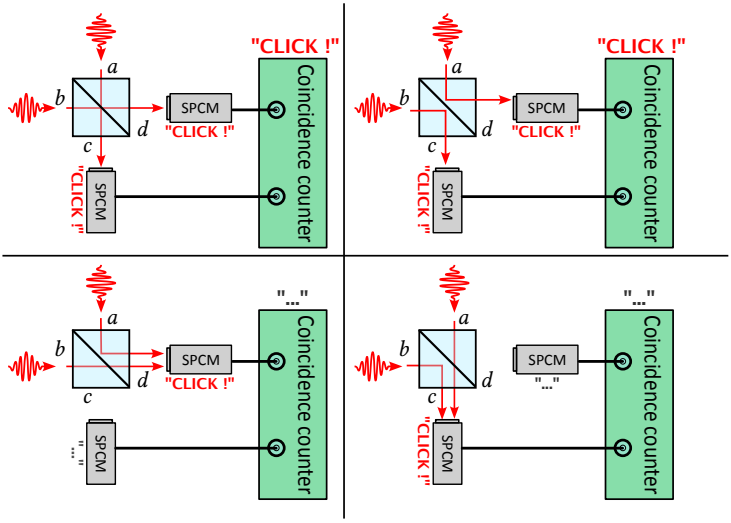

Figure 2.1: Two indistiguishable photons arrive simultaneously on a beam splitter. Two single-photon detectors at the output c and d record which way the photons went out.

If the photons were classical particles, the 4 cases would always be equiprobable, in the case where the reflectivity and transmitivity of the beam splitter are equal. But according to the quantum theory, if the two particles are **indistinguishable** there is no way to know which particle is which at the output of the beam splitter, and therefore there is only 3 possible **observations** :

- we observe one photon in each output ;
- we observe two photons in output c ;

- we observe two photons in output d.

Then, according to quantum mechanics, the probability of observing a photon in each output results from the **interference** between the two **classical trajectories** $(a,b) \to (c,d)$ and $(a,b) \to (d,c)$. It then depends on the **relative phase** associated to those trajectories.

In our case, two photons are **indistinguishable** when their properties (polarization, frequency, transverse mode) can not be distinguished with our experimental setup. Note that the two photons do not need to be identical, which would imply that they have identical properties, for them to be indistinguishable. For instance, two photons with different frequencies (or energies) behave as indistinguishable photons as long as the experimental setup does not allow one to measure the difference in their frequencies. As a consequence, establishing whether two photons are indistinguishable or not depends on the experimental setup which is used.

1.2 Formalism

In classical electromagnetism, a beam splitter is modelled by a **real unitary matrix** , that links the **electrical fields** $\mathcal{E}_{a,b}$ of the inputs to the electrical fields $\mathcal{E}_{c,d}$ of the outputs:

$$\begin{pmatrix} \mathcal{E}_c \\ \mathcal{E}_d \end{pmatrix} = U \begin{pmatrix} \mathcal{E}_a \\ \mathcal{E}_b \end{pmatrix} \quad \text{with} \quad U = \begin{pmatrix} t & r \\ -r & t \end{pmatrix} . \tag{2.1}$$

The unitarity property $U^\dagger U = \mathbb{1}$ stands for the **energy conservation** between the input and the output of the beamsplitter. It leads to a relationship between the reflectivity and transmitivity coefficient of the beam splitter.

$$r^2 + t^2 = 1 . \tag{2.2}$$

A $50/50$ beam splitter corresponds to the case where $r = t = 1/\sqrt{2}$.

In quantum optics, the complex electromagnetic field is replaced by **creation and annihilation operators** :

$$\mathcal{E}_a \to \{\hat{a}, \hat{a}^\dagger\} , \ \mathcal{E}_b \to \{\hat{b}, \hat{b}^\dagger\} , \ \mathcal{E}_c \to \{\hat{c}, \hat{c}^\dagger\} , \ \mathcal{E}_d \to \{\hat{d}, \hat{d}^\dagger\} . \tag{2.3}$$

The beam splitter links those operators in the same way than with the electric fields :

$$\begin{pmatrix} \hat{c} \\ \hat{d} \end{pmatrix} = U \begin{pmatrix} \hat{a} \\ \hat{b} \end{pmatrix} \quad \text{and} \quad \begin{pmatrix} \hat{c}^\dagger \\ \hat{d}^\dagger \end{pmatrix} = U \begin{pmatrix} \hat{a}^\dagger \\ \hat{b}^\dagger \end{pmatrix} . \tag{2.4}$$

The unitarity property of the matrix U ensures that **the number of photons is conserved** between the input and the output :

$$\hat{c}^\dagger \hat{c} + \hat{d}^\dagger \hat{d} = \hat{a}^\dagger \hat{a} + \hat{b}^\dagger \hat{b} . \tag{2.5}$$

The quantum state that corresponds to a situation where two photons enter in a and b is obtained by using the operators $\hat{a}^\dagger$ and $\hat{b}^\dagger$ on the state which corresponds to the **electromagnetic vacuum** : $\hat{a}^\dagger\hat{b}^\dagger|\text{vacuum}\rangle$. By inverting the relation 2.4, one can link this input state to the output state:

$$\begin{aligned}\hat{a}^\dagger\hat{b}^\dagger|\text{vacuum}\rangle &= (t\hat{c}^\dagger - r\hat{d}^\dagger)(r\hat{c}^\dagger + t\hat{d}^\dagger)|\text{vacuum}\rangle \\ &= (tr\hat{c}^\dagger\hat{c}^\dagger + t^2\hat{c}^\dagger\hat{d}^\dagger - r^2\hat{d}^\dagger\hat{c}^\dagger - rt\hat{d}^\dagger\hat{d}^\dagger)|\text{vacuum}\rangle\,. \end{aligned} \tag{2.6}$$

In the case of a $50/50$ beam splitter, we can use the commutativity of the operators acting on the different modes of the electromagnetic field. The last expression then become:

$$\hat{a}^\dagger\hat{b}^\dagger|\text{vacuum}\rangle = \frac{1}{2}(\hat{c}^\dagger\hat{c}^\dagger - \hat{d}^\dagger\hat{d}^\dagger)|\text{vacuum}\rangle\,. \tag{2.7}$$

The interpretation of this equation is straightforward: at the output of the beam splitter, the states corresponding to the situation where two photons are at the output c or d are equiprobable, but the probability of having a photon on each output is zero. Therefore **we never observe any coincidence** between the detectors c and d.

2 Experimental realization

2.1 Description of the experimental setup

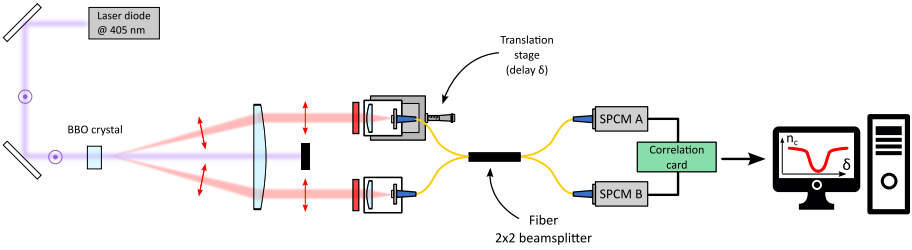

Figure 2.2: View from above. We see the laser diode, two mirrors to set the alignement, the non-linear crystal, the optics for the conjugation and two fibered collimators. The optical path of the pump beam and the photons pairs are sketched.

To observe the HOM effect, one needs to create pairs of indistinguishable photons and send them into a beam splitter (see figure 2.2). To do so, we will use

a parametric down-conversion process inside a $\chi^{(2)}$ non-linear crystal (BBO) than can convert a pump photon at $\lambda_p = 405\,\mathrm{nm}$ into a pair of photons at $2\lambda_p = 810\,\mathrm{nm}$. The twin photons are emitted symmetrically with respect to the pump axis, within a cone of about 3° of aperture. The pump beam, emitted from a laser diode, is horizontally polarized. The twin photons created in this process, are vertically polarized.

The twin photons are then injected inside two polarization-maintaining monomode fibers, thanks to a pair of fibered collimators and an optical doublet, whose focal point is set inside the crystal. An interferometric filter at $810\,\mathrm{nm}$ allows us to get rid of most of the stray lights. The fibered light then enters inside a module made of two waveguides that will play the role of the beam splitter. The waveguides are mounted very close to each other so that the transverse mode of the light propagating in each waveguide overlap the other one. The fibers are connected to a detection module using Avalanche PhotoDiodes (APD). A FPGA card is used to count the number of detected photons in each output. A simultaneous detection on each output is counted as a **coincidence**. A Labview code is then used to display the number of events and coincidences.

2.2 Single photon detection module

The single photon detection module is an exceptional tool, adapted for this kind of experiment. It is made of four fibered channels, linked to four APDs. On each channel, the detection of a photon triggers the emission of a $25\,\mathrm{ns}$ TTL pulse ($0\,\mathrm{V}$ to $5\,\mathrm{V}$). We will just use two channels out of four for this experiment, labeled A and B.

Warning ! Those detectors are very, very expensive and would be destroyed by a strong photon flux! Always check that the interferometric filters are installed to protect the photodiodes. Wait for the teacher authorization to switch on the detectors, and make sure that the main lights are off and the door is closed.

2.3 Event and Coincidence counter

The FPGA card counts the TTL pulses emitted by the detectors (after a conversion from $0\,\mathrm{V}$ to $5\,\mathrm{V}$ to $0\,\mathrm{V}$ to $3{,}3\,\mathrm{V}$), and the number of coincidences between the A and B pulses within an adjustable integration time. To count the coincidences, the FPGA card proceeds as follows: when a pulse arrives on channel A, a time window of adjustable duration is open; if a pulse arrives on channel B before this window is closed, a coincidence is counted. The card send the counting information to the computer via a RS232 link, and the informations are displayed by a Labview code. All the connections are already done, and we

SW16	SW17	τ (ns)
off	off	~ 70
on	off	~ 20
off	on	~ 14
on	on	~ 7

Table 2.1: Duration of the coincidence window.

payed attention to the fact that the cables linking the APD to the coincidence counters have the same length.

Q1 Why do the cables need to have the same length?

$\rightsquigarrow$ Perform the following settings and measurements:

- Before doing anything else, switch on the FPGA card, then start the Labview program.
- Switch off every lights and turn the photons counters on.
- Measure the number of dark counts. The lower this number, the better the detectors are.
- Switch on a distant light and check that the number of detected photons stays way below 10^6 photons/s.

2.4 Number of accidental coincidences.

For now, since the light sources are chaotic, the photons arriving in A and B are not correlated, and therefore the coincidences are accidental. We note n_A and n_B the **counting rate** (average number of photons per second) on channels A and B, n_{f} the rate of accidental coincidence, and τ, the duration of the coincidence window.

Q2 *Show that the rate of accidental coincidence is given by :* $n_f = n_A\, n_B\, \tau$.

The last two switches of the FPGA card, SW16 and SW17, allow one to choose the duration of the coincidence window (see table 2.1). The numbers given in this table are approximate and must need be measured.

$\rightsquigarrow$ Measure the rate of accidental coincidences for each of the four configurations and calculate the durations of the four coincidence windows using the formula established in question 2.

This measure allows one to check the behavior of the coincidence counters. Call the teacher if the results are different from the value of table 2.1.

2.5 Pump diode

The pump diode is a $405\,\mathrm{nm}$ laser with about $60\,\mathrm{mW}$ of output power. The light emitted by the diode is linearly polarized. The wearing of security glasses is mandatory!

$\rightsquigarrow$ Make the following settings:

- Press the two buttons to turn on the temperature regulator of the diode. The temperature is already set to obtain the correct wavelength. Don't try to change it.
- Press the two buttons to turn on the current supply of the diode, and set the current at maximum (about $95\,\mathrm{mA}$).
- Briefly check the alignement of the beams (they should be already well aligned).

2.6 Parametric conversion

The photons pairs are produced by parametric down conversion in non-linear crystals β-BaB2O4 (baryum β-borate, BBO for short). During the non-linear process, a photon of the $405\,\mathrm{nm}$ pump can be converted in a pair of twin $810\,\mathrm{nm}$ photons. Recall that the two photons of the pair may have slightly different energies (or wavelenghts) since only their sum is set by the energy of a $405\,\mathrm{nm}$ pump photon (energy conservation in the process of parametric down conversion).

The BBO is a negative uniaxial birefringent crystal. We use a type I phase matching, meaning that the twin photons have the same polarization.

Q3 Recall what are the two conditions satisfied by a non-linear process. Which one is called the phase matching condition?

The pump beam is orthogonal to the entrance plane of the crystal. The optical axis of the crystal and the axis of the pump are forming an horizontal plane (see figure 2.3).

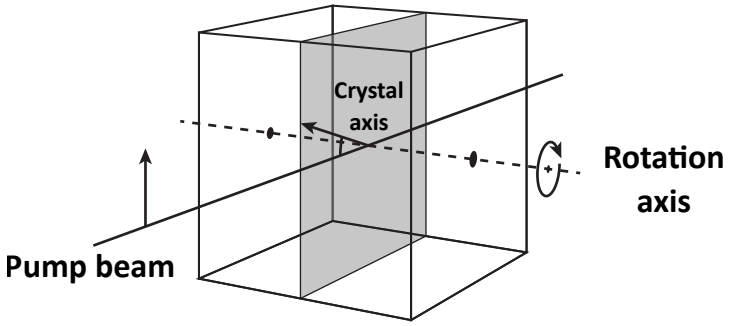

Figure 2.3: Orientation of the optical axis of the crystal with respect to the pump axis.

The pump is horizontally (extraordinary) polarized and the $810\,\mathrm{nm}$ twin photons emitted from the crystal are vertically (ordinary) polarized. The refractive indexes n_o and n_e which characterize respectively the crystal axis and the orthogonal axis are given in table 2.2. From those indexes, one can calculate the index n_θ seen by the pump while it propagates through the crystal:

$$1/n_\theta^2 = \sin^2(\theta)/n_o^2 + \cos^2(\theta)/n_e^2\,. \tag{2.8}$$

θ being the angle between the propagation axis and the crystal axis (see figure 2.3).

wavelength (nm)	n_o	n_e
405	1,691 835	1,567 071
810	1,660 100	1,544 019

Table 2.2: Refractive index of the BBO crystal along its optical axis, at a temperature of $293\,\mathrm{K}$.

Q4 Using a spreadsheet (Excel), calculate $n_\mathrm{e}(405, \theta)$ as a function of θ in the near range of $\theta = 30^\circ$. For what precise angle θ is type I collinear phase tuning achieved?

If we deviate slightly from this precise θ angle by modifying the crystal's inclination, we'll still obtain a type I, but non-collinear, phase tuning.

Q5 The collimators are positioned in such a way that they are forming with the crystal an isosceles triangle, with a 3° aperture. What should be the angle θ for the twin photons to be correctly collected by the collimators?

2.7 Settings of the collimators

The optical fibers are polarization-maintaining fibers. Their own axis are parallel to the horizontal and vertical axis. One of the own axis can be spotted thanks to a tip on the connector.

Q6 Why are those polarization-maintaining fibers crucial to observe the HOM effect?

Now you need to image the area of emission of the photons pairs onto the core of each fibers, by tuning the orientation of the collimators. This is a difficult setting because the fibers' cores have a diameter of $5\,\mu\mathrm{m}$ only. A trick is to make light propagates in the other direction (from the collimators to the crystal) by injecting a $670\,\mathrm{nm}$ auxiliary laser at the output of the polarization-maintaining fibers. You then have two beams coming out of the collimator. Focalise them inside the crystal and superimpose them to the pump beam. Of course you need to take the filter away from the collimator because they would cut the $670\,\mathrm{nm}$ light. Don not forget to put them back before switching the photon counters on again.

Warning ! You must switch the single photon detection module off every time the fibers are disconnected, and every time the filter are taken away from the collimators. Don not forget to put them back before switching the photon counters on again. Always protect the fibers' extremity with a cap.

Even with this method, it is difficult to inject the fibers. You will have to be very cautious (and probably try several times) to set the collimators correctly. However, as soon as you manage to inject a small fraction of the twin photons, the setting becomes a lot easier, you then just have to optimize the number of coincidences by fine-tuning the position of the collimators.

Remark The screws of the collimators' mounts are the only elements you need to touch during this setting. If you lose all the signal in the process (and you are not able to recover it) call the teacher.

$\rightsquigarrow$ Measure the coincidences rates.

Q7 Calculate the rate of accidental coincidences.

Q8 Do you need to account for them?

2.8 Observation of the HOM effect

Once the coincidence rate is high enough (about $600\,\mathrm{coincidences/s}$), you are ready to observe the HOM effect. One of the collimators is mounted on a translation stage. Record the number of coincidences as you gently move the translation stage (for instance by step of $10\,\mu\mathrm{m}$). To lower the uncertainty of your measurements, you need to raise the number of detected coincidences, so you need to count coincidences over a longer time interval. The fluctuations of the number of coincidences N_c measured during a time T is linked to the photonic shot noise, which follows a Poisson law. It means that the standard deviation $\sigma[n_\mathrm{c}]$ on the coincidence rate $n_\mathrm{c} = N_\mathrm{c}/T$ verifies :

$$\sigma[n_\mathrm{c}] = \frac{\sigma(N_\mathrm{c})}{T} = \frac{\sqrt{N_\mathrm{c}}}{T} = \sqrt{\frac{n_\mathrm{c}}{T}}\,., \tag{2.9}$$

which leads to the relative uncertainty :

$$\frac{\sigma[n_\mathrm{c}]}{n_\mathrm{c}} = \frac{1}{\sqrt{N_\mathrm{c}}} = \frac{1}{\sqrt{n_\mathrm{c}T}}\,. \tag{2.10}$$

Q9 Assuming you count an average of $100\,\mathrm{coincidences/s}$, what is the standard deviation on the coincidence rate? How long should the time interval be to reduce this deviation by a factor of 10?

In practice, you will count the coincidences during a time interval of 10 or $20\,\mathrm{s}$.

$\rightsquigarrow$ Plot the coincidence rate as a function of the position of the translation stage. Add the error bars on your graph.

Q10 Interpret the curve.

$\rightsquigarrow$ What is the depth of the dip?

Q11 Why does it not go to zero?

$\rightsquigarrow$ What is the the full width at half minimum of the dip?

Q12 Compair it to the coherence length of the $810\,\mathrm{nm}$ photons, which is given by the the filter ($10\,\mathrm{nm}$ width).

The width of the HOM dip is given by the energy difference of the twin photons created.

Q13 Explain why, using the notion of indistinguishability of the photons detected.

It is now possible to add interference filters of width $5\,\mathrm{nm}$.

Q14 What width of dip should we get in this case?

$\rightsquigarrow$ It is necessary to slightly change to pump wavelength and set it at $404\,\mathrm{nm}$ so that the twin photons are indeed transmitted by the pair of superimposed filters. To do so, you can increase the resistance of the temperature controller up to a value typically between $12,9k\Omega$ and $13,3k\Omega$. You can use the spectrometer to check the pump wavelength.

Careful, changing the pump wavelength implies to slightly relalign the collimators to collect the pairs of photons and measure coincidences. With these narrower filter and working around $808\,\mathrm{nm}$ the typical counts and coincidence rates are much smaller than in the previous case and require longer integration time.

$\rightsquigarrow$ If you have time, add the $5\,\mathrm{nm}$ filters in front of the $10\,\mathrm{nm}$ wide filters and repeat the HOM dip measurements.

$\rightsquigarrow$ Measure the new width of the HOM dip.

Q15 Compare it with the new energy difference of the photons detected using the $5\,\mathrm{nm}$ width filters.

P 3

NV center magnetometry

Contents

1 Learning objectives

At the end of this labwork session, you'll be able to :

- use a method to a align a light beam ("walking the beam")
- measure the RF spectrum of NV centres
- analyze the RF spectrum of NV centers under an externally applmied magnetic field
- reconstruct a vectorial magnetic field from this RF spectrum
- describe a method to reconstruct weak magnetic fields such as the magnetic field of the Earth.

2 Introduction

An NV center is a crystalline defect of diamond. It's also known as a "colored center", because on a macroscopic scale, when these defects are present in very large numbers, they give diamond a colored hue. Since diamond is made up of a network of carbon atoms, the NV center consists of the substitution of one of these atoms by a nitrogen atom (N), directly adjacent to a vacancy (V). (see Fig. 3.1).

In the quantum world, electrons are described by a wave function. The wave functions of electrons around an atom are confined (because the electrons remain close to the nucleus). The confinement of this wave gives rise to the quantization of its energy states, in the same way that a wave (e.g. a light wave) sees its modes of propagation confined by the existence of boundary conditions, in a cavity or a waveguide.

In the case of NV centers, the disruption of the crystal lattice causes the wave function of certain electrons to be confined to the defect. It is therefore often said that an NV center behaves like an artificial atom: while crystalline diamond is a large-gap semiconductor, the defect introduces electronic energy levels within this gap.

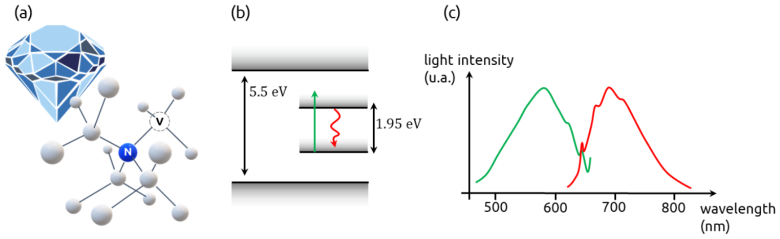

Figure 3.1: Diamond NV center. (a) Schematic representation of an NV center, with a nitrogen atom (N) next to a vacancy (V).(b) Energy levels of diamond. Diamond is a wide-gap semiconductor. The presence of an NV center creates a sublevel within the gap.

The optical transition of the defect is at 637 nm. The interaction between this defect and the crystal, via phonons, causes a significant broadening of this transition. In practice, the absorption spectrum of the defect consists of a broad lobe centered around 550nm. Fluorescence at this level undergoes a Stokes shift, and takes the form of a broad lobe centered around 700 nm, in the red part of the visible spectrum. Each lobe is around 200 nm wide.

Although NV centers are naturally present in diamond, it is possible to introduce NV centers in controlled densities into diamond samples (usually synthesized).

2.1 Defect geometry

Diamond is a crystal with a...diamond-like structure. It is a crystal with a blende structure, in which all sites are occupied by carbon atoms. It can be described as a face-centered cubic structure in which half the tetrahedral sites are occupied, two in the lower half of the cube describing the mesh, along a small diagonal, and two in the upper half, along the other small diagonal
.

The structure of an NV center is inscribed in this mesh, by substitution of one of the carbon atoms by a nitrogen, and creation of a gap by replacement of one of the surrounding carbon atoms.

The natural axis of symmetry of an NV center is the axis connecting the nitrogen atom to the gap. By construction, there are therefore 4 possible orientations of an NV center in a diamond crystal, corresponding to the 4 possible vacancy positions for a given nitrogen atom. (see Fig 3.2).

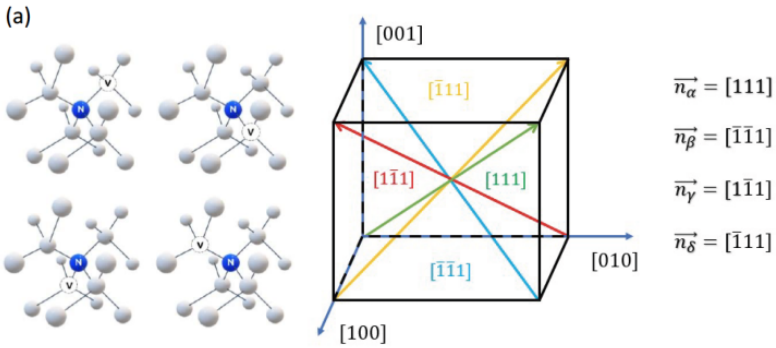

Figure 3.2: The four possible orientations of NV centers in a solid diamond crystal and corresponding Miller notations.

The corresponding directions can be assigned to so-called Miller indices. These are an notation system allowing to define orientations with respect to the crystalline axis if the system.

Here, we define the known orientation of the diamond sample with respect to the lab reference frame as (X, Y, Z). You can find at the end of this textbook an appendix explaining in more details the relation between the Miller indices and the axes (X, Y, Z).

3 Energy levels and spin

An NV center has a total spin $S = 1$. The fundamental level and the excited level of the optical transition of interest are therefore spin triplets: they are characterized by the quantum number m_S, which can take on the values 0,1, depending on the projection of the spin on the quantization axis (which is therefore the axis of the NV center). (see Fig 3.3).

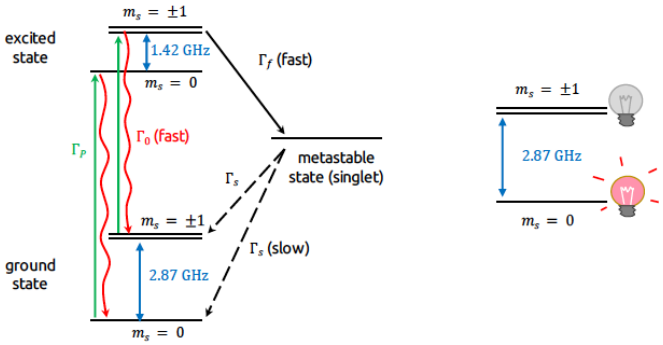

Figure 3.3: Energy level structure of an NV center, comprising a triplet of ground states and a triplet of excited states

The energy degeneracy between the $|m_S = \pm 1\rangle$ and $|m_S = 0\rangle$ levels is partially overcome by spin-spin interaction. These two sets of levels are separated by an energy whose corresponding frequency is $D \approx 2.87\text{GHz}$ for the fundamental triplet and $D' \approx 1.42\text{GHz}$ for the excited triplet.

It is therefore possible to use a laser to induce an optical transition from one of the fundamental levels to the excited state of the same spin.

Moreover, one can use a radio-frequency antenna tuned at $2,87\,\text{GHz}$ to induce transitions within the levels $m_s = 0$ and $m_s = \pm 1$.

A crucial point in the energy level structure of an NV center is the presence of a metastable singlet state. The excited state $|m_S = 0\rangle$ is not coupled to this metastable state and will always decay to the corresponding ground state by emitting a photon. For excited states $|m_S = \pm 1\rangle$, however, there is a probability of non-radiative de-excitation from the levels to the metastable state, i.e. without photon emission.

> In other words, when the NV center is placed in the $|m_S = \pm 1\rangle$ states, it emits less fluorescence as it de-excites: this property is at the heart of the experiments that will be carried out during the course of the labwork.

3.1 Zeeman effect

The energy levels of the NV center are given by the Hamiltonian of the system. In the $(x_{\text{NV}}, y_{\text{NV}}, z_{\text{NV}})$ basis related to the NV center, with the z_{NV} axis aligned with the NV center, this Hamiltonian is written :

$$\hat{H} = hD\hat{S}^2_{z_{NV}} + hE(\hat{S}^2_{x_{\mathrm{NV}}} - \hat{S}^2_{y_{\mathrm{NV}}}) + \Gamma(\mathbf{B}\cdot\hat{\mathbf{S}}) \tag{3.1}$$

where

- $D \approx 2.87\,\mathrm{GHz}$ is the zero-field separation factor of the fundamental levels, related to the spin-spin interaction.
- E is a splitting factor related to imperfections in the crystal lattice,
- $\Gamma \approx 28\,\mathrm{MHz.mT^{-1}}$ is the gyromagnetic factor. More precisely, one writes $\Gamma = g\mu_B$, with g the Landé factor and μ_B the Bohr's magneton associated with the $\mathbf{S}$ spin of the NV centers.
- $\mathbf{B}$ represents the external magnetic field that can be applied.
- $\mathbf{S}$ represents the spin operator and its components, the Pauli spin matrices;

Under some approximations, the Hamiltonian can be simplified to contain only the contribution of the magnetic field aligned with the center NV :

$$\hat{H} \approx hD\hat{S}^2_{z_{NV}} + \Gamma(B_{z_{\mathrm{NV}}}S_{z_{NV}}) + hE(\hat{S}^2_{x_{NV}} - \hat{S}^2_{y_{NV}}) \tag{3.2}$$

This Hamiltonian explains the $2,87\,\mathrm{GHz}$ splitting between level $m_s = 0$ and the levels $m_s = \pm 1$ degeneracy lift of the $ketm \pm 1$ levels. Moreover, the degeneracy between levels $m_s = \pm 1$ can be lifted by two contributions :

- at zero field, a first contribution arises from the deformations of the crystal lattice (term in E)
- in addition, a second contribution to the splitting arises from the amplitude of the projection of the magnetic field onto the axis of the NV center: this is the Zeeman effect, modeled by the term $(B_{z_{\mathrm{NV}}}S_{z_{NV}})$.

The frequencies of both levels $m_S = -1$ and $m_S = +1$ are given by :

$$f_{\pm} = D \pm \sqrt{E^2 + (\Gamma B_{z_{\mathrm{NV}}})^2} \tag{3.3}$$

For intense fields, the Zeeman splitting is therefore given by :

$$\boxed{\Delta f_{\mathrm{Zeeman}} = f_+ - f_- \approx 2\Gamma B_{Z_{NV}} \approx 56\cdot\mathrm{MHz/mT}.B_{z_{NV}}} \tag{3.4}$$

3.2 Preliminary questions

The session consists in carrying out *Optically Detected Magnetic Resonance* (or ODMR) measurements. The protocol is as follows: the fluorescence of an NV center illuminated by a laser is detected. The NV center itself is placed on an RF antenna. The fluorescence intensity is observed by switching on the RF antenna and performing a frequency sweep around the transition between the $|m_S = 0\rangle$ and $|m_S = \pm 1\rangle$ states of the fundamental triplet.

P1 Schematically represent the ODMR spectrum of a single NV center at zero field ($B = 0$), then at non-zero field.

P2 How does this ODMR spectrum measure the amplitude of a magnetic field component?

A diamond crystal can contain numerous NV centers, in 4 possible orientations. A fluorescence experiment thus simultaneously probes 4 different populations of NV centers, each associated with a different projection of the same magnetic field on the center's orientation. An ODMR plot can therefore display up to 4 pairs of dips, thus with exhibiting 4 different Zeeman splittings.

P3 Schematically represent the ODMR spectrum of a diamond crystal containing numerous centers at zero field, then at non-zero field.

4 Optical setup

WARNING !!!

In this TP, the maximum power of the 532 nm laser is 140 mW, i.e. over 100 times the eye's permanent damage threshold.

Please wear safety goggles when the laser is in operation.
For any changes to be performed on the optical table, lower the laser power below 1 mW, then open the boxes before adjusting.

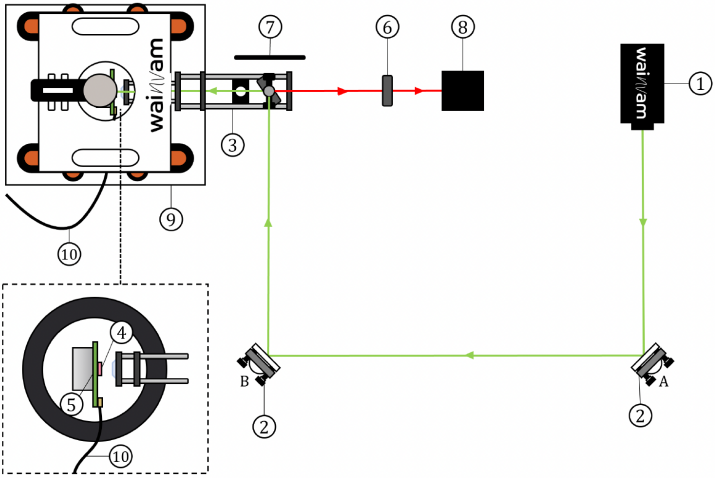

Figure 3.4: Setup schematic 1 - Laser source. 2 - Alignment mirrors. 3 - Caged system comprising irises, dichroic mirror and aspherical focusing lens. 4 - NV-doped diamond sample. 5 - RF antenna, sample support. 6 - High-pass filter (lambda). 8 - Detector. 9 and 10 - Coils and their power supplies.

The optical set-up (see Figure 3.4) consists of a 532 nm laser, sent by two mirrors to a dichroic mirror, towards an asphere lens focusing the beam on a small diamond sample rich in NV centers, placed on an RF antenna, and in the middle of three pairs of coils allowing magnetic fields to be applied along the X, Y and Z axes (linked to the laboratory reference frame). The red fluorescence of the NV centers follows the opposite path, but is transmitted by the dichroic mirror, towards a photodiode.

The laser excitation power level and the photodiode detection signal can be

controlled via the WAINTEACH control software.

5 Experiments

5.1 Aligning the beam ("beam walking")

$\rightsquigarrow$ Switch on the laser and set the drive current up to few mA.

Before starting measurements, fine-tuning the alignment of the laser on the sample might be necessary. To do this, one may adjust the micrometric screws on the two mirrors, so that the beam passes through two diaphragms, whose straight line joining the two centers defines the optical axis of the setup.

As the rest of the set-up has already been adjusted, it is not necessary (and not recommended) to touch other elements of the set-up. If you feel the need (or curiosity!) to do so, please call the teacher.

$\rightarrow$ You can optimize further the mirror orientation by optimizing the collection of the fluorescence signal by the photodiode. To do so, connect the output of the photodiode to the oscilloscope.

$\rightarrow$ When the laser is adequately focused onto the crystal, one can easily notice a strong orange fluorescent hue, even easier to wear with the safety goggles on.

5.2 Zero field measurement

The aim of this first experiment is to carry out an ODMR measurement at zero field - without applying a magnetic field to the coils.

$\Rightarrow$ With the boxes closed, turn up the laser power in a range between 20 mW and 80 mW.

$\Rightarrow$ Start the software **kwanteach-sw** using the shortcul icon on the desktop. In the software window, click the "load wainteach" button.

$\Rightarrow$ Display the "ODMR Acquisition" tab in the Kwanteach software (voir Figure 3.5).

$\Rightarrow$ Record a first ODMR spectrum, for example between $2,8\,\mathrm{GHz}$ and $2,94\,\mathrm{GHz}$, with RF power set at 0 dBm.

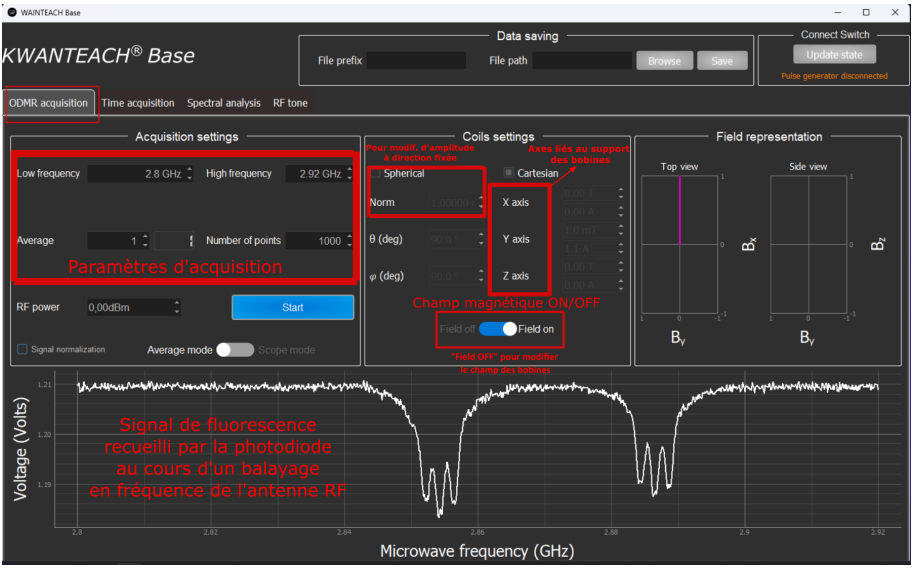

Figure 3.5: Interface du logiciel dans l'onglet "ODMR acquisition".

⇒ Save this acquisition (and subsequent ones) in the same folder, using the software's "save" function.

⇝ Click on the recorded plots to show a cursor that will enable you to precisely display the corresponding frequency.

Q1 Note the center frequency corresponding to fluorescence drop. How do you explain this drop? What transition between levels in the NV center does this center frequency correspond to?

Q2 If you look carefully, , you should see two peaks within the central peak. Which Hamiltonian term explains the physical origin of these two peaks? Comment.

5.3 Measurement in an unspecified magnetic field

⇒ Bring the horseshoe magnet close to the sample, from the top of the coils. Repeat the spectrum measurement.

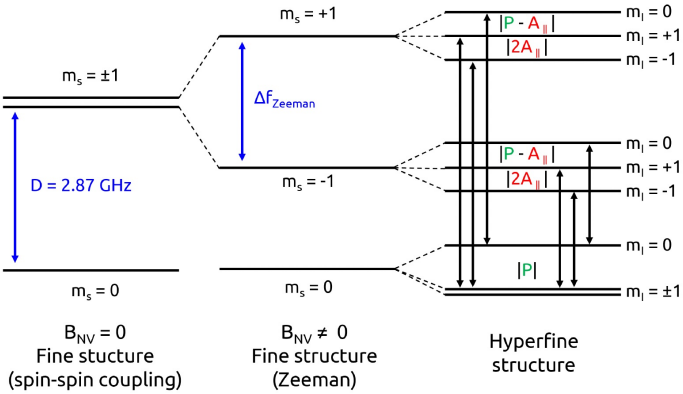

Figure 3.6: Details of the energy level structure of a single NV center, down to its hyperfine structure..

Q3 What do you observe? Describe the changes observed and explain qualitatively why the shape of the ODMR spectrum has changed.

Q4 Use the hyperfine level structure described on Figure 3.6), and comment the number of observable peaks in this non-specified magnetic field.

5.4 Influence of the magnetic field orientation

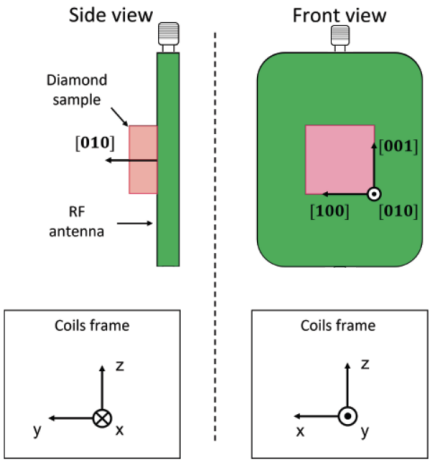

Figure 3.7: Diagram of the sample orientation within the coils applying the magnetic field. The diamond is cut perpendicular to the orientation [010] - each of the 3 axes of the coils corresponds to one of the crystalline axes of the diamond lattice.

The diamond sample is oriented along the axes shown in figure 3.7. The aim of this section is to study the effect of field orientation on the ODMR spectra.

The measurement bench allows a magnetic field with a controlled orientation to be applied using three pairs of coils. **Helmholtz coils** are used here: each pair consists of two identical circular coils with radius R, positioned parallel to each other and facing one another at a distance d equal to their radius. The advantage of this commonly used configuration is that it produces a highly uniform magnetic field at the center of the setup, along the axis connecting the coils, and over a region comparable in size to R. By combining three pairs of coils aligned along the X, Y, and Z axes of the laboratory frame, one can exploit the linearity of Maxwell's equations to sum the contributions of each pair and generate a magnetic field with an arbitrary orientation at the center of the system.

$\Rightarrow$ A gaussmeter is used to measure magnetic fields. Due to a significant offset, differential measurements must be performed to obtain accurate values along a given axis. For example, to measure the component of the field along the OXOX axis, the gaussmeter should be oriented first along $+X$, then along

X, by rotating the Hall probe by $180\,\mathrm{deg}$.

Q5 Measure the magnetic field in the room along the three orientations X, Y, Z. Estimate the Earth's magnetic field. A compass can be used to verify the direction of magnetic North.

Repeat the measurement by placing the gaussmeter at the center of the coils, with the system powered off. Then, apply several current values to the coils and verify that the readings provided by the gaussmeter are consistent with those displayed by the software.

The diamond sample is oriented according to the axes shown in Figure 3.7. The aim of this section is, on the one hand, to study the effect of the magnetic field orientation on the ODMR spectra.

Q6 Recall the possible orientations of the NV centers in the crystal axis system. Associate each of these orientations with a unit vector in the coil axis system X, Y, Z.

$\Rightarrow$ Apply a magnetic field of approximately 2 mT along the Y axis, the normal to the sample.

Q7 What is the projection of this field onto the four possible NV center orientations? Use your answer to comment on the shape of the resulting ODMR spectrum.

Q8 If the magnetic field had a different projection onto each of the four possible NV center orientations, what would be observed? Try to identify a field orientation that would result in the maximum number of peaks.

Q9 Align the magnetic field along the direction $\beta = \frac{1}{\sqrt{3}}(1,1,1)$. Why do two pairs of peaks appear? Why do these two pairs of peaks have very different amplitudes? Identify each of these peaks.

5.5 Mesasuring the gyromagnetic ratio

The aim of this section is to study the influence of the field norm on Zeeman splitting, for a class of NV centers with a given orientation.

$\Rightarrow$ Keep the magnetic field oriented along direction β.

$\Rightarrow$ Once the direction of the magnetic field is set, use the "Spherical" tab in the "Coils settings" panel to vary the magnetic field strength from 0 to 2.5 mT in steps of 0.5 mT.

$\Rightarrow$ For each applied field value, and after averaging over 5 consecutive sweeps, record the frequency position of the central peak of each of the two observed triplets.

Q10 Use your measurement to plot the evolution of the Zeeman splitting with respect to the amplitude of the applied magentic field. Deduce the gyromagnetic factor Γ.

5.6 Measuring the Earth magnetic field

In practice, the magnetometer never rests in a rigorously zero magnetic field, even when the coils are switched off: it rests in the Earth's magnetic field (and other parasitic fields).

Q11 Using your previous gaussmeter measurements, provide an estimate of the expected Zeeman splitting amplitude for an NV center oriented vertically.

The goal of this section is to determine the magnitude and orientation of the Earth's magnetic field. More generally, the method you will follow can be used to measure and characterize weak and unknown magnetic fields at very small scales.

Measurement guidelines

Measuring a magnetic field with a magnetometer is based, on the one hand, on the idea that the Zeeman splitting of a pair of peaks is linked to the norm of the projection of the magnetic field on the direction associated with an NV center, and on the other hand, on the exploitation of the 4 possible NV center orientations to obtain 4 different projections of the same magnetic field vector on different directions.

The magnetic field of the coils is therefore added to that of the earth's magnetic field to obtain adequate ODMR spectra. A complete procedure to reconstruct the ambient magnetic field from a sequence of ODMR measurements is detailed in the appendix to this session's textbook.

Experimental protocole

⇒ Record the frequency position of the central peak of the two outermost triplets;

⇒ Acquire a second spectrum *by reversing the direction of the applied magnetic field*. The total field experienced by the NV centers becomes $\vec{B}_{tot}^{-} = \vec{B}_{Earth} - \vec{B}_{\alpha}$;

⇒ Again, record the frequency position of the central peak of the two outermost triplets;

⇒ Repeat these measurements by applying a magnetic field along the other crystalline orientations β, γ, and δ, each time in both opposite directions.

Q12 Use the Excel sheet available on the couputer and report your measurement results enabling you to calculate the projection of the ambient magnetic field onto each one of the four different crystalline orientations. The table then provides a way to compute the magnetic field components in the reference frame of the lab, X, Y and Z. Comment on the main sources of uncertainties of your setup and suggest solutions to reduce them as much as possible.

Appendix: magnetic field reconstruction

Expression of Zeeman splitting as a function of magnetic field projections

To reconstruct the magnetic field from ODMR spectra, each ODMR line must first be assigned an NV center class and orientation. To do this, we need to go back to the projection of the magnetic field onto each orientation.

The two split frequencies $f_{i_\pm}$ associated with a given NV center orientation $\mathbf{n_i}$ (with $i = \alpha, \beta, \gamma, \delta$) are expressed as :

$$f_{i,\pm} = f_0 \pm \gamma |\mathbf{B}_{\mathrm{tot}}| \cos\theta_i \tag{3.5}$$

with $theta_i$ the angle between the magnetic field vector and the crystal orientation vector.

In the approximation where the ambient field is much weaker than that applied by the coil, this angle is given by :

$$\frac{\mathbf{B_{coil}} \cdot \mathbf{n_i}}{|\mathbf{B_{coil}}||\mathbf{n_i}|} \approx \cos\theta_i \tag{3.6}$$

The sign matters and the cosine can be negative, so that $f_{i+} > f_{i-}$ if $\cos\theta_i > 0$, and $f_{i+} < f_{i-}$ if $\cos\theta_i < 0$. The Zeeman splitting, which can be positive or negative, is then expressed as :

$$\Delta f_i = |f_{i+} - f_{i-}| \times \mathrm{sign}(\cos(\theta_\mathrm{i})) \tag{3.7}$$

Measuring a magnetic field component

In the labwork, two consecutive spectra are measured by reversing the direction of the magnetic field, resulting in two splitting measurements.

$$\mathbf{B}_\mathrm{tot} = \mathbf{B}_\mathrm{Earth} + \mathbf{B}_\mathrm{coil} \longrightarrow \Delta f_i^+$$

$$\mathbf{B}_\mathrm{tot} = \mathbf{B}_\mathrm{Earth} - \mathbf{B}_\mathrm{coil} \longrightarrow \Delta f_i^-$$

Using the projection angle θ_i, we can write :

$$\Delta f_i^+ = 2\gamma B_\mathrm{Earth} \times \cos\theta_i + 2\gamma B_\mathrm{coil} \times \cos\theta_i \tag{3.8}$$

and likewise,

$$\Delta f_i^- = 2\gamma B_\mathrm{Earth} \times \cos\theta_i - 2\gamma B_\mathrm{coil} \times \cos\theta_i \tag{3.9}$$

Combining the two expressions gives :

$$\frac{\Delta f_i^+ + \Delta f_i^-}{4} = B_\mathrm{Earth} \times \cos\theta_i = B_\mathrm{Earth,i} \tag{3.10}$$

i.e. the measurement of the projection of the value of the earth's magnetic field on the direction $\mathbf{n_i}$.

Crystal orientations and field reconstruction

The orientations of the various NV center classes can be linked to the axes of the laboratory's frame of reference $\mathbf{n}_\alpha$,$\mathbf{n}_\beta$, $\mathbf{n}_\delta$,$\mathbf{n}_\gamma$

$$[111] \longrightarrow \mathbf{n}_\alpha = \frac{1}{\sqrt{3}}\begin{pmatrix}1\\1\\1\end{pmatrix}$$

$$[\bar{1}\bar{1}1] \longrightarrow \mathbf{n}_\beta = \frac{1}{\sqrt{3}}\begin{pmatrix}-1\\-1\\1\end{pmatrix}$$

$$[\bar{1}11] \longrightarrow \mathbf{n}_\gamma = \frac{1}{\sqrt{3}} \begin{pmatrix} 1 \\ -1 \\ 1 \end{pmatrix}$$

$$[1\bar{1}1] \longrightarrow \mathbf{n}_\delta = \frac{1}{\sqrt{3}} \begin{pmatrix} -1 \\ 1 \\ 1 \end{pmatrix}$$

This translates directly into a system of equations linking the Cartesian components of the field to those projected onto the crystal orientations:

$$\begin{aligned}
\sqrt{3} \times B_{\mathrm{Earth},\alpha} &= +B_{\mathrm{Earth,x}} + B_{\mathrm{Earth,y}} + B_{\mathrm{Earth,z}} \\
\sqrt{3} \times B_{\mathrm{Earth},\beta} &= -B_{\mathrm{Earth,x}} - B_{\mathrm{Earth,y}} + B_{\mathrm{Earth,z}} \\
\sqrt{3} \times B_{\mathrm{Earth},\gamma} &= +B_{\mathrm{Earth,x}} - B_{\mathrm{Earth,y}} + B_{\mathrm{Earth,z}} \\
\sqrt{3} \times B_{\mathrm{Earth},\delta} &= -B_{\mathrm{Earth,x}} + B_{\mathrm{Earth,y}} + B_{\mathrm{Earth,z}}
\end{aligned}$$

which gives :

$$\begin{aligned}
B_{\mathrm{Earth,x}} &= \frac{\sqrt{3}}{4}(B_{\mathrm{Earth},\alpha} - B_{\mathrm{Earth},\beta} + B_{\mathrm{Earth},\gamma} - B_{\mathrm{Earth},\delta}) \\
B_{\mathrm{Earth,y}} &= \frac{\sqrt{3}}{4}(B_{\mathrm{Earth},\alpha} - B_{\mathrm{Earth},\beta} - B_{\mathrm{Earth},\gamma} + B_{\mathrm{Earth},\delta}) \\
B_{\mathrm{Earth,z}} &= \frac{\sqrt{3}}{4}(B_{\mathrm{Earth},\alpha} + B_{\mathrm{Earth},\beta} + B_{\mathrm{Earth},\gamma} + B_{\mathrm{Earth},\delta})
\end{aligned}$$

P 4

Saturated absorption Sub-Doppler spectroscopy

Contents

At room temperature, the main cause of the broadening of atomic transitions in a gas is the Doppler effect. Saturated absorption spectroscopy, developed in the 1970s, makes it possible to overcome this broadening and resolve the hyperfine structure of atomic transitions. The aim of the practical work is to carry out saturated absorption spectroscopy of the D1 line of rubidium in order to observe its hyperfine structure. The source used is a laser diode tunable in wavelength around 795 nm.

1 Preliminary study

1.1 Doppler broadening

We consider an atomic gas of two-level atoms and denote ν_0 the frequency of the atomic transition. Doppler broadening, which is largely predominant at room temperature, results from the dispersion of the velocities of the atoms in the gas. The gas is illuminated by a laser beam of frequency ν propagating along the axis Oz in the positive direction. Among the atoms, only those whose V_z projection of the velocity along Oz satisfies the relation

$$\nu_0 = \nu\,(1 - V_z/c) \tag{4.1}$$

are in resonance with the wave and can absorb and re-emit light (c is the speed of light). Thus, if we sweep the laser frequency, **we obtain an absorption line profile that reflects the distribution of atomic velocities in the direction of the laser beam**.

P1 Quickly explain the demonstration of the formula (4.1).

Statistical physics shows that the velocity distribution of atoms in a perfect gas follows the Maxwell-Boltzmann law:

$$f(V_z) = \left(\frac{m}{2\pi \mathrm{k_B} T}\right)^{1/2} \exp\left(\frac{-mV_z^2}{2\mathrm{k_B}T}\right). \tag{4.2}$$

In this equation, V_z is the velocity along the z axis, T is the temperature of the gas, m is the mass of the atoms ($1.41\ 10^{-25}\,\mathrm{kg}$ for rubidium) and $\mathrm{k_B}$ is Boltzmann's constant ($1.38\ 10^{-23}\,\mathrm{J/K}$).

P2 Show that the width at half-height of the line broadened by the Doppler effect is :

$$\Delta\nu = \sqrt{8\ln 2}\sqrt{\frac{\mathrm{k_B}T}{m}}\frac{\nu_0}{c}\,. \tag{4.3}$$

P3 Use the formula 4.3 to calculate the Doppler broadening at $T = 20^\circ$ of the rubidium D1 line (centred at $795\,\mathrm{nm}$).

1.2 Structure of the rubidium D1 line

The rubidium cell you are going to use contains the two stable isotopes of the atomic species in the proportions of their natural abundance: 72% rubidium 85 and 28% rubidium 87. The wavelength of study ($795\,\mathrm{nm}$) corresponds to the transition from the fundamental level $5\mathrm{S}_{1/2}$ to the excited level $5\mathrm{P}_{1/2}$. The hyperfine structure is detailed in figure 4.1 for both isotopes.

P4 How many lines should we theoretically observe? Arrange these lines in ascending order of resonance frequency.

P5 Taking Doppler broadening into account, which lines can be resolved with a simple absorption spectrum? At what temperature would we need to go down to resolve the entire hyperfine structure? Knowing that the natural width of the excited levels is $6\,\mathrm{MHz}$, at what temperature would we have to go down to be able to measure it? How can this be achieved?

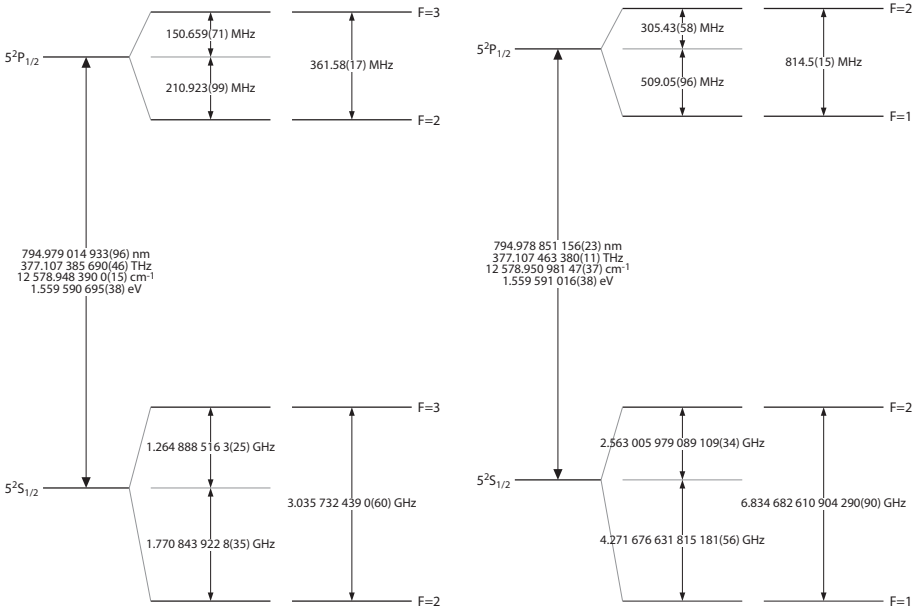

(a) Rubidium 85 **(b)** Rubidium 87

Figure 4.1: Hyperfine structure of the D1 line of the two rubidium isotopes. The figure is taken from: Daniel A. Steck, *Rubidium D Line Data*, available online at `http://steck.us/alkalidata`.

1.3 Saturation of absorption

Let's now return to a two-level gas of atoms. In general terms, the absorption $\mathcal{A}$ (in cm^{-1}) of a laser beam of frequency equal to the atomic transition frequency is given by the effective resonance scattering cross-section σ_0 (in cm^2) weighted by the difference between the densities of atoms in the fundamental level, n_1, and in the excited level, n_2 (in cm^{-3}). This difference in density depends on the intensity I (in $\mathrm{W.cm}^{-2}$) of the laser beam and therefore on the absorption $\mathcal{A}$. This process of circular dependence ($\mathcal{A}$ depends on $n_1 - n_2$, which depends on I, which depends on $\mathcal{A}$) gives rise to the phenomenon of absorption saturation. In concrete terms, we show that:

$$\mathcal{A} = \sigma_0 \times (n_1 - n_2) \quad \text{avec} \quad n_1 - n_2 = \frac{n_\mathrm{t}}{1 + I/I_\mathrm{sat}}\,, \tag{4.4}$$

where n_t is the total density of atoms and I_sat is an intensity characteristic of the transition, called the **saturation intensity**, which is $1.6\,\mathrm{mW/cm}^2$ for the atomic transition under consideration. The ratio $s = I/I_\mathrm{sat}$, which is used in

the equation 4.4, is called the **saturation parameter**.

P6 Make a qualitative comparison of the absorption in the limiting cases $s = I/I_{\text{sat}} \ll 1$ and $s = I/I_{\text{sat}} \gg 1$. What about absorption in the case of high intensity ($s \gg 1$). **This phenomenon is called absorption saturation**.

P7 Give the limit of the populations n_1 and n_2 in the case of strong saturation. Give an interpretation of absorption saturation by considering the evolution of the spontaneous emission rate as a function of intensity.

P8 Is it possible to invert the populations on a 2-level system? Explain why.

1.4 Application to sub-Doppler spectroscopy (pump-probe method)

Consider two laser beams of the same frequency ν and counter-propagating (superimposed but propagating in opposite directions). The first beam, called the pump beam, propagates in the positive direction of the Oz axis and has sufficient intensity to saturate the absorption on the transition in question. The second beam, called the probe beam, propagates in the negative direction of the Oz axis and has too low an intensity to saturate the transition on its own. We are interested here in the absorption of the probe beam in the presence of the pump beam when their frequency is varied around the frequency of the atomic transition.

According to equation 4.1, for a given frequency ν, the atoms which absorb the pump are those for which $V_z = -c\,(1 - \nu/\nu_0)$ and the atoms which absorb the probe are those for which $V_z = +c\,(1 - \nu/\nu_0)$. There are then two cases, represented in figure 4.2 :

- if $\nu \neq \nu_0$, the atoms which absorb the pump and those which absorb the probe belong to different velocity classes. In this case, the presence of the pump has no effect on the absorption of the probe;

- if $\nu = \nu_0$, the same atoms absorb the pump and the probe, i.e. atoms with zero velocity along z ($V_z = 0$). As the pump is sufficiently intense to saturate the absorption, the probe is absorbed very little (absportion is reduced) at this precise frequency $\nu = \nu_0$.

The absorption line profile of the probe therefore has a dual structure, with a narrow peak centred on the frequency of the atomic transition superimposed on the profile broadened by the Doppler effect. As you will see in the course of the labwork, the resolution offered by pump-probe spectroscopy is such that

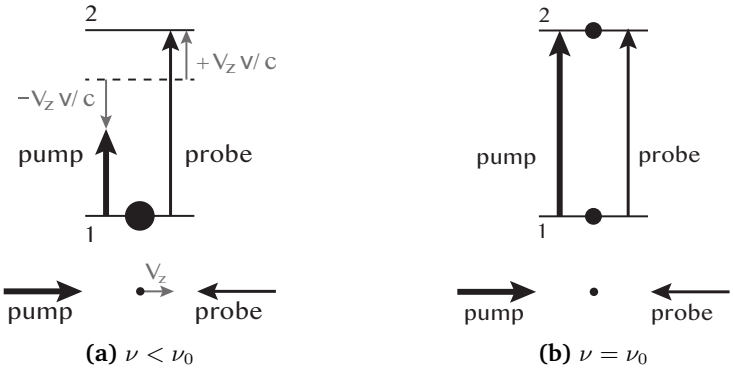

(a) $\nu < \nu_0$ **(b)** $\nu = \nu_0$

Figure 4.2: Influence of the Doppler effect in the pump-probe configuration.

it can reveal the hyperfine structure of the atomic transition. Each transition then appears as a distinct peak in the Doppler profile, as shown in Figure 4.3.

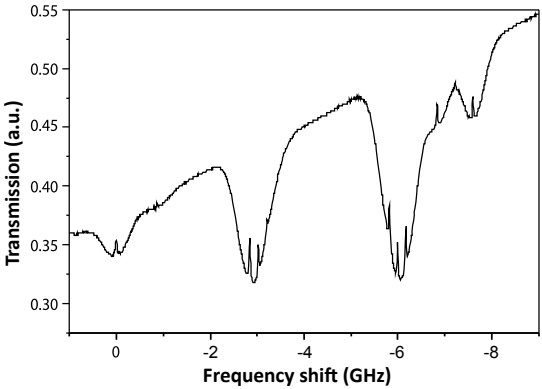

Figure 4.3: Absorption spectrum around $795\,\mathrm{nm}$ obtained by the pump-probe method. The lines of the hyperfine structure appear as narrow peaks against a background broadened by the Doppler effect. The figure is adapted from: Svenja A. Knappe *et al.*, *Microfabricated saturated absorption laser spectrometer*, Optics Express **15**, 6293–6299 (2007).

P9 What is the intrinsic width of the saturated absorption peak? What are the reasons why this peak might appear wider?

1.5 Laser Diode Characteristics

The tunable laser used here is a DBR795PN laser diode, typically employed to address the D1 line of rubidium. The letters DBR stand for "Distributed Bragg Reflector": a Bragg grating is used as a reflector at one end of the gain medium. The emission frequency of the diode depends on two parameters: the equilibrium temperature TeqTeq of the junction and the injection current ii of the diode. The emission frequency decreases with both the regulated temperature TeqTeq and the injection current ii (which slightly heats the medium), mainly due to the increase in the refractive index of the epitaxial layers with temperature. The laser "redshifts" as the current increases. In this lab session, we will vary the emission frequency using only the injection current. The full specifications of the laser diode are provided in Table 4.1.

Power	$40\,\mathrm{mW}$
Wavelength	$795\,\mathrm{nm}$
Current tuning of the wavelength	$+0,0014\,\mathrm{nm/mA}$
Temperature tuning of the wavelength	$+0,06\,\mathrm{nm/K}$
Spectral width	$0,25\,\mathrm{nm}$

Table 4.1: Caracteristics of the laser diode model DBR795PN used in this lab session. Complete specfications are available online on thorlabs.com

P10 Compare the spectral width of the laser with the intrinsic linewidth of the transition. Which one of the two will set the observed width after suppression of the Doppler broadening ?

2 Experimental realization

Precautions for using the laser diode Never disconnect the cables connecting the laser diode to its power supply. **The maximum power delivered by the diode is of the order of 30 to 50 mW, which is enough to cause irreversible eye damage in direct vision**. As the eye is not very sensitive to this wavelength, the beam can reach you without you noticing. So be careful not to put your eyes at bench level. Remove or hide any reflective objects that may be at beam level (watches, bracelets, rings, chains, bracelets, belt buckles, etc.). Check that all optical elements are firmly attached to the board when the diode is transmitting. Finally, use the laser safety glasses provided at the entrance to the room.

General precautions All the optical elements used are fragile, expensive and difficult to obtain (particularly the cell containing the rubidium). You will be making difficult adjustments, in the dark, and with a near-infrared viewfinder (which is not very convenient). So move the elements carefully, clamp the feet carefully after each modification and don't leave anything lying around the edge of the board.

2.1 Laser diode

The tunable laser used here is a "DBR" (Distributed Bragg Reflector) laser diode, which provides single-mode operation at a very fine instantaneous laser linewidth (around MHz, i.e. around 2 $10^{-6}\,\mathrm{nm}$!!). However, fluctuations in current and temperature will introduce fluctuations in this frequency and cause it to broaden. In practice, the actual frequency linewidth is therefore higher, of the order of a few tens of MHz.

The laser diode package includes an optical fiber to prevent perturbing backward light reflection into the cavity [1], and the light is directly injected into a single mode polarizing maintaining optical fiber.

The laser emission frequency is a function of two parameters: the equilibrium temperature T_{eq} of the junction and the intensity i of the diode injection current. The emission frequency decreseases both with T_{eq} andwith i (the wavelength increases with the current). In this labwork, we will vary the emission frequency using the current alone. The full characteristics of the laser diode used are detailed in the document at your disposal.

Temperature controller The junction equilibrium temperature is measured by a thermistor. The set temperature is fixed by a resistance value. Its value is preset so that the entire spectrum around line D1 can be observed by sweeping the current alone. **In principle, you will not need to change this setting**. If, however, you need to change the set temperature, to move away from a mode jump for example, be careful to do so only in very small steps. A sudden change would take you too far away from resonance and it would be difficult to find it again afterwards.

Current supply By default, set the current to around $120\,\mathrm{mA}$ so that you can view the beam using the infra-red card (or simply on a piece of paper).

[1] Laser diodes are very sensitive to reflections (even very weak ones) from the beam towards the cavity, which can introduce significant fluctuations in the emission length. It is therefore necessary to use an optical isolator. This blocks the reverse return of light by using a Faraday rotator placed between two polarisers. The Faraday rotator used rotates a 45° rectilinear polarisation in the same direction regardless of the direction in which the light travels, so that if the polarisers are oriented to allow light propagating in one direction to pass, they will necessarily block light propagating in the other direction.

Q1 If we want to observe all the transitions of the D1 line of rubidium for both isotopes, over what range should the current in the laser diode be varied? (To answer this, you will need to find the relevant information in the provided document...)

Q2 Compare the spectral linewidth of the laser with the natural linewidth of the atomic transition. Which of these two linewidths will determine the width of the absorption lines once the Doppler effect is eliminated?

2.2 Fluorescence and absorption spectra

⇝ Place the cell in the path of the laser beam and adjust the observation camera so that the inside of the cell is clearly visible.

⇝ In total darkness, slowly vary the value of the current. In this way, you should be able to observe the fluorescence of the rubidium in the D1 line using the camera: the path of the laser beam shines in the cell for a precise value of current!

⇝ Once you have obtained fluorescence, complete the set-up described in figure 4.4. To visualise the lines of the two isotopes contained in the cell, sweep the diode's emission frequency by modulating the driving current with a triangular signal.

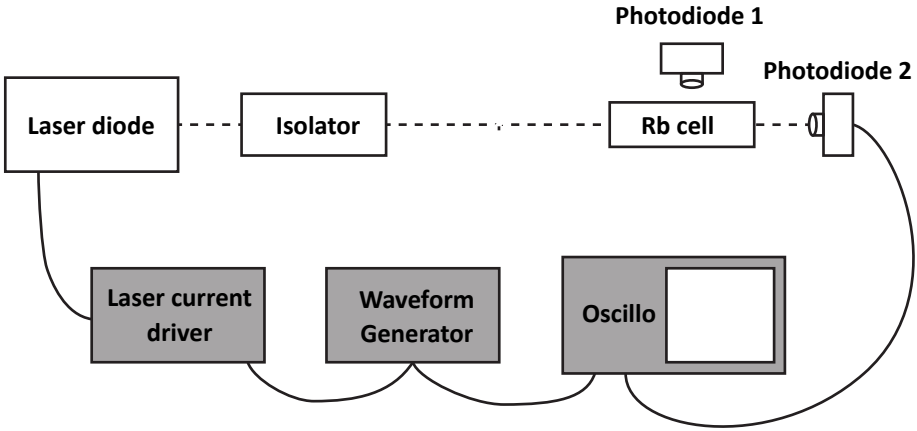

Figure 4.4: Schematic of the setup when measuring directly fluorescence and absorption.

$\rightsquigarrow$ Switch on the GBF and set it to produce a low-amplitude triangular signal at a frequency of around 10 Hz. Display the GBF signal on one of the oscilloscope channels.

$\rightsquigarrow$ Place one of the two photodiodes carefully against the cell (without contact), perpendicular to the laser beam, to capture part of the fluorescence signal. Monitor the photodiode signal on the other channel of the oscilloscope (set the adjustable gain to maximum) .

$\rightsquigarrow$ Modify the amplitude of the modulation applied to see the different fluorescence lines expected. Improve the signal obtained (by averaging if necessary.

$\rightsquigarrow$ Save the displayed signals with an USB stick (or take a photo of the screen, after you've turned on "stop").

Q3 Identify the different lines on the oscillogram and briefly explain how you did this.

Q4 Calibrate the oscillogram using the largest gap between two lines as a reference. Measure and check the spacing and relative positions of the different lines. Check that the width of the lines corresponds to that expected from the Doppler effect (or at least is of the right order of magnitude).

$\rightsquigarrow$ Place the second photodiode behind the cell and display the absorption spectrum on the oscilloscope channel previously occupied by the GBF (the GBF is moved to the synchro input). **Caution: adjust the gain to make sure you don't saturate the signal coming out of the photodiode, which happens very quickly!**.

$\rightsquigarrow$ Observe the fluorescence and absorption spectra simultaneously.

$\rightsquigarrow$ Observe the changes in the absorption spectrum when a density is added before the cell.

$\rightsquigarrow$ Now observe what happens if you place the density after the cell, and compare it with the previous situation (density before the cell).

$\rightsquigarrow$ Using the power meter provided, **measure the values of the saturation parameter** $s = I/I_{\mathbf{sat}}$ for the intensity incident on the cell (with or without density).

Q5 Explain why the phenomenon of absorption saturation is clearly demonstrated qualitatively.

2.3 Sub-Doppler spectroscopy of hyperfine levels

The pump-probe setup is shown in Figure 4.5. The pump and probe beams must be superimposed at the gas cell.

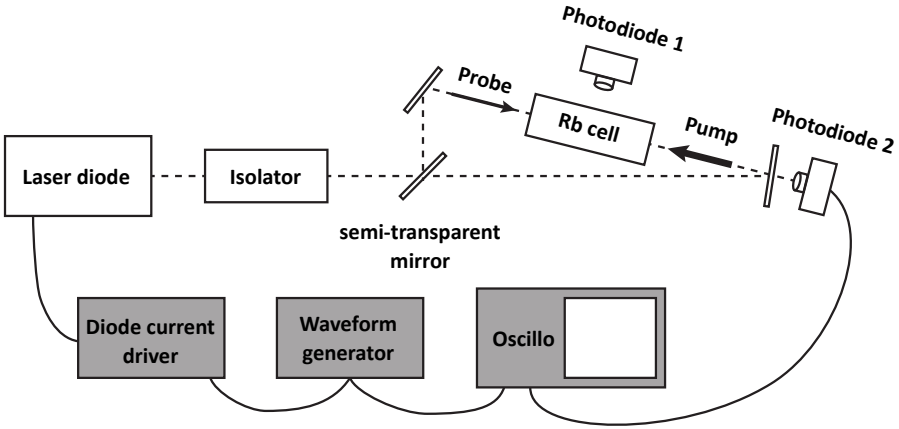

Figure 4.5: Setup in pump-probe configuration..

⇝ Do not touch the power supply or GBF settings!

⇝ First place and adjust all the components, excluding the cell and photodiodes. Carefully superimpose the pump and probe beams, observing the laser spots on on separating plates with the infrared viewer.

⇝ Using the power meter, measure the values of the saturation parameter $s = I/I_{\text{sat}}$ for the pump and probe in this configuration.

⇝ Then position the cell and the photodiodes to visualise absorption on the probe beam and the fluorescence.

⇝ Save the displayed signals with an USB stick (or take a photo of the screen, after you've turned on "stop").

Q6 For the two isotopes, identify the lines of the hyperfine structure (using figure 4.1). Measure the relative positions of the hyperfine lines and compare the values obtained with the expected values. Also measure the width of the observed lines.

Q7 What do they correspond to?

In Doppler profiles covering two atomic transitions (as for rubidium 85), instead of 2 absorption lines you should observe 3 lines. The third line appears precisely in the middle of the 2 expected lines. This phenomenon is called crossover.

Q8 Explain the origin of the crossover line. To do this, repeat the reasoning given in section 1.4 for the case of an atom with two excited states.

Q9 Compare the absorption and fluorescence spectra. Is it possible to see the same saturation signature in the fluorescence spectra? Explain why.

P 5

Spectroscopy of an atomic beam

This lab illustrates the first stage of laser atom cooling experiments, namely the production of a atomic beam from an oven, which will then be captured in a magneto-optical trap. You will carry out spectroscopy of the atomic beam using a laser, most specifically the absorption and fluorescence spectroscopy of a line of the hyperfine structure of rubidium 85 around $780\,\mathrm{nm}$.

Contents

P11 Fluorescence rate of a two-level atom.
In this tutorial, atoms will be modelled as two-level systems. The interaction between a laser beam and a two-level atom is described by the optical Bloch equations (OBE). The stationary solution of the OBEs for the fraction of atoms in the excited state is given by

$$\Pi_e = \frac{1}{2}\frac{s}{1+s}\ , \tag{5.1}$$

where the saturation parameter writes

$$s = \frac{I/I_s}{1+4\Delta^2/\Gamma^2}\ , \tag{5.2}$$

as a function of the laser detuning to the atomic transition

$$\Delta = (\omega - \omega_0) - \mathbf{k} \cdot \mathbf{v} \ . \tag{5.3}$$

The fraction of atoms in the ground state is simply deduced from that in the excited state:

$$\Pi_g = 1 - \Pi_e. \tag{5.4}$$

In the equations above, we have used the following notations:

- ω, I and $\mathbf{k}$ are respectively the pulsation of the laser beam, its intensity and its wave vector;
- ω_0, I_s and $1/\Gamma$ are respectively the Bohr pulsation of the atomic transition, its saturation intensity and the lifetime of the excited state.
- $\mathbf{v}$ is the velocity of the atom in the laboratory reference frame.

Finally, remember that the fluorescence rate of a two-level atom is equal to $\Pi_e\Gamma$.

Q10 Name the function representing the fluorescence spectrum of an atom, i.e. the change in fluorescence rate as a function of detuning. Determine its total width at half-maximum in the low-intensity limit. $I \ll I_s$.

Q11 Explain why the fluorescence and absorption spectra of the laser by an atom have an identical profile as a function of the laser detuning.

Q12 What effect causes the term $-\mathbf{k} \cdot \mathbf{v}$ in the expression of the detuning Δ (Equation 5.3) ?

Q13 In a gas at equilibrium at a temperature T, the fluorescence spectrum broadened by the Doppler effect has a total width at half-maximum equal to

$$\Delta\omega = \sqrt{8\ln 2}\,\sqrt{\frac{k_B T}{m}}\,\frac{\omega_0}{c}. \tag{5.5}$$

In this equation, $k_B = 1.38 \times 10^{-23}$J/K is Boltzmann's constant, $m = 1.41 \times 10^{-25}$ kg is the mass of a rubidium atom and c is the speed of light in vacuum. Calculate the Doppler shift expected in a cell at room temperature ($T \sim 20°$C) for the rubidium line centred at $780\,\mathrm{nm}$.

P12 Distribution of velocities in the atomic beam.
The atomic beam is obtained from a rubidium vapour produced by heating a metal sample in an oven to a temperature of $T \simeq 100\,^{\circ}\mathrm{C}$. This vapour escapes from the oven through a first circular orifice of diameter $D_1 = 5\,\mathrm{mm}$. A second orifice of diameter $D_2 = 1\,\mathrm{cm}$ placed at a distance $L \simeq 20\,\mathrm{cm}$ from the first one filters the distribution of transverse velocities, thus creating an atomic jet.

Q14 Assuming that the gas is at thermodynamic equilibrium in the oven, give the energy distribution of the atoms, then their velocity distribution, expressed as a function of the norm of the velocity vector $v = \|\mathbf{v}\|$.

Q15 Estimate numerically the average $\langle v \rangle = \sqrt{9\pi k_B T/8m}$ of the norm of the velocity vector at the exit of the oven.

Q16 Assuming that the velocity of an atom along the axis of the circular orifices is equal to $\langle v \rangle$, estimate the maximum transverse velocity that will allow this atom to reach the last chamber. To make the calculation easier, consider that $D1 = D2 = 1\,\mathrm{cm}$.

1 Absorption spectrum

In this section you will first measure the absorption spectrum of a laser beam of wavelength $780\,\mathrm{nm}$ through a spectroscopy cell at room temperature, then through the atomic beam produced by the oven. The optical set-up is shown in figure 5.1 below.

The natural abundance of the two isotopes of Rubidium is $\sim 72.2\%$ for the 85 isotope and $\sim 27.8\%$ for the 87 isotope..

IMPORTANT Make sure the laser diode is set to the following values: selected current (« set ») $I_{\text{set}} = 143{,}5\,\mathrm{mA}$ and set temperature $T_{\text{set}} = 19{,}550\,^{\circ}\mathrm{C}$.

Absorption spectrum through the cell at room temperature

$\rightsquigarrow$ Scan the laser diode current using the RIGOL function generator connected to the external modulation input of the laser diode controller and display on the oscilloscope 4 resonances such as those shown in figure 5.2. To do this, choose a symmetrical triangular sweep pattern, a modulation frequency of the order of $100\,\mathrm{Hz}$ and a peak-to-peak modulation amplitude of the order of $300\,\mathrm{mV}$ (and a zero offset voltage).

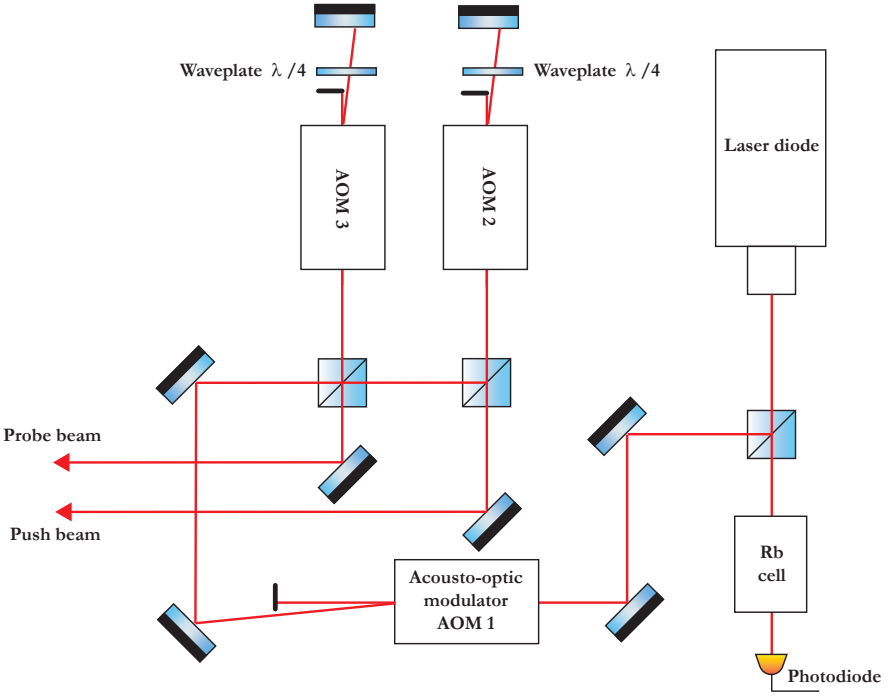

Figure 5.1: Description of the optical table. The light source is a laser diode emitting around $780\,\mathrm{nm}$. Part of the beam is used for spectroscopy in the glass cell. The other part of the beam is sent through a first single-pass AOM. The laser beam is then split into two beams, each injecting a double-pass AOM. The probe and push beams thus generated are sent to the vacuum chamber.

Each of these resonances actually comprises several unresolved atomic transitions: the difference in energy between the hyperfine sub-states of the excited state is smaller than the Doppler shift at ambient temperature.
An energy diagram of the hyperfine structure of rubidium isotopes 85 and 87 is given in the appendix.

Q17 The lines observed in Figure 3 are identified through the isotope (85 or 87) and the F hyperfine state of the ground state. Justify this identification by checking that the relative distance between the two lines of each isotope

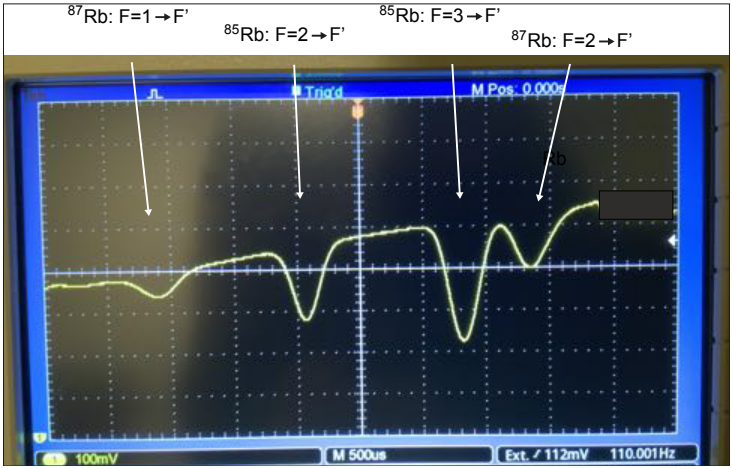

Figure 5.2: Absorption spectrum in the cell. This spectrum was obtained using the same set-up as the one you have, by measuring the laser intensity transmitted through the cell using an amplified photodiode and sweeping the frequency of the laser diode. It shows 4 lines linked to the hyperfine structure of the 85 and 87 isotopes of rubidium around $780\,\mathrm{nm}$ (see the energy diagrams in the appendix).

corresponds to what is expected from the energy diagrams.

Q18 Using the same data, determine the coefficient of proportionality between the current modulation voltage and the optical frequency of the laser.

Q19 Measure the total width at half-maximum of the two rubidium 85 resonances. Compare your result with the natural width expected for a transition, i.e. $\Gamma/2\pi = 6{,}1\,\mathrm{MHz}$, and with the width calculated in question Q4.
Comment your result.

Absorption spectrum through the atomic beam In this section, you will measure the absorption spectrum of a jet of rubidium atoms using the probe beam shown in figure 5.3.

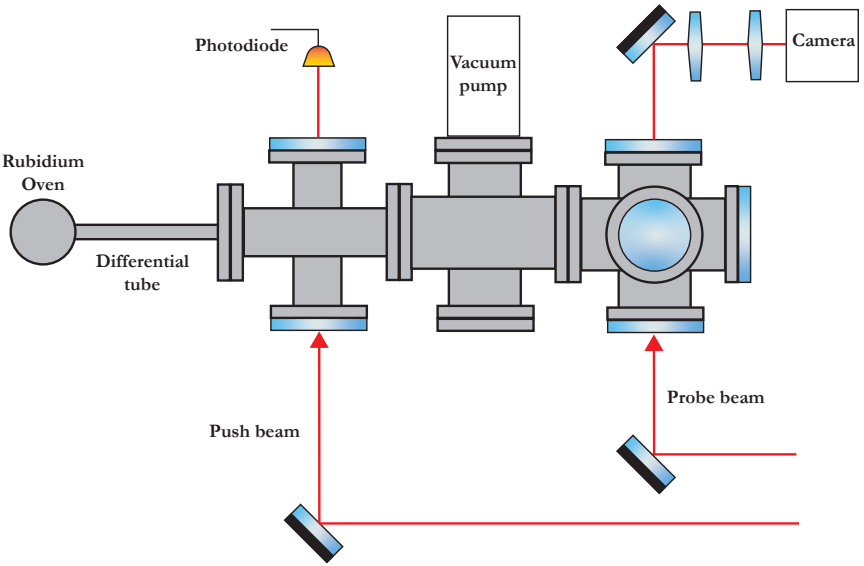

Figure 5.3: Description of the vacuum chamber. The jet of rubidium atoms is produced in an oven heated to around $100\,°\mathrm{C}$ and whose outlet is bounded by a narrow cylinder. The jet propagates from left to right in the diagram. The transverse velocity distribution of the jet is characterised in the rightmost chamber, either by absorption of the probe beam using a photodiode (not shown), or by fluorescence induced by the same probe beam using a camera. In the intermediate chamber, a push beam can deflect the atomic beam before it reaches the probe.

Initial settings. The AOM2 and AOM3 acousto-optic modulators are driven using the SIGLENT arbitrary function generator, which has two output channels. It will be ensured for both output channels that a sinusoid of frequency $200\,\mathrm{MHz}$ and amplitude $100\,\mathrm{mV}$ is sent to the two acousto-optic modulators.

$\rightsquigarrow$ Simultaneously observe the signals from the photodiodes in the cell and the jet using an oscilloscope.

Q20 What obvious difference(s) can you see between the two absorption signals?

⇝ Modify the amplitude of the laser diode current sweep so that only the most intense absorption line is observed in the cell. The absorption spectrum from the atomic beam should now look like that shown in figure. 5.4.

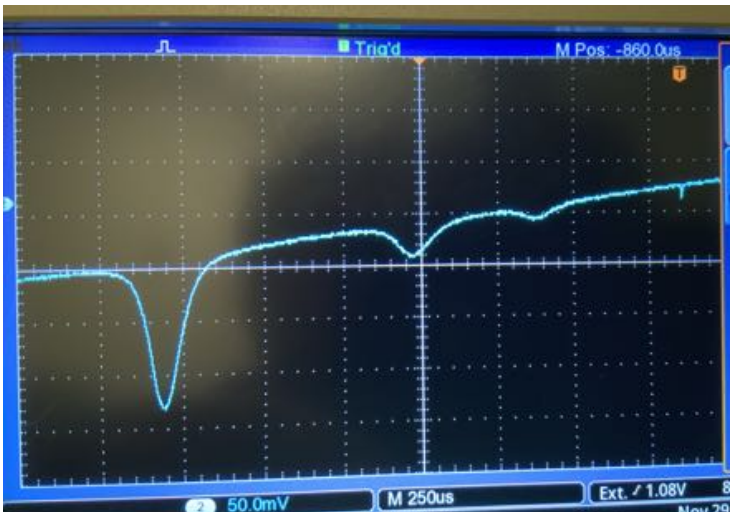

Figure 5.4: Absorption spectrum through the atomic jet. This spectrum was obtained using the same set-up as the one you have, by measuring the laser intensity transmitted through the vacuum chamber and the atomic jet, using an amplified photodiode and sweeping the frequency of the laser diode.

Q21 Using the energy diagrams given in the appendix, identify the atomic transitions visible in the absorption spectrum of the atomic beam.

Q22 Measure the total width at half-maximum of the most intense absorption line across the jet.
From the expression for Doppler broadening given in equation 5.5, estimate an "effective" temperature corresponding to your linewidth measurement. Why can't this be a 'true' temperature?

Q23 Discuss the value of the atom jet for spectroscopic measurements.

Q24 Give a rough estimate of the frequency resolution achieved by external modulation of the laser diode current.
In the next section, we will see that this resolution limit can be greatly reduced by using an acousto-optic modulator (AOM) to sweep the laser beam frequency.

2 Fluorescence spectrum

You are now going to observe the fluorescence spectrum of the atomic jet using a camera positioned perpendicular to the probe beam.

$\rightsquigarrow$ Using modulation of the laser diode current to vary the frequency of the laser beam (procedure identical to the previous section), observe the fluorescence resonance on the camera.

Q25 Determine the orientation of the probe beam and the atomic beam on the camera image.

$\rightsquigarrow$ Disable the laser diode current sweep and add a $50\,\Omega$ termination to the controller's external modulation input. Slowly modify (a few MHz at a time) the frequency of AOM No. 3 driven by the SIGLENT generator until the fluorescence resonance on the camera is restored.

$\rightsquigarrow$ Determine the frequency range that needs to be covered to visualise the entire fluorescence resonance, i.e. the minimum (respectively maximum) frequency below (respectively above) which the fluorescence signal is negligible.

Q26 What is the first observation you can make about the resolution of the frequency sweep performed using the AOM compared with that performed by modulating the laser diode current?

$\rightsquigarrow$ We want to measure the shape of the observed resonance precisely. To begin, acquire a fluorescence image using the camera control software. Elect an area of interest (ROI) covering the entire sensor in the direction of the laser beam but only the fluorescence signal in the direction of the jet. Extract the average number of grey levels $N_{\text{n.g.}}$ calculated by the histogram function.

$\rightsquigarrow$ We also want to ensure that we are working within a linear response regime, defined by a saturation parameter s less than the unit.
To determine this regime in the experiment, we begin by choosing the AOM frequency for which the fluorescence signal (i.e. the average number of grey

levels $N_{\text{n.g.}}$ in the ROI) is maximum. Keeping this frequency fixed, we vary the amplitude of the signal sent to the AOM by the SIGLENT generator: for each value of the amplitude chosen, we measure both $N_{\text{n.g.}}$ and the voltage V_{PD} on the photodiode of the probe beam.

Q27 Plot the curve $N_{\text{n.g.}}$ as a function of V_{PD} and identify the linear and saturated fluorescence regimes. Determine the maximum value of amplitude of the AOM drive signal below which the variation of $N_{\text{n.g.}}$ is linear with V_{PD}.

$\rightsquigarrow$ Measure the number of grey levels in the ROI as a function of the frequency of the AOM drive signal. Choose about ten frequency values spread over the range you determined in question Q16.

Q28 Plot the fluorescence spectrum obtained as a function of the AOM drive frequency. Determine its total width at half-height and compare it with that of the absorption spectrum by the atomic beam. Be careful to take into account the double passage through the AOM, which shifts the laser beam frequency by twice the AOM drive frequency!

$\rightsquigarrow$ When the drive frequency of the AOM is varied, the diffraction efficiency changes as we move away from the Bragg condition. This effect is likely to alter the measurement of the fluorescence spectrum and can be corrected. To do this, measure V_{PD} as a function of AOM frequency over the range used for the previous measurement in order to calibrate the variation in optical power of the probe beam. Correct the fluorescence spectrum measurement to compensate for the effect of the variation in probe beam power.

Q29 Plot the corrected spectrum and compare it with the raw spectrum. Does it seem necessary to take into account the modulation of the optical power of the probe beam?

$\rightsquigarrow$ Reproduce the measurement of the fluorescence spectrum for the maximum value of the optical power of the probe beam and plot the new spectrum obtained.

Q30 Compare the width of this spectrum with that of the spectrum obtained at low power and comment on the effect of saturation.

3 OPTIONAL SECTION - Mechanical action of light on atoms

If you have time, you can deal with this optional section.

In this final section, we study the mechanical effect of laser light on the atomic jet. This effect is similar to that exerted by sunlight on the tail of a comet: the radiation pressure exerted by the sunlight bends the tail of the comet.

The radiation pressure force exerted by the laser light on the atom at two levels is written,

$$\mathbf{F}_{\text{rad}} = \hbar\mathbf{k}\frac{\Gamma}{2}\frac{s}{1+s} \ . \tag{5.6}$$

$\rightsquigarrow$ Add the pusher beam to the empty chamber at the end of the oven. Set the power of the push beam to its maximum and vary its frequency until an effect on the fluorescence resonance is observed.

Q31 Interpret the modification of the spectrum by the mechanical action of the laser beam at the oven outlet.

Q32 Estimate the variation in impulse experienced by an atom passing through a laser beam.

Q33 Discuss the best beam size for measuring the velocity distribution of the atomic beam.

4 Annexe

Hyperfine structure of the D2 line of rubidium isotopes 85 and 87. The figures are taken from documents posted online by Daniel Steck at the following address `http://steck.us/alkalidata/`.

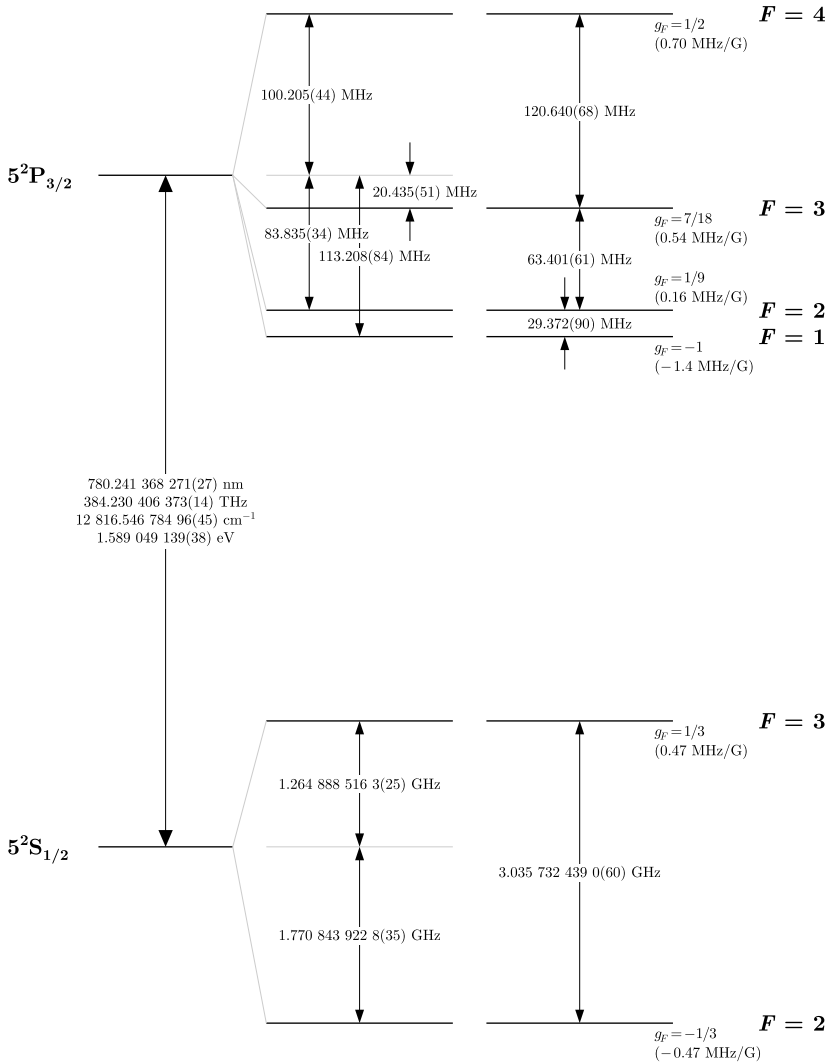

Figure 5.5: Hyperfine structure of the D2 transition of rubidium 85.

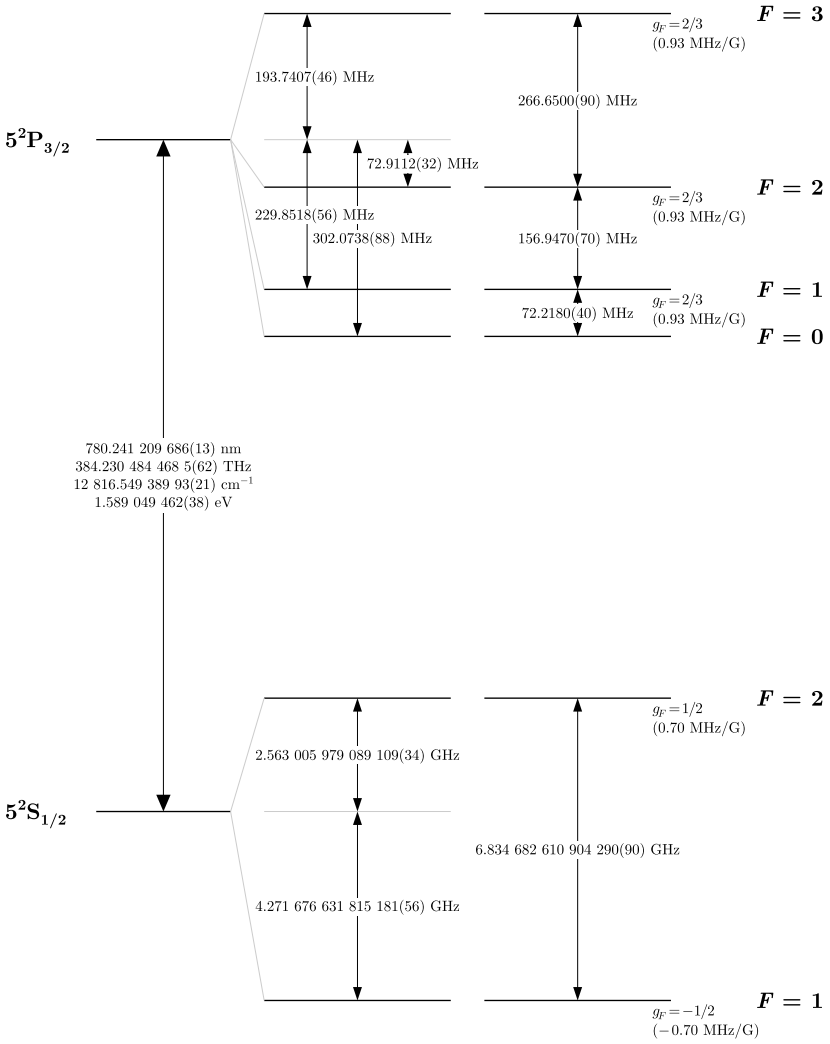

Figure 5.6: Hyperfine structure of the D2 transition of rubidium 87.

P 6

Single-Photon Interferences : Grangier-Roger-Aspect experiment

Contents

1 Introduction

The Grangier-Roger-Aspect (GRA) experiment provided a perfect illustration of wave-corpuscle duality, namely the ability of individual quantum systems, referred to as particles - in this case, a single photon - to form interference, i.e. an experimental signature typically associated with waves.

This experiment was carried out in 1985-1986. The notion of single-photon sources, and how to approach them experimentally, was a relatively emerging subject. In particular, the question was whether a sufficiently attenuated light source could constitute a single-photon source, in the quantum sense of the term (the answer is no: see the Appendix.).

The Grangier-Roger-Aspect (GRA) experiment was carried out at Orsay, in the former 503 building of Institut d'Optique, following on from the Bell inequality violation experiments. In particular, it exploited the same photon source, which was in fact a source of *pairs* of photons. The designers of the GRA experiment were the first to produce a *heralded photon source*. Each of

the two beams emanating from the twin-photon source does not initially have the character of a single-photon source. However, based on measurements of the first beam (containing "heralding" photons), the second beam can be conditioned to exhibit single-photon flux behavior.

The aim of this labwork session is therefore both to study the operating principle of such a source and to use it to reproduce the results of the GRA experiment.

1.1 The corpuscular character of the photon

What is a single photon?

Let's consider the $\mathcal{E}$ electromagnetic field occupying a certain volume V of space. Solving Maxwell's equations within this volume V, combined with boundary conditions, allows us to decompose this field $\mathcal{E}$ as a superposition of $\mathcal{E}_m$ modes.

In classical physics, the energy of each of these field modes can take on arbitrary values, related to the square modulus of their amplitude $|\mathcal{E}_{\Updownarrow}|^2$. In quantum physics, field modes cannot take on arbitrary energy values: the energy of electromagnetic field modes is quantized, according to the same rules as quantum harmonic oscillators. The energy E_m of the m mode of frequency ω writes :

$$E_m = \hbar\omega(n + \frac{1}{2})$$

where n is the number of mode excitations, also called *quanta*. It is convenient to use the concept of Fock states, or number states, to designate the quantum state of a field. A field containing exactly n photons is then denoted $|n\rangle$.

A photon is a single excitation, a quantum of a mode of an electromagnetic field .

In general, a pure quantum field state can be written as a superposition of Fock states:

$$|\Psi\rangle = \sum_i c_i|i\rangle$$

i.e. as a superposition of 0-photon states (vacuum), 1-photon states, 2-photon states, etc...

A single photon refers to the quantum state of a mode of the electromagnetic field in its first excited state: it is more formally written as $|1\rangle$ – and by extension, the word photon also refers to the $\hbar\omega$ amount of energy associated with this excitation.

An ideal single-photon source is therefore a light source producing a field whose state, when measured, is systematically found to be in the $|1\rangle$ state. The quantum state of the field produced by this source is therefore a pure state written :

$$|\Psi_{\mathrm{SPS}}\rangle = |1\rangle$$

where SPS stands for *Single Photon Source*).

Conversely, the other quantum states of light can be measured in multiphoton states $|n\rangle$ with $n \geq 2$: for a pure state, Fock's decomposition into states includes terms in $|2\rangle$, $|3\rangle$, and so on. **Most importantly, this property is true even for extremely attenuated sources**.

A brief discussion of other types of quantum states commonly used to describe different light sources, which are not single-photon sources, such as thermal sources and coherent sources, is given in the Appendix.

Principle of HBT interferometry

The experimental demonstration of the corpuscular nature of a single-photon source is based on a principle: **a single photon can only be detected at a single location**. A way to proceed is therefore by measuring coincidences between two detectors placed at two different locations.

The adequate setup is that of **a Hanbury-Brown and Twiss interferometer, usually abbreviated to HBT** (see Figure 6.1). It consists of a simple 50/50 splitter, whose two output ports lead to two avalanche photodiodes, denoted A and B, placed at equal distance from the splitter.

A coincidence measurement consists in measuring the probability that the two channels A and B detect a photon (almost) simultaneously. Two cases are of interest here:

- For an ideal single-photon source, the electromagnetic field of the mode contains only a single photon at each instant. The $|1\rangle$ photon can be transmitted or reflected by the splitter - but never split into two components on each of the A and B paths. When the detectors are well synchronized, it is therefore impossible to detect coincidences with an ideal single-photon source. This is known as **photon antibunching**.

- If the light source has multi-photon state components, such as $|2\rangle$, each photon can be reflected or transmitted as it passes the splitter. So, 50% of the time, one photon is detected on channel A and the other on channel B : **any light source other than a single-photon source gives rise, at least occasionally, to coincidences.**

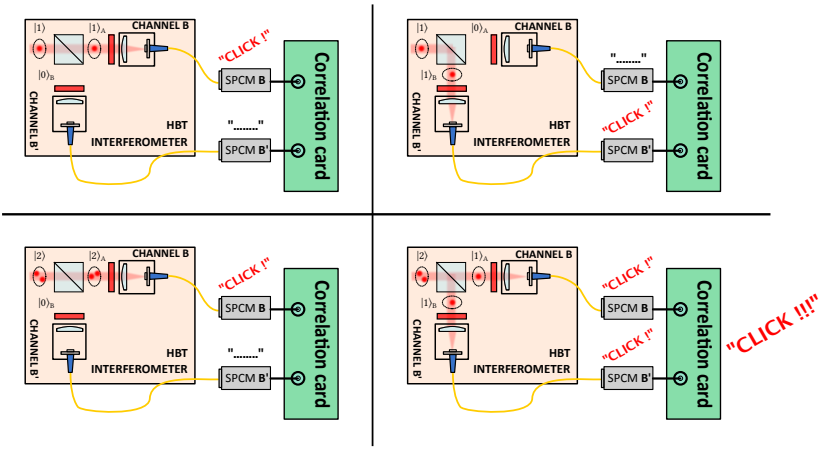

Figure 6.1: Principle of the experimental test of the statistical nature of a source by coincidence measurements. A single-photon source at the input to an HBT interferometer never generates coincidences, unlike other sources which contain multiphoton states

.

A more detailed discussion of the formalism of the quantum theory of photodetection applied to the case of coincidence detection is given in the Appendix.

Parameter $g^{(2)}(0)$

An HBT interferometer measures an objective parameter to characterize the statistical properties of the source: the intensity autocorrelation function $g^{(2)}(0)$. In the classical formalism, this function evaluates the intensity fluctuations of a light source.

$$g^{(2)}(\tau) = \frac{\langle \hat{n}(t)\hat{n}(t+\tau)\rangle}{\langle \hat{n}\rangle^2}$$

The interferometer's separator, assumed to be lossless and perfectly balanced, has two output channels enabling us to evaluate the $g^{(2)}$ function of the initial mode by simultaneous measurements on the two distinct output modes A and B. Using the number operators attached to the two channels, we write :

$$g^{(2)}(0) \equiv g^{(2)}_{BB'}(0) = \frac{\langle \hat{n}_B \hat{n}_{B'}\rangle}{\langle \hat{n}_B\rangle \hat{n}_{B'}\rangle}$$

At zero delay, the function $g^{(2)}$ is interpreted as the ratio of the probability of observing coincidences P_{AB}, to the individual probabilities of ob-

serving detection events, P_B and $P_{B'}$. These probabilities are directly proportional to the count rates. We denote with the letter R the count rates in $[\mathrm{counts.s}^{-1}]$ and with the letter N the number of counts during the integration time Δt in [blows], we have $N_B = R_B \Delta t$ and $N_{B'} = R_{B'} \Delta t$ and coincidences $N_{BB'} = R_{BB'} \Delta t$ between B and B'.

$$g^{(2)}_{AB}(0) = \frac{P_{BB'}}{P_B P_{B'}} = \frac{N_{BB'}}{N_B N_{B'}} = \frac{R_{BB'}}{R_B R_{B'} \Delta t}$$

Since the number of coincidences for a single-photon source is zero, the expected theoretical result is $g^{(2)}_{BB'}(0) = 0$ – and more generally, a value of $g^{(2)}_{BB'}(0)$ significantly smaller than 1 is proof of the quantum, anti-bunched nature of photons. Conversely, any combination of photon fluxes from thermal or coherent sources can only yield $g^{(2)}_{BB'}(0) \geq 1$.

1.2 Single-photon interference

The evolution of quantum states, even those associated with objects described as "corpuscular", is described by the Schrödinger equation, which is intrinsically a *wave* equation. It is therefore possible to observe interference phenomena - which is the hallmark of undulatory objects - even with a flux of single photons.

To observe interference, it's convenient to use...an interferometer. For the sake of simplicity, we discuss here the case of a single-photon source, providing $|1\rangle$ states sent to the input of a Mach-Zehnder interferometer (see Figure 6.2)[1].

The quantum state after the first splitter is simply written:

$$|\Psi^{\mathrm{in},1}_{\mathrm{SPS}}\rangle = |1\rangle \longrightarrow |\Psi^{\mathrm{out},1}_{\mathrm{SPS}}\rangle = \frac{|1_A\rangle|0_B\rangle + i|0_A\rangle|1_B\rangle}{\sqrt{2}}$$

where i appears as the phase factor between reflection and transmission coefficients, ensuring the unitarity of the transformation. It is possible to adjust the length of the interferometer arms, so as to introduce a step difference δ between the two arms, associated with a phase shift $\varphi = \frac{2\pi\delta}{\lambda}$. The input state of the separator closing the interferometer is written :

[1]The substance of the discussion is the same for Michelson, Fizeau or Young's slit interferometers!

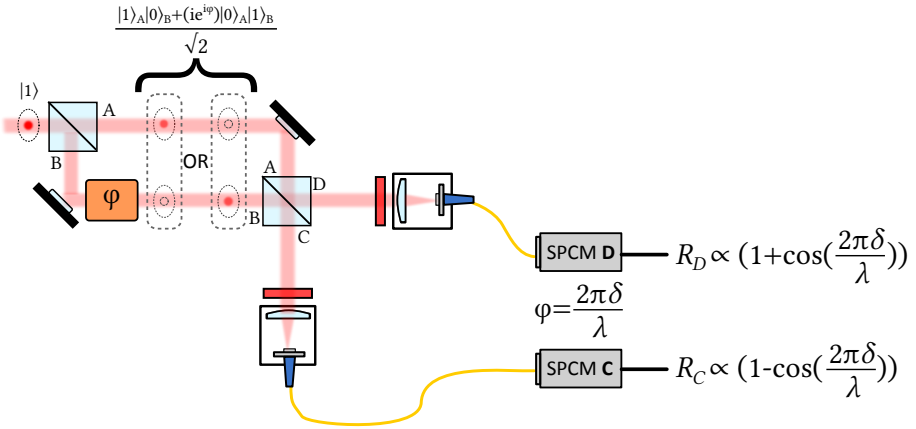

Figure 6.2: Mach Zehnder interferometer illuminated by a single photon state at the input of the first splitter. The quantum state of the field is written as a superposition of states once inside the interferometer. The two outputs of the Mach-Zehnder are connected to avalanche photodiodes: the average hit rates on each channel display the same dependence on the step difference as the intensity observed using a classical input light source: they are the same two-wave interference fringes

.

$$|\Psi_{\mathrm{SPS}}^{\mathrm{in},2}\rangle = \frac{|1_A\rangle|0_B\rangle + ie^{i\varphi}|0_A\rangle|1_B\rangle}{\sqrt{2}} \tag{6.1}$$

$$\longrightarrow |\Psi_{\mathrm{SPS}}^{\mathrm{out},2}\rangle = \frac{1}{\sqrt{2}}\left[\left(\frac{|1_C\rangle|0_D\rangle + i|0_C\rangle|1_D\rangle}{\sqrt{2}}\right) + ie^{i\varphi}\left(\frac{i|1_C\rangle|0_D\rangle + |0_C\rangle|1_D\rangle}{\sqrt{2}}\right)\right] \tag{6.2}$$

$$= \left(\frac{1-e^{i\varphi}}{2}\right)|1_C\rangle|0_D\rangle + \left(\frac{1+e^{i\varphi}}{2}\right)|0_C\rangle|1_D\rangle \tag{6.3}$$

As in classical physics, the field at the output of an interferometer is written as a recombination of different amplitudes that have passed through the two arms of the interferometer. The number of counts measured by a detector per unit of time is then directly proportional to the probability of detection on the same channel. On channel C, for example :

$$R_D \propto P_D = |\langle 0_C|\langle 1_D|\Psi_{\mathrm{SPS}}^{\mathrm{out},2}\rangle|^2 = \frac{1}{2}(1+\cos\frac{2\pi\delta}{\lambda})$$

The count rate is written as the result of two-wave interference, and therefore evolves sinusoidally with the optical path difference between the two arms. A single photon is therefore...a wave!

1.3 Heralded photon source

The set-up used is based on a spontaneous parametric conversion process in a BBO crystal. Illuminated by a pump beam from a laser diode at 405 nm, the crystal generates two beams containing twin photon pairs at 810 nm, a signal beam (s) and an idler beam (i).

The pump is in a coherent state, comprising different number states. By converting pump photons, the crystal can generate photon pairs, but it can also generate double pairs, triple pairs, etc. from several pump photons. Formally, the quantum state in each beam is a correlated mixture of number states between the two arms. For the sake of simplicity, we write it here as a linear combination of several Fock states[2]:

$$|\Psi_{SPDC}\rangle = \sum_{i=0}^{+\infty} c_n|n\rangle_s|n\rangle_i = c_0|0\rangle_s|0\rangle_i + c_1|1\rangle_s|1\rangle_i + c_2|2\rangle_s|2\rangle_i + ...$$

On each of the s or i channels considered independently, we do *not* have a single-photon flux, but a superposition with multi-photon components: the expected value of $g_{AB}^{(2)}(0)$ is greater than 1.

[2]Refer to the Appendix for an advanced discussion of the quantum state generated by the crystal

The correlation properties between the two beams in state $|\Psi_{SPDC}\rangle$ are very interesting: if, when taking a measurement on channel i, we find the field in a $|1\rangle_i$ state, then, by projection and necessarily, the corresponding field on channel s at the exact instant of this measurement must be in the $|1\rangle_s$ state..:

$$\langle 1|_i \Psi_{SPDC}\rangle = |1\rangle_s$$

We speak of **conditioning the measurement.**

Experimentally, conditioning is carried out by recording coincidence events. The detection of a photon on the i channel generates a short coincidence time window in an electronic circuit. This is known as a **heralding photon**: the window represents the brief interval of time during which the quantum state of the s-channel field is perfectly known, and is precisely a single photon $|1\rangle_s$. This photon is the heralded photon.

Measurements are then carried out on the s channel - in this case, in this labwork session, by sending it through a Michelson interferometer and then an HBT interferometer. After having equalized the optical and electronic delays between the heralding channel i and the signal channel s, we select only those events that give rise to coincidences between the two channels. These events correspond to measurement results for the s channel performed only on a $|1\rangle_s$ state. It is as if we had used a single photon source in our set-up: we call it a "heralded photon source".

2 Experiments

2.1 Presentation of the setup

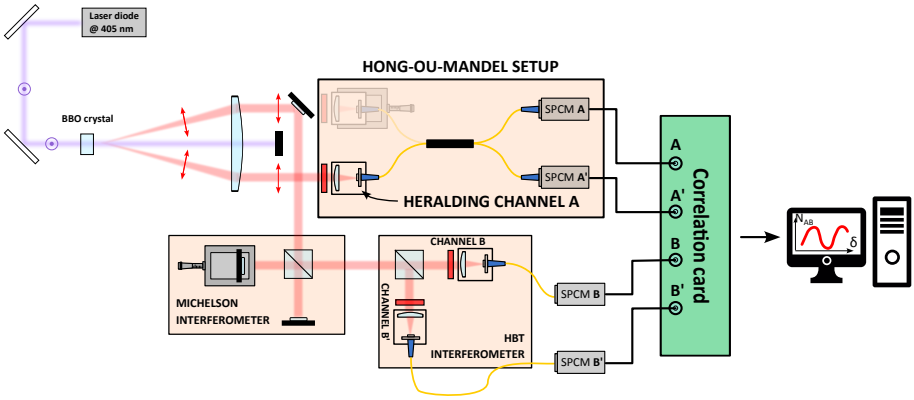

Figure 6.3: Optical assembly diagram.

The experimental set-up is an extension of the setup dedicated to the study of the HOM effect.

A laser diode at 405 nm pumps a BBO crystal, generating two beams along the edges of a cone whose apex angle is close to 3 degrees. One beam is sent to a fibered collimator, whose output is connected to an avalanche photodiode. This is the heralding channel, denoted A.

Photons from the second, "heralded" channel are reflected by a mirror to a Michelson interferometer, with one mirror mounted on a piezoelectric translation stage.

The Michelson's output channel is connected to an HBT interferometer, whose output channels B and B' feature fibered collimators connected to avalanche photodiodes.

Channels A, B, and B' are connected to an ALTERA DE2 FPGA board, which records the detection rates per time unit on each channel, and calculates the different coincidence rates of interest:

.

The FPGA board can process signals from up to 4 different detectors: we're using three here. The board sends back to the computer an array of up to 8 32-bit numbers, representing the data from 8 different counters. The first 4 elements of the array are the single counts from up to 4 detectors (counter 0 - counter 3), in this order: A, B, A'(not used), B'. The last 4 elements are the

	SW0	SW1	SW2	SW3
AB	1	1	0	0
	SW4	SW5	SW6	SW7
ABB'	1	1	0	1
	SW8	SW9	SW10	SW11
AB'	1	0	0	1
	SW12	SW13	SW14	SW15
BB'	0	1	0	1

Table 6.1: Tableau résumant les positions attendues des interrupteurs pour le VI coincidence$_r s232.vi$.

coincidence counts (Counter 4 - Counter 7). Coincidences are determined by the settings of switches SW0 - SW15 on the DE2 board. Each counter uses four switches to determine which coincidence it counts - counter 4 uses switches SW0 - SW3, counter 5 uses switches SW4 - SW7, etc. When a switch is activated, the corresponding LED lights up. With this arrangement, any of these 4 counters can determine any arbitrary coincidence between 2, 3 or 4 detectors. In our case, different coincidences are counted: to correctly retrieve the information, make sure switches SW0 and SW1 are on, while SW2 and SW3 must be off - switches SW4 to SW15 are only important in the case of a 4-detector configuration (see Table 6.1).

- The rates R_A, R_B, $R_{B'}$ are the raw, unconditioned count rates recorded on the different detection channels.

- The rates R_{AB} and $R_{AB'}$ are the detection rates conditioned by the heralding channel - in practice, these are the coincidences between A and B, or A and B', recorded at the Michelson output, with the heralding process by A allowing selection of the "single photon" states. R_{AB} and $R_{AB'}$ therefore correspond to the interference signal in equation (1.2).

- The rate $R_{BB'}$ is the unconditioned coincidence rate between the two channels of the HBT interferometer. It can therefore be used to determine the value of $g^{(2)}(0)$ for one of the two beams from the SPDC process, which is not a single-photon source.

- The rate $R_{ABB'}$ is a 3-detector coincidence rate, and is interpreted as the HBT interferometer coincidence rate, between B and B', conditioned by the heralding channel A . It allows us to trace back to the value of $g^{(2)}(0)$, when the beam state is placed in the single-photon state. It is this very rate that demonstrates the source's antibunching properties.

In a three-detector configuration, the experimental definition of $g^{(2)}$ must be modified. Since the relevant detection events can only occur when an electronic gate is opened by the heralding channel, the count and coincidence probabilities are equal to the number of events divided by the total number of generated gates, i.e. normalized by the number of detections on the heralding channel.

$$P_B = \frac{N_{AB}}{N_A} \qquad P_{B'} = \frac{N_{AB'}}{N_A} \qquad P_{BB'} = \frac{N_{ABB'}}{N_A}$$

so that we obtain :

$$g^{(2)}_{\mathrm{ABB'}}(0) = \frac{N_{ABB'}N_A}{N_{AB}N_{AB'}}$$

For an ideal photon source, $N_{AB} \neq 0$ because a SPDC beam is not a stream of single photons, but we have $N_{ABB'} = 0$, and therefore $g^{(2)}_{3\,\mathrm{det.}}(0) = 0$.

2.2 Settings

Alignment of the Michelson interferometer

This session is an extension of the TP HOM session. The alignment procedure described below assumes that this part of the set-up is correctly adjusted and allows observation of the HOM "dip", the signature of two-photon interference between the two SPDC beams.

$\rightsquigarrow$ Switch on the piezoelectric stage, then run Thorlabs' Kinesis software to control its position.

$\rightsquigarrow$ **WITH UTMOST CARE, AND WITHOUT TOUCHING ITS SURFACE**, flip the mirror mounted on...its *flip mount* to reflect the photons present in the left part of the emission cone.

Before you start acquiring measurements, it is crucial to check that the Michelson interferometer is correctly aligned and that the photons leaving the BBO crystal are sent to their respective detectors. The precision of the adjustment must be extremely fine to be certain that the photon sent to the Michelson is indeed the twin of the photon sent to the heralding channel A.

The first step is to check the Michelson's alignment, by making sure that interference fringes are indeed observed on the Michelson's output channel. To do this, we use a fiber checker, connected to the output of an optical fiber linked to the collimator. This fiber checker contains a laser diode emitting at around $750\,nm$, and enables a beam to be sent back from the collimators, passing through the Michelson interferometer and the rest of the setup in the

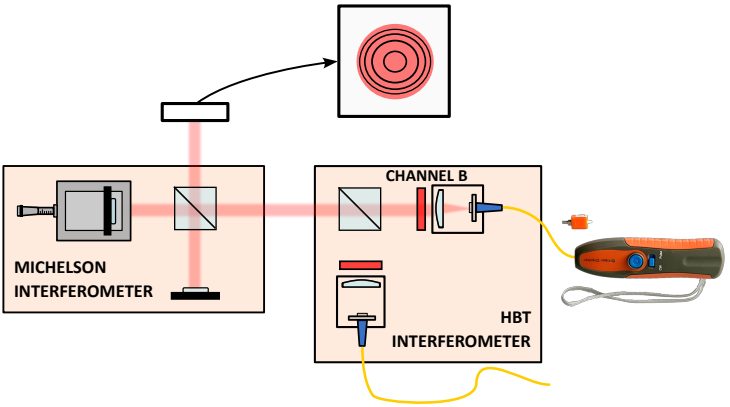

Figure 6.4: Use the fiber checker to align the Michelson in the opposite direction

.

opposite direction. This beam is intense and visible, so it will be possible to observe fringes at the output of the interferometer if the setting is close to optical contact).

CAUTION ! Fibers need to be handled with the utmost care, and as infrequently as possible. For this reason, NEVER disconnect the fiber outputs connected to the collimators, as this operation is never necessary.

⇝ **Check that the power supply to the photodiodes is switched off**. Then, on the photodiode housing, disconnect the fiber corresponding to the B detection channel.

⇝Connect the checker to channel B. Don't forget to replace the plug on the corresponding photodiode input so as not to leave it exposed.

⇝ Place a converging lens at the Michelson's input: it forms a cone of incidence angle at the interferometer's input. Then place a screen at the output of the interferometer. If the set-up is not too out of alignment, you should obtain interference rings. If necessary, adjust the M1 mirror (the fixed one, not mounted on the wedge) to superimpose the beams as best you can, then obtain rings by achieving parallelism between the mirrors.

⇝ From a uniform air gap configuration, scroll through the rings using the piezoelectric translation stage to get as close to the optical contact as experimentally possible, trying to achieve a uniform, flat interference pattern.

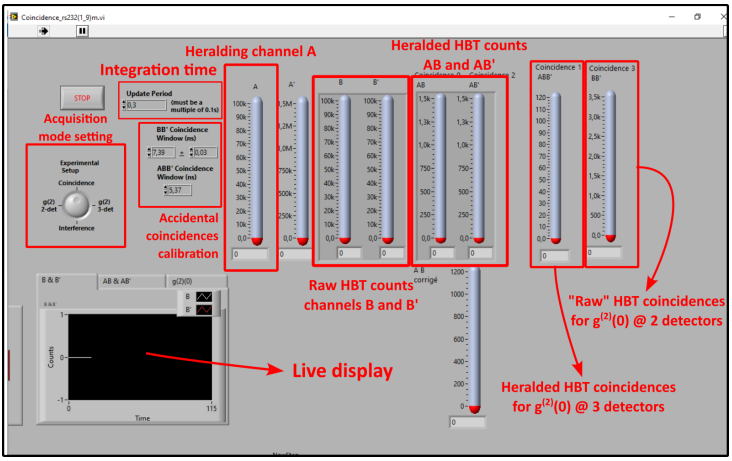

Figure 6.5: Fenêtre du VI Labview de mesure des coïncidences.

⇝Once this has been done, check that connecting the checker to channel B' produces the same interference pattern. If necessary, gently adjust the of the collimator to obtain fringes similar to the previous situation.

Fine collimator alignment

Now that the Michelson is properly aligned, we need to check that the two collimators at the output of the HBT assembly are both able to intercept the same photons from the BBO crystal.

P1 Explain why we need to maximize the number of coincidences detected and not necessarily the number of single hits received on the detectors.

⇝ Remove the checker, and reconnect all the fibers to the detectors.

⇝ Switch on the pump diode temperature control box and start the servo drive.

⇝ **CAUTION : Always switch on the coincidence circuit power supply BEFORE switching on the avalanche photodiodes, and switch off the photodiodes before switching on the stabilized power supply!**

turn on the coincidence circuit power supply of the ALTERA DE2 board.

On the computer, launch the Labview VI “Coincidences .vi.” and start acquisition.

⇝With the room lights off, switch on the power supply to the photodiode box and observe the appearance of a signal on the interface.

⇝With the room lights off, what do the counts generated by the photodiodes correspond to?

⇝Turn on the laser diode current control box. Starting with zero current, gradually increase the current while monitoring the number of strokes detected by the detectors: this should be in the order of a few thousand to a few tens of thousands.

CAUTION : avalanche photodiodes are EXTREMELY FRAGILE! Always ensure that the rate of detected counts is well below one million counts per second!

⇝ On the Labview interface, use the knob selector to choose the "**g(2) 3 det.**" mode. Read off the number of counts on the different channels, as well as the number of coincidences AB and AB'.

⇝ Place a screen to cut off one of the Michelson's two channels. Adjust the alignment of a first collimator, trying to maximize the number of coincidences. The settings are very sensitive, so be careful not to lose all your coincidences!

⇝ Optimize the setting of the second collimator, then block the other Michelson channel. Wherever possible, adjust the collimators and slightly rewind the Michelson mirrors to maximize and balance the number of coincidences received by the two collimators from the fluxes of the two Michelson channels.

If no coincidences or counts are visible on the photodiodes, it it best to first find a suitable approximate position for the collimators without trying to find even a weak signal and losing the alignment.The checker can then be used in reverse propagation, from the HBT detection channels B and B', and from heralding channel A. We then use the degrees of freedom of the collimators to observe that the beams from B and B' are well focused in the BBO crystal, at the same location as heralding channel A. This roughly ensures that the collimator collects a few photons from the crystal, providing a starting point for optimizing the setting.

2.3 Measurements

Recall that the source's intensity auto-correlation coefficient is written :

$$g^{(2)}_{\mathrm{GRA}}(0) = \frac{N_{ABB'} N_A}{N_{AB} N_{AB'}}$$

If it is zero, for an ideal single-photon source, the expected *experimental* value can be modeled and is different from 0: to do this, we need to take into account

that, under realistic conditions (coincidence window of non-zero size, detector efficiency, etc.), several events are actually recorded as triple $N_{ABB'}$ or double N_{AB} and $N_{AB'}$ coincidences :

- **Accidental double coincidence** As in the HOM experiment, double coincidences arising from the detection of two independent photons on two detectors during the coincidence window must be taken into account. The number $N_{acc}^{(1+1)}$ is written :

$$N_{\text{acc}}^{(1+1)} = (N_A N_B + N_A N_{B'}) \frac{\Delta t}{T_{\text{int}}^2}$$

  So the total number of coincidences measured experimentally is $N_{AB} = N_{AB,\text{source}}^{(2)} + N_{AB,\text{acc}}^{(1+1)}$. By definition, a source of pairs is highly correlated and naturally produces large numbers of coincidences. When the "xperiment is correctly set up, the number of accidental coincidences can be neglected before the number of desired coincidences, those of the source pairs: $N_{AB} \approx N_{AB,\text{source}}^{(2)}$.

- **Purely accidental triple coincidence :** Three photons from different, and therefore independent, pairs reach the detectors on channels A, B and B' during the same coincidence window Δt. The number $N_{acc}^{(3)}$ of this accidental triple coincidence counted over the time T_{int} wrties :

$$N_{acc}^{(3)} = \frac{N_A N_B N_B'}{T_{\text{int}}^3} \Delta t^2$$

  Where T_{int} is the integration time.

- **Normal double coincidence with an accidental third count:** In this case, two photons from a pair generate a coincidence on paths A and B or paths A and B' and a count is recorded on the third detector during the coincidence window. The number $N_{acc}^{(2+1)}$ of accidental triple coincidences events recorded during the time T_{int} is written :

$$N_{\text{acc}}^{(2+1)} = (N_{AB} N_{B'} + N_{AB'} N_B) \frac{\Delta t}{T_{\text{int}}^2}$$

The coincidence window is chosen to be very small compared to the measurement time, on the order of a few nanoseconds. Moreover, for a source of photon pairs, we have $N_{AB} \gg N_A N_B$, which means that accidental triple coincidences of the $(2+1)$ type predominate. Finally, the number of triple coincidences actually measured as such experimentally is therefore written :

$$N_{ABB'} = N_{\text{source}}^{(3)} + N_{\text{acc}}^{(3)} + N_{\text{acc}}^{(2+1)} \approx N_{\text{source}}^{(3)} + N_{\text{acc}}^{(2+1)}$$

with in the case of an ideal photon source $N^{(3)}_{\text{source}} = 0$. This gives a minimum experimental bound to the measurement of the value of $g^{(2)}(0)$:

$$g^{(2)}_{GRA}(0) \geq \frac{N^{(2+1)}_{acc} N_A T_{int}}{N_{AB} N_{AB'}}$$

Q1 Justify that $g^{(2)}_{GRA}(0) \propto N^{inc}_{ph} \Delta t$ with N^{inc}_{ph} the number of photon pairs generated by the SPDC source).

Q2 Based on the previous question, how can $g^{(2)}_{GRA}(0)$ be minimized? What practical problem(s) might we then encounter?

Q3 What is the statistical distribution of pair emission events from the non-linear crystal? Deduce the standard deviation $sigma(N_i)$ of the uncertainties in counting an average number of events (counts or coincidences) N_i over the time interval T_{int}.

Q4 What average number of events do you need to detect over a time T_{int} to estimate the rates of counts or coincidences with a relative uncertainty of 1%? With an uncertainty of 10% ? In each case, what is the signal-to-noise ratio (SNR) associated with the measurement?

Q5 Assuming all detectors and splitters to be perfect, plot the evolution of the value of $g^{(2)}(0)$ as a function of the number of pairs detected, for measurement times of $T_{\text{int}} = 1s$, taking a coincidence window $\Delta t = 10\,\text{ns}$. What is the minimum value of $g^{(2)}(0)$ that can be reached for a rate of 10^5 pairs per second?

2-detector $g(2)(0)$

Experimentation and analysis of results requires accurate estimation of uncertainties.

$\rightsquigarrow$ Once the alignment has been optimized, use the knob selector to switch to $g(2)(0)\,2\,\text{det.}$ mode, measuring the unconditioned correlations between the two outputs of the HBT interferometer.

$\rightsquigarrow$ Select an integration time window $T_{\text{int}} = 10\,s$. Report the corresponding values for N_B, $N_{B'}$ and $N_{BB'}$.

Q6 Calculate the corresponding count and coincidence rates, in number of events per second, and carefully estimate the associated uncertainties.

Q7 What is the proportion of accidental coincidences between detectors A and B? If necessary, propose a corrected value for the coincidence flux and its uncertainty.

Q8 Use your previous measurements or the calculation directly returned by the interface to measure a two-detector $g^{(2)}(0)$ at the Michelson output (now between channels A and B). Carefully estimate the uncertainties in your result.

Q9 Is the probed SPDC beam a single-photon source?

Measurement of a 3-detector $g(2)(0)$

$\rightsquigarrow$ Turn off photodiodes.

$\rightsquigarrow$ Carefully swap the coaxial cables of channels A and B located behind the photodiodes.

$\rightsquigarrow$ Select an integration time $T_{\text{int}} = 10\,s$.

Q10 Find the corresponding values for N_A, N_B, $N_{B'}$, N_{AB}, $N_{AB'}$ and $N_{ABB'}$.

Q11 Find the values of $g^{(2)}(0)$ at 3 detectors directly calculated via the interface after each integration cycle.

An intrinsic difficulty of the 3-detector set-up is that it relies on the measurement of coincidences between all three channels in the set-up, which, single-photon source or not, is a rare and infrequent event, unless you have sources delivering very high fluxes, which would then threaten to damage the photodiodes.

In other words, for integration times limited to a few seconds, it is almost certain to obtain a number of coincidences $N_{ABB'} = 0$. If the calculation then necessarily yields $g(2)(0) = 0$, only a reliable estimate of the uncertainties can tell whether the measurement is conclusive or not. This final estimate is then entirely dependent on the uncertainties in the measurements of counts and double coincidence rates on the different detectors.

Q12 From the measurements of the number of counts and coincidences recorded over the time T_{int}, calculate once again the corresponding counts and coincidence rates and their uncertainties.

Q13 Considering the uncertainties on the counting of the different events independent of each other, give an expression for the relative error $\Delta g^{(2)}_{\mathrm{GRA}}(0)$ of your measurement of $g^{(2)}_{\mathrm{GRA}}(0)$. Which terms dominate the relative error?

Q14 Assuming that triple coincidences are limited by accidental coincidences $(2+1)$, estimate the number of triple coincidences you need to detect to obtain a relative error of 10 pc on the measurement of $g^{(2)}_{\mathrm{GRA}}(0)$.

$$N_{AB}(\Delta x) = \frac{N_0}{2}(1 + C\cos(\frac{4\pi\Delta x}{\lambda}))$$

where Δx represents the displacement of the mirror mounted on the piezoelectric stage relative to the optical contact.

$\rightsquigarrow$ Check that the number of coincidences between G and A or B is non-zero, typically of the order of at least a few dozen coincidences per second.

$\rightsquigarrow$ If necessary, improve the set-up: start by blocking one of the Michelson arms, and optimize the coincidences measured on each detector pair by adjusting the position of the corresponding Michelson mirror. Then do the same by blocking the other channel. The number of coincidences provided by each of the two arms should be equivalent.

Q15 We'll try to obtain the interference period, to check that it corresponds to the wavelength of the photons converted by SPDC. Applying the Shannon-Nyquist theorem, what is the maximum carriage distance between two consecutive points that must be respected in order to correctly determine the wavelength? Check that the minimum shifting distance of the wedge allows this criterion to be met.

$\rightsquigarrow$Open the Kinesis software for controlling the piezoelectric stage. Use the **"Closed loop"** mode to position the stage.

$\rightsquigarrow$ Use the software's **"step-by-step"** translation mode to move the stage by its minimum displacement increment.

Q16 For a well-chosen counting time T_{int}, plot the evolution of the number of coincidences N_{AB} as a function of the displacement of the piezoelectric wedge. Add error bars to represent your uncertainties about the coincidence count, explaining how you evaluate the uncertainties. Also take into account the uncertainty in the position of the shim at each translation step.

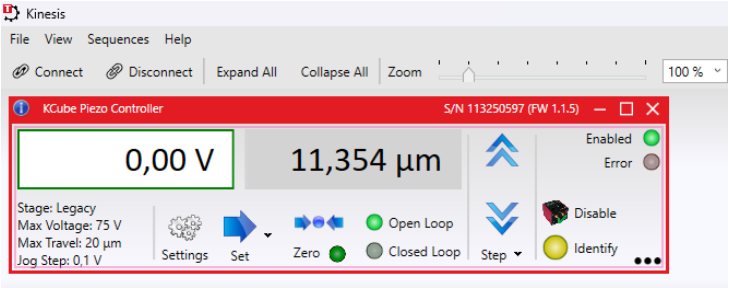

Figure 6.6: Fenêtre de contrôle du logiciel Kinesis.

Q17 Using a weighted least-squares method, fit a sinusoidal model to your experimental data. What is the period of this sinusoid? Can you find the wavelength of the photon injected into the Michelson interferometer? Evaluate the contrast of these interference fringes.

2.4 Conclusion and interpretations

The two main results of this set-up seem strongly contradictory:

- The measurement of $g^{(2)}(0)$ by HBT interferometry suggests that a photon is never split in two by a splitter, but rather takes one or other of the output paths.
- However, the observation of interference bangs at the Michelson's output can only be explained by a wave model.

This paradox is that of **wave-corpuscle duality**. This notion has a subtle link with the notion of quantum indiscernibility, and in our experiment, with the concept of **which-path information**.

Q18 At the output of a Michelson, what can you say about the path information of each photon detected?

Q19 If the Michelson's two mirrors were now replaced by two detectors, what would we observe in terms of counts and (conditioned) coincidences on them? What can you say this time about the path taken by the photons successively detected?

Q20 Using equation (6.3), justify that the observation of interference is the consequence of the indistinguishability between several quantum paths. What parallels can you draw with the HOM experiment?

Q21 In your own words, explain what you think is fundamentally wave-like and what is fundamentally corpuscular in the description of a single photon.

Appendix : Quantum states of light

Coherent states

In addition to the single photon state, there are other quantum states of importance in describing the different states of light.

Light can be placed in a so-called coherent "state", which is a pure quantum state written as a superposition:

$$|\Psi_{\text{coh.}}\rangle = e^{-\frac{|\alpha|^2}{2}} \sum_{n=0}^{+\infty} \frac{\alpha^n}{\sqrt{n!}} |n\rangle$$

By construction, the coherent state is one whose behavior reproduces that of coherent light described in classical physics: it is therefore typically the state associated with laser light. The probability of measuring n photons is then :

$$P_{\text{laser}}(n) = |\langle n|\Psi_{\text{coh.}}\rangle|^2 = e^{-|\alpha|^2} \frac{\alpha^{2n}}{n!}$$

The statistical distribution of the number of photons in the mode of a coherent source is a **Poisson law**. It is not a single-photon source.

We can look at the $g^{(2)}(0)$ of such a source, particularly in the case of a strongly attenuated source ($\alpha \longrightarrow 0$). We then see that the source converges to the empty state of the $|0\rangle$ field, but its statistical properties persist.

At low flux, we can intuitively understand that the coincidence events measured in an HBT interferometer are almost exclusively related to the weight of the two-photon $|2\rangle$ component of the field: when two photons arrive at a splitter, 50% of the time they emerge separated. The probability of coincidence P_{AB} is then typically equal to $P(2)/2$. The $g^{(2)}(0)$ of the source can therefore be quickly estimated by the ratio $P(2)/P(1)^2$, which expresses the relative frequency of coincidence events compared to independent detection events on the two channels. For a coherent source,

$$g^{(2)}(0) \approx 2P(2)/P(1)^2 = 2\frac{\alpha^4}{2\alpha^2 \cdot \alpha^2} = 1$$

This ratio does not depend on the intensity of the source: even if the source is strongly attenuated (and the average number of photons in the mode lowered), the relative weight of the 2-photon states compared to the 1-photon states remains the same. The $g^{(2)}(0)$ is always greater than 1.

(Pseudo-) Thermal state

When the field of a mode results from a statistical mixture of several incoherent, statistically independent contributions, the measured quantum state is no longer a pure state. It can only be written using more sophisticated tools, such as the density matrix. This is the case with so-called **thermal**, or **chaotic** sources: the field of a mode is then the resultant of numerous independent spontaneous emission processes. The state is then written :

$$\rho_{\text{th}} = \sum_n \frac{\langle \hat{n} \rangle^n}{(1 + \langle \hat{n} \rangle)^{n+1}} |n\rangle\langle n|$$

The density matrix is diagonal, which corresponds to an incoherent statistical mixture of Fock states. The probability of measuring n photons is given by :

$$P_{\text{th}}(n) = \frac{\langle \hat{n} \rangle^n}{(1 + \langle \hat{n} \rangle)^{n+1}}$$

This factor results from the laws of statistical physics applied to a mode of the electromagnetic field considered in thermodynamic equilibrium at temperature T. The average number $\langle \hat{n} \rangle$ of photons in the mode is then given by the Bose-Einstein statistic:

$$\langle \hat{n} \rangle = \frac{1}{e^{\beta \hbar \omega} - 1}$$

Furthermore, the geometric progression in n of the $P(n)$ terms is directly related to the incoherent nature of the source. For independent spontaneous emission events associated with a probability λ^2 of emission, then the probability of obtaining a number n of photons is proportional to λ^{2n} :

$$P_{\text{th}}(n) = k\lambda^{2n}$$

with the closure relation

$$\sum_n P_{\text{th}}(n) = 1 = k \sum_n \lambda^{2n} = \frac{k}{1 - \lambda^2}$$

which shows that $k = 1 - \lambda^2$. We can then easily identify :

$$P_{\text{th}}(n) = (1 - \lambda^2)\lambda^{2n} = \left(\frac{1}{1 + \langle \hat{n} \rangle} \right) \left(\frac{\langle \hat{n} \rangle}{1 + \langle \hat{n} \rangle} \right)^n \longrightarrow \lambda^2 = \frac{\langle \hat{n} \rangle}{1 + \langle \hat{n} \rangle} = e^{-\beta \hbar \omega}$$

So the thermal state can be written as $\rho_{\text{th}} = (1 - \lambda^2) \sum_n \lambda^{2n} |n\rangle\langle n|$.
Decreasing the intensity of the source decreases the average number of photons, i.e. we are in the limit $\lambda \to 0$. In this limit, the density matrix converges to that of the pure $|0\rangle_i$ state: we gradually obtain the field vacuum.

Furthermore, we have $\lambda^2 \approx \langle\hat{n}\rangle$, so that $P_{th}(n) \approx (\langle\hat{n}\rangle)^n$. As in the previous case, we can quickly estimate a value for $g^{(2)}(0)$:

$$g^{(2)}(0) \approx 2P(2)/P(1)^2 = 2\frac{\langle\hat{n}\rangle^2}{\langle\hat{n}\rangle\langle\hat{n}\rangle} = 2$$

Here again, the ratio does not depend on the intensity of the source: even with an extremely attenuated source, the expected number of coincidences relative to the average flux received is a non-zero constant in the case of the thermal source.

Quantum state generated by SPDC

In second-order nonlinear optics processes such as SPDC, a photon from the pump beam is converted into a pair of photons *signal* and *idler* (complementary). The reciprocal process also exists: second harmonic generation.

In the quantum-mechanical sense, SPDC is a coherent process: the state of the field is obtained by a unitary evolution from a pure initial state to a final state that is also pure. In the vocabulary of optics, non-linear processes like SPDC are coherent because they are generated at each instant by a coherent field, namely the laser field driving the laser-matter interaction.

The initial state is the vacuum of the electromagnetic field in the two output modes, $|0_\mathrm{s}\rangle|0_\mathrm{i}\rangle$. The Hamiltonian of the SPDC process that applies to this state is written :

$$\hat{H}_\mathrm{SPDC} \propto \chi^{(2)}\left(\hat{a}_s^\dagger\hat{a}_i^\dagger - \hat{a}_s\hat{a}_i\right)$$

and shows the creation or annihilation of pairs. The associated unitary evolution is written :

$$|\psi(t)\rangle_\mathrm{SPDC} = \mathrm{e}^{-i\hat{H}_\mathrm{SPDC}/\hbar}|0_\mathrm{s}\rangle|0_\mathrm{i}\rangle$$

and it can be shown, with the help of several theorems describing the normal ordering of operators, that the field state generated by SPDC is written as [3]:

$$|psi(r)\rangle_{mathrmSPDC} = \mathrm{sech}(r)\sum_{n=0}^{+\infty}\tanh^n(r)|n\rangle_s|n\rangle_i$$

where r is a complex number, called the squeezing parameter, and describes the interaction with the pump – its value depends on the complex amplitude

[3] (see, for example, Stephen M. Barnett, Paul M. Radmore, *Methods in theoretical quantum optics*, Oxford series in optical and imaging sciences 15, page 76, eq 3.7.50, (1997) ; or D. B. Horoshko et al, *Thermal-difference states of light: Quantum states of heralded photons*, Phys. Rev. A **100**, 053831(2019)

of the pump field, the nonlinear response coefficient $\chi^{(2)}$, etc.

The state presents perfect photon number correlations between the mode of the *signal* beam and that of the *idler* beam: if we measure a number m of photons in the s mode, then the i mode contains exactly the same number m of photons. It is therefore a highly entangled state.

The quantum state associated with only one of the two modes (e.g. the *signal*) is calculated by performing the partial trace on the states of the other mode (i.e. the *idler*). The density matrix of the total system is written :

$$\rho = |\psi(r)\rangle\langle\psi(r)| = \mathrm{sech}^2(r) \sum_{n,m} \tanh^{n+m}(r) |n\rangle_s\langle m|_s \otimes |n\rangle_i\langle m|_i$$

The partial trace of the idler mode is :

$$\begin{aligned}
\rho_s = \mathrm{Tr}_i(\rho) &= \sum_k \langle k|_i \rho |k\rangle_i \\
&= \mathrm{sech}^2(r) \sum_{k,n,m} \tanh^{n+m}(r) \delta_{k,n}\delta_{k,m} |n\rangle_s\langle m|_s \;\Rightarrow\; k = n = m \\
&= \mathrm{sech}^2(r) \sum_n \tanh^{2n}(r) |n\rangle_s\langle n|_s \\
&= (1-\lambda^2) \sum_n \lambda^{2n} |n\rangle_s\langle n|_s
\end{aligned}$$

We find that the quantum state associated with one (of the two) SPDC modes is in a **thermal state** as described above: a statistical mixture of Fock states, weighted by geometrically progressing probabilities. We directly identify $\lambda^2 = \tanh^2(r) = \frac{\langle\hat{n}\rangle}{1+\langle\hat{n}\rangle} = e^{-\beta\hbar\omega}$.

To sum up: the *two mode* quantum state resulting from SPDC is indeed a pure state, a **coherent superposition of two-photon states**. The quantum correlations it possesses are measurable via joint measurements on the two photons exploiting quantum interference effects, like measurements of the Bell parameter.

Conversely, detection measurements performed on only one of the two modes ignore, by definition, the correlations between the two modes. Phase information - initially derived from the phase of the pump beam - is therefore lost. The result of each measurement on an individual mode appears to be dictated by independent spontaneous emission events, with probability proportional to λ^2 : **the single-mode quantum state is a statistical mixture of number states according to a thermal distribution**.

Furthermore, for a low-intensity SPDC source, the field state converges to the empty state: $\lambda^2 \longrightarrow 0 \Rightarrow \rho_s \longrightarrow |0\rangle_s\langle 0|_s$.

Conditional detection of a heralding photon

Although SPDC is a photon pair generation process, the statistical distribution of photons in one of the two generated modes does not behave at all like a single photon source. The aim is to place one of the two beams in a state as close as possible to the Fock $|1\rangle$ state. This means actively exploiting the correlation between the two beams.

The strategy is as follows: we know that if the first mode contains exactly one photon, then the second mode contains exactly one photon too. We can therefore perform a measurement on the first mode. The detection of a photon on this first channel is the heralding signal: this event indicates that the twin beam also contains a photon at the same instant. The heralding photon is of course no longer usable, as it has been absorbed. But the heralded photon is still available. In a very short time window, synchronized with the announcement photon, the state of the heralded field is known: it is a state with "at least one photon".

For detectors with unit efficiency, but unable to resolve the photon number, we can define two measurement operator operator $\Pi_{\text{off},i} = |0\rangle_i\langle 0|_i$ referring to no detection on mode i, detection operator $\Pi_{\text{on},i} = \mathbb{1}_i - |0\rangle_i\langle 0|_i$ corresponding to the detection of at least one photon on mode i.

We can now turn our attention to the quantum state of the s mode, measured in conjunction with the observation of a photon on the s channel:

$$\rho_s^{\text{cond.}} = \text{Tr}_i(\Pi_{\text{on},i}|\psi(r)\rangle\langle\psi(r)|) = \sum_k \langle k|_i \rho |k\rangle_i \quad = (1-\lambda^2)\sum_{n=1}^{+\infty} \lambda^{2n}|n\rangle_s\langle n|_s$$
$$= \rho_s - (1-\lambda^2)|0\rangle_s\langle 0|_s$$

More properly renormalized (the trace must be equal to 1), the matrix is written:

$$\rho_s^{\text{cond.}} = \frac{1-\lambda^2}{\lambda^2}\left(\frac{1-\lambda^2}{-}|0\rangle_s\langle 0|_s\right)$$

The measured conditional state is the previously calculated thermal state, truncated by the vacuum contribution of the $|0\rangle_s\langle 0|_s$ field. When the field is sufficiently weak, the state obtained is the pure one-photon state:

$$\lambda^2 \longrightarrow 1 \Rightarrow \rho_s^{\text{cond.}} \longrightarrow |1\rangle_s\langle 1|_s$$

P 7

HBT Interferometry : photon source statistics

Contents

1 Learning objectives

At the end of this session you will be able to :

- Create a speckle and adjust its grain size by focusing a laser in a scattering medium.
- Use the various components of a confocal scanning microscope for fluorescence measurements (excitation channel, wide-field imaging collection, etc.).)
- Align the confocal microscope in the opposite direction (by reverse light propagation)

- Set up the detection pinhole to perform fluorescence spatial mode filtering
- Produce a 2D photoluminescence map to search for single emitters.
- Perform an intensity autocorrelation measurement ($g^{(2)}(t)$) to discern photon flux statistics from a laser, a pseudo-thermal source and a single-photon source.

2 Introduction

In 1956, two radio astronomers, Robert Hanbury Brown and Richard Twiss, designed a new type of stellar interferometer to measure the angular diameter of unknown cosmic objects. The method used until then had been that of a Michelson stellar interferometer.[1].

In any amplitude interferometer, the interference term is proportional to the product of the collected fields: observing the interference fringes is therefore akin to measuring the correlation between the fields. Hanbury Brown and Twiss demonstrated that there are in fact still correlations in the intensity signal of the two fields collected by the interferometer, and that these correlations also allow the angular diameter of the star to be traced. So there is no need to physically recombine the fields to make them interfere before detection. All that is needed is a precise measurement of the intensity of the two signals, then an electronic calculation of the correlation between the two signals to obtain the desired information.

So what is the link between this astronomy experiment and quantum photonics?

The HBT experiment uses a light source (a star or something else...) and a pair of detectors placed on either side of a splitter. The individual signals and the correlation of the two signals are recorded for symmetrical and non-symmetrical positions of the two detectors relative to the splitter, to measure temporal and spatial correlations.

The existence of correlations between the two signals has a very simple wave explanation: when a wave passes a beamsplitter, its amplitude is divided into 2, so the intensity signal is also divided into 2 identical replicas.
What if, instead of detecting a "continuous" signal such as photocurrent,

[1]The Michelson interferometer is an amplitude interferometer used to trace the diameters of stars by observing the interference fringes formed by the recombination of the fields collected by two separate mirrors. The contrast of the interference pattern is related to the mirror separation distance and the angular size of the star.

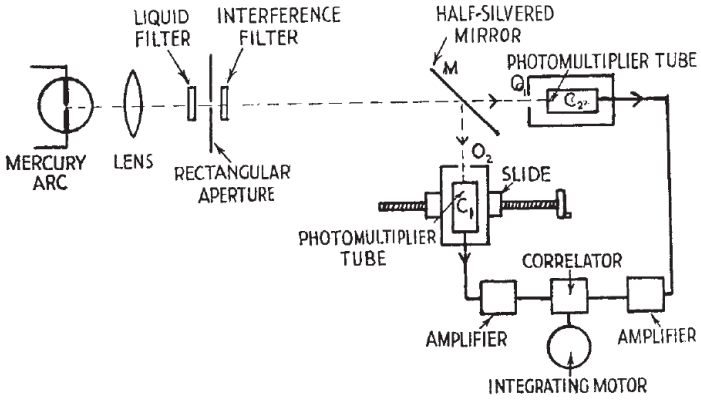

Figure 7.1: Figure of the HBT interferometer experimental set-up, as described in the historical article on the experiment: Robert Hanbury Brown, Richard Twiss "Correlation between Photons in two Coherent Beams of Light," *Nature* 177 (**1956**), 27-29.

we considered light to be made up of photons, unbreakable on a splitter?

It was this experiment, carried out by Hanbury Brown and Twiss, that launched a revolution in optics. For the flux of a mercury arc lamp, the two scientists show that photon arrival times are correlated - in this case, it is shown that photons do not arrive in a random flux, but statistically "bunched" in packets [2].

The impact of this experiment led to the development of an appropriate quantum framework to model the detection process, interferometry experiments, and distinguish the different statistical properties of light: this is the coherence theory of Roy Glauber, who was awarded the Nobel Prize in 2005 for his work.

The aim of this labwork is to help you rediscover a modernized version of this experiment, which is now widely used to characterize a light source through its statistical properties.

First, in an updated version of the HBT experiment, we'll observe the correlations between a laser and a so-called pseudo-thermal source, mimicking the behavior of light from a star based on the rapid blurring of a coherent speckle.

[2] "Correlation between Photons in two Coherent Beams of Light," Nature 177 (1956), 27-29.

Secondly, we will study the statistics of a flux made up of **single photons**. The HBT experiment enables us to confirm the emission of single photons from a source, a key issue in photonic quantum technology. The sources in question here will be **single NV centers**, embedded in nanodiamonds, probed using a confocal scanning microscope. The principle of single-photon sources is often based on the ability to isolate a single quantum emitter.

These different experiments will lead us to measure the intensity autocorrelation coefficient $g^{(2)}(0)$, in order to confirm the difference in quantum nature of different sources and to reconcile the concept of single photon with its intrinsic wavelike nature.

3 Correlation functions and photodetection

Field operators and number operator

In quantum physics, the electric field in a mode (for example, the monochromatic field in a cavity mode) is described by the creation and annihilation operators $\hat{a}^\dagger$ and $\hat{a}$:

$$\hat{E}^{(+)}(t) \propto \hat{a}e^{-i\omega t}, \quad \hat{E}^{(-)}(t) = \left[\hat{E}^{(+)}(t)\right]^\dagger \propto \hat{a}^\dagger e^{i\omega t}.$$

The field intensity, linked to the energy transported, is then related to the operator number $\hat{n}$:

$$\hat{n} = \hat{a}^\dagger \hat{a}.$$

The average of this operator over a considered state of the field gives the average number of photons in the mode: $\langle \hat{n} \rangle$, and its variance describes photon fluctuations:

$$(\Delta n)^2 = \langle \hat{n}^2 \rangle - \langle \hat{n} \rangle^2.$$

To detect a photon is to absorb it. The detection process is therefore intrinsically linked to the action of the annihilation operator $\hat{a}$ on the field under study. The probability $P(t)$ of detecting a photon at time t is written :

$$P(t) \propto \langle \hat{E}^{(-)}(t)\hat{E}^{(+)}(t) \rangle = \langle \hat{n}(t) \rangle$$

The key point compared to the classical case is that the order of the operators is imposed by the detection process. The probability of coincidence between two detectors (or two clicks at separate times) is :

$$P(t, t+\tau) \propto \langle \hat{E}^{(-)}(t)\hat{E}^{(-)}(t+\tau)\hat{E}^{(+)}(t+\tau)\hat{E}^{(+)}(t) \rangle$$

The member on the right is, to within one normalization factor, the correlation function of order 2 in intensity (and order 4 in field) associated with the state

of light, which we denote $g^{(2)}(\tau)$. Experimentally, this correlation function can be measured using coincidence measurements between two detectors, based on the principle of the HBT experiment.

For $\tau = 0$,

$$g^{(2)}(0) = \frac{\langle \hat{a}^\dagger \hat{a}^\dagger \hat{a} \hat{a} \rangle}{\langle \hat{a}^\dagger \hat{a} \rangle^2}.$$

Using the algebraic identities of bosonic operators, we can rewrite :

$$g^{(2)}(0) = \frac{\langle \hat{n}(\hat{n}-1) \rangle}{\langle \hat{n} \rangle^2} = 1 - \frac{1}{\langle \hat{n} \rangle} + \frac{(\Delta n)^2}{\langle \hat{n} \rangle^2}.$$

This explicit link between $g^{(2)}(0)$ and photon number fluctuations shows that light can be characterized via its intensity variance. The preceding formalism shows that there is a subtle link between:

- the distribution of photon arrival times (statistically more numerous coincidences at zero delay suggest that "photons travel together"),
- and **the distribution of the number of photons in the quantum state describing light** (more numerous coincidences suggest that light can be measured more frequently in multi-photon states.)

These last two points illustrate the complementarity principle between phase and photon number in describing the quantum state of light. By associating photons with a wave packet describing their probability of presence in a light flux, phase relations between packets are likely to create interference, grouping photons when constructive and ungrouping them when destructive.

Classical and non-classical statistical regimes

- **Coherent states (ideal laser)**: Ideal laser light is described by the absence of intensity fluctuations. More formally, it is written as a coherent state (or Glauber state, see Appendix).

  The statistical distribution of the number of photons is Poissonian, such that $(\langle (\Delta n)^2 \rangle = \langle n \rangle)$, so $(g^{(2)}(0) = 1)$.

- **Thermal states (chaotic light)**: Thermal light is that of a field in thermodynamic equilibrium with the matter emitting it. The iconic case would be that of a monochromatic component of the field emitted by a black body.

  Statistical physics arguments applied to light demonstrate that photon statistics follow a Bose-Einstein law such that $\langle (\Delta n)^2 \rangle = \langle n \rangle^2 + \langle n \rangle)$, hence $g^{(2)}(0) = 2$.

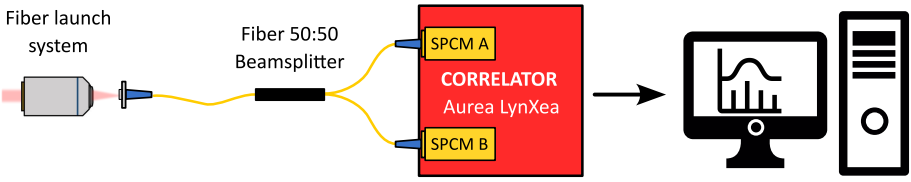

Figure 7.2: HBT interferometer used for coincidence measurements

A thermal source exhibits photon bunching (*bunching*), also known as a super-Poissonian source.

- **One-photon states** One-photon states are pure states that reduce to the $|1\rangle$ state. The photon statistic therefore reduces to a Dirac in $n = 1$ in the ideal case. More broadly, we have $(\Delta n)^2 < \langle n \rangle$, so $g^{(2)}(0) < 1$. The source exhibits **photon bundling** (*antibunching*), we also say that its statistics are **sub-Poissonian**.

The case $g^{(2)}(0) < 1$ is impossible to explain by classical field theory. It is therefore a strong criterion for the non-classicity of light.

4 Experiments performed

4.1 Setup overview

The TP setup is based on an HBT interferometer, here in a fibered version (see Figure 7.2). A microscope objective collects light from various sources and injects it into the input of a fiber with a 50:50 splitter. The two fiber ports at the splitter's output are connected to the two detectors forming the two channels of a LynXea correlator (Aurea Technology).

CAUTION: Avalanche sensors are extremely fragile! Never switch on the LynXea when the ambient light is on, or if the lasers in the various channels of the assembly are not strongly attenuated.

ALWAYS leave the fibers connected to the LynXea. It is almost never necessary to remove them. Leaving the fibers in place preserves the cleanliness of the fibers and fiber connectors, while avoiding exposing the detectors.

The correlator records the arrival times of photons in each of the two channels, and plots the histogram of relative arrival times between two detection events, giving the function $g^{(2)}(\tau)$ and its value at $g^{(2)}(\tau) = 0$, which corresponds to pure coincidence between the two channels.

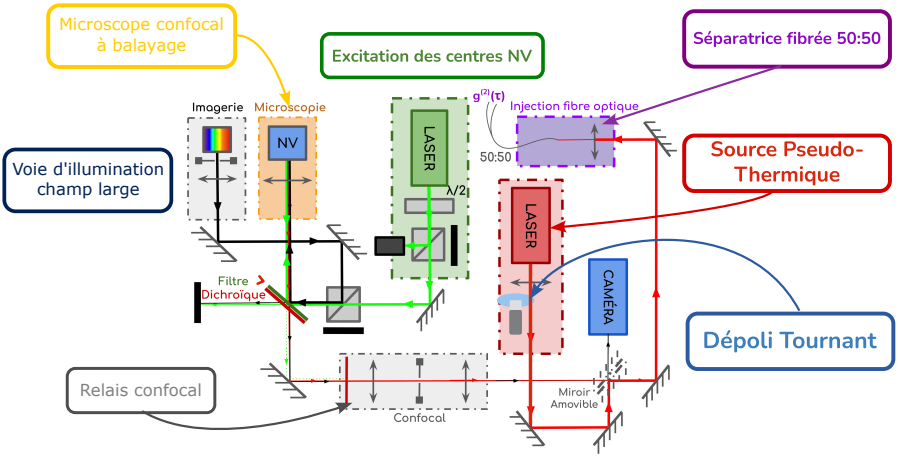

Figure 7.3: Setup overview.

Upstream of the interferometer, a first channel is dedicated to the TP pseudo-thermal source, which will be used to study both the statistical properties of chaotic and laser sources.

A second channel, which takes up the bulk of the setup, is connected to the output of a scanning confocal microscope, used to excite and collect fluorescence from nanodiamond samples.

4.2 Pseudo-thermal source and laser

Thermal sources refer to all sources emitting photons by incandescence, which is one of several spontaneous emission processes. The field generated by such sources is the sum of random phase contributions from a multitude of independent sources, namely the atoms that make up the thermal source.

A laser source can be used to provide a large number of photons while mimicking the principle of a mixture of phase-shifted sources[3]

The principle behind the creation of a pseudo-thermal source is based on the manipulation of an optical speckle. A speckle is an interference pattern created by the scattering of coherent light by a random medium. The intensity at each point of this pattern is the result of interference between a multitude of secondary sources - the scatterers in the medium - each of which has a different

[3]The experiment was inspired by F. T. Arecchi, E. Gatti, and A. Sona, "Time distribution of photons from coherent and Gaussian sources". Sona, "Time distribution of photons from coherent and Gaussian sources," *Phys. Lett.* 20, 27-29 (1966).

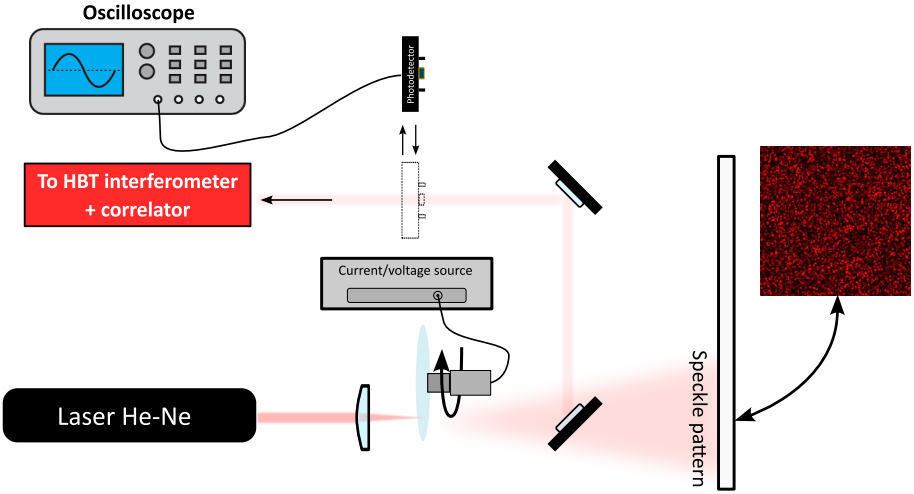

Figure 7.4: Arecchi wheel for measuring the coherence of a thermal source.

phase. A speckle light grain thus is a region of space where the superposition of all the random fields from the medium's scatterers gives rise to constructive interference.

The TP experiment uses a frosted glass slide illuminated by a beam from a He-Ne laser. The laser is focused into the ground glass: there is an inverse relationship between the size of the coherence volume excited by the laser and the angular size of the speckle grains (see Figure 7.4). If the diameter of the laser spot on the diffuser is D, then D also represents the maximum possible distance between two scatterers. By placing a screen in the far field at a distance L from the diffuser, the fringe spacing of the interference pattern resulting from these two secondary sources will be on the order of $\lambda L/D$—this corresponds to the smallest possible fringe size. This leads to the conclusion that the typical size of a speckle grain is equivalent to the size of the Airy disk in the imaging configuration of the system.

The screen is mounted on a motor and can be rotated at speeds of up to over 5,000 rpm. Consider a speckle of light at the start of the experiment: when, after rotation, the laser spot illuminates a new area of the ground glass, the distribution of scatterers is completely different. The light collected at this same point is the result of a new random draw on the number and phase of the secondary sources illuminated by the laser: interference can give either a constructive or destructive result. Once the frosting has been rotated, the intensity

signal received by a detector fluctuates randomly on the same principle as the fluctuations of a heat source.

The rotation of the ground glass remains periodic and not rigorously random, so that we speak of a *pseudo*-thermal source. The correlation time of the intensity fluctuations depends in particular on the rotation speed of the frosting, and can therefore be used to explore slower correlations, more easily accessible to experiment.

Observation of time correlations in the photocurrent signal

$\rightsquigarrow$ Check that the LynXea correlator is switched off, then switch on the He-Ne laser.

$\rightsquigarrow$ If necessary, remove the ground glass from the optical path. Position the removable mirror so that the laser beam is directed at the HBT interferometer.

$\rightsquigarrow$ By adjusting the two mirrors in the laser path, roughly align the laser with the optical axis of the microscope objective.

$\rightsquigarrow$ Place the converging lens at the laser output and insert the rotating frosting (keeping it stationary). You should instantly see a pattern of speckle being diffused by the screen (on the wall of the room facing the fixture, for example).

$\rightsquigarrow$ Change the orientation of the frosting if necessary, so that the speckle pattern is partly intercepted by the mirrors forming the laser path. Check that part of the speckle pattern illuminates the entrance pupil of the microscope objective.

$\rightsquigarrow$ Gently move the converging lens along the optical axis to change the size of the speckle grains. Adjust the speckle size so that the entrance pupil of the collection lens is essentially a single speckle grain.

Q1 Why is this setting important? What do you expect to see in terms of intensity fluctuations if the interferometer simultaneously collects light from a large number of speckle grains?

$\rightsquigarrow$ Insert the photodiode in the optical path of the fixture and position it so that the active area lies within a speckle grain.

$\rightsquigarrow$ Visualize the photocurrent signal on the oscilloscope, keeping the grond glass at rest.

Q2 Describe what you observe. Are the fluctuations you observe characteristic of Gaussian noise? White noise?

⇝ Using the voltage source, rotate the ground plate by applying voltages up to around +15 V.

⇝ Adjust the oscilloscope trigger and time window to observe around a single period of the signal and its intensity fluctuations on the screen.

Q3 Describe again what you observe. Are the fluctuations you observe characteristic of Gaussian noise? White noise?

Q4 Gradually increase the applied voltage, and therefore the motor speed: how does the time signal on the photodiode change?

Q5 Use the tachometer to measure actual motor speed as a function of applied voltage. By briefly analyzing the time signals on the oscilloscope, propose an estimate of the correlation time of fluctuations in intensity as a function of motor rotation speed.

Q6 Using a USB key, acquire a few signals and plot the histogram of the voltage values contained in the signal.

Q7 When the diffuser is at rest, what do the remaining fluctuations correspond to? Estimate their correlation time once again, and plot the histogram of the voltage values. Comment on the distributions obtained in both situations studied.

Correlation of photon arrival times – photon bundling

Oscilloscope visualization illustrates the existence of correlations in a signal associated with the intensity of a pseudo-thermal source. This observation is made on the photocurrent, a continuous macroscopic quantity. The coherence time is then the characteristic time of the observed fluctuations.

The aim of this section is to observe the same phenomenon in an experimental setting where a photon flux is detected. The photons are detected using avalanche photodiodes, and the focus is now on the statistics of the photon arrival times on the detectors of an HBT interferometer.

⇝ Remove the photodiode from the light path, and check that we still have a single speckle grain collected by the microscope objective.

⇝ Place the variable optical density slightly upstream of the objective pupil, to ensure that the laser speckle is clearly attenuated.

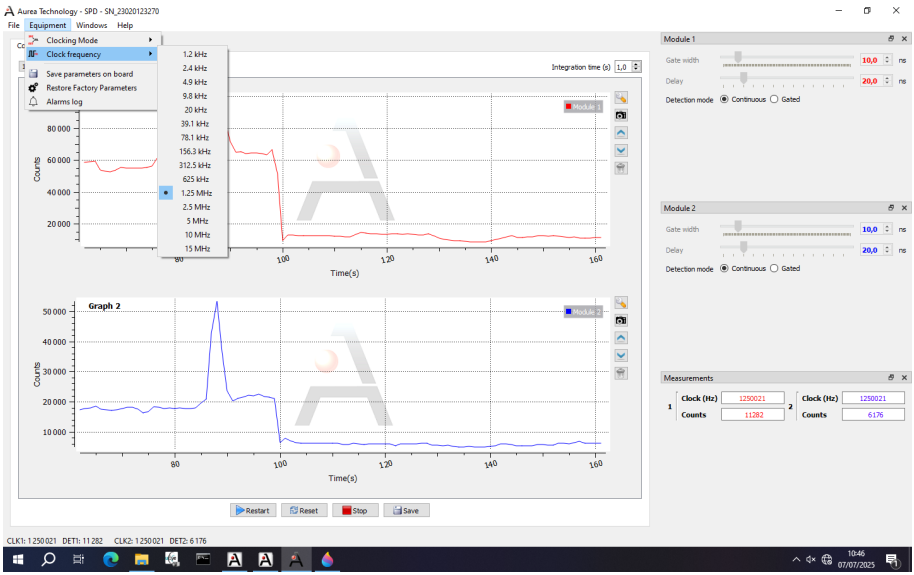

Figure 7.5: Window of the Aurea, in photon counting mode, displaying the signal from both detectors.

⇝ Turn off the overhead lights in the room, block the laser beam completely, then switch on the LynXea box and initialize the Aurea "**Launcher**". First, select the "**Photon Counting**" option.

⇝ The window shown represents the detection counts per integration time window on the LynXea's two input channels. If necessary, select the "**Continuous**" detection mode for both channels (right-hand panel of the software window).

⇝In the "**Equipment/Clock Frequency**" menu, select a clock frequency of 78.1 kHz. The process of counting and time-tagging detections by LynXea is described in the Appendix.

⇝ With the laser beam blocked, check that the number of strokes on each channel is of the order of a few hundred counts per second: this is the level of the detector's dark counts.

⇝ Unblock the laser beam and observe the increase in the number of hits on the detectors. Adjust the density position to obtain several tens of thousands of shots and ensure that it remains well below one million count per second.

⇝ Adjust the X, Y and Z settings of the fiber injection stage to maximize the

signal detected. This will ensure that your setup is pre-aligned for the upcoming experiments.

Q8 Note the count rates on each detector. What statistical law can you use to describe the fluctuations in the number of counts recorded over one integration period? Deduce the standard deviation of the expected fluctuations from the mean value, and check whether these correspond to your observations.

$\rightsquigarrow$ Using the “Launcher” of the Aurea software, start the “Photon Timing” correlation module.

Aurea’s correlation module enables you to acquire and measure correlations between the successive arrival times of photons on the two detectors placed at its two inputs.

Principle of correlation measurements . The **Cross correlation** mode operates on the principle of a "**Start-Stop**" measurement. A clock, whose frequency has been set in the previous step, supplies a periodic signal. When, during a clock cycle, a photon is detected on channel 1, a chronometer, based on a second, much higher-frequency clock, starts. It stops when a detection event is registered on channel 2, or if no detection occurs, at the end of the clock cycle. The duration of the delay between the two detection events, as measured by the timer, is recorded. As this process is repeated, the software processes and displays the histogram of recorded delay values.

The temporal resolution of each histogram interval is set by the Start-Stop clock rate, and is $13\,\mathrm{ps}$. The value of the maximum measurable delay is set by the frequency of the first clock. For example, at 78.1 kHZ, this delay is $12.8\,\mathrm{ps}$.

If necessary, use the acquisition mode selection menu ("**Caliper**" button to choose the **Cross Correlation** mode (see Figure (7.6)).}.

In the ALU window, you can select "**Ch1-Ch2**" or vice versa to swap the role of the start or stop channel, and therefore the sign of the measured delays. The "**Stop conditions**" panel allows you to specify either a total acquisition time, or a number of samples to be acquired, or to let the histogram be acquired continuously, using the value "-1" as a setpoint.

The delay values forming the histogram can be exported using the "**Save raw data**" button at bottom right. The histogram figure itself can be saved with "**Save histogram**".

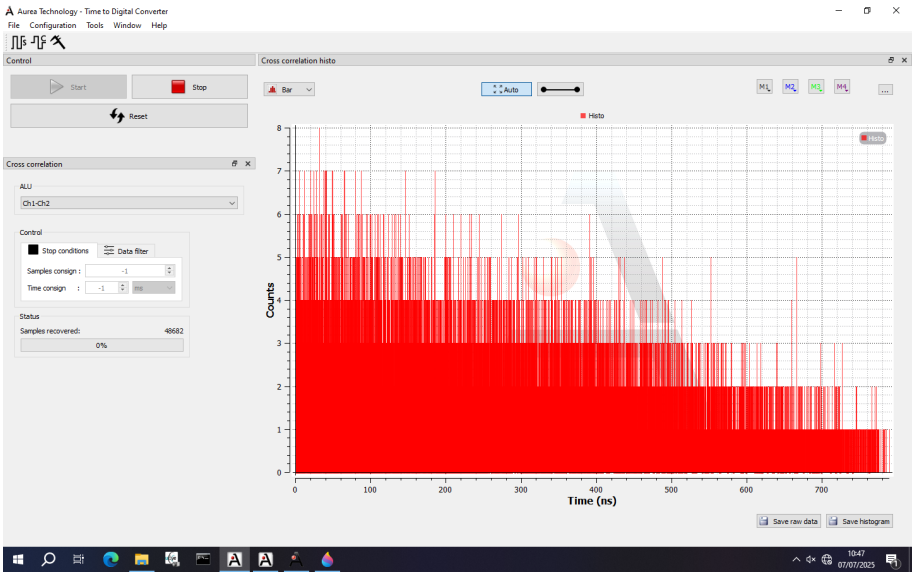

Figure 7.6: Software window of the correlation module of Aurea's LynXea.

Q9 With the lens stopped, make an initial measurement of the histogram. From your measurement, explain how we can estimate the coincidence rate between the two detectors within a given narrow coincidence window. Also explain how we can estimate the number of accidental coincidences for the same width of coincidence window.

Q10 Comment on the histogram obtained. In particular, how do you interpret the drop in the number of occurrences of the highest delay values? What can you say about the photon correlation properties of laser light?

⇝ Now rotate the screen. Check, in the "**Counting**" window, that the signal received on average by the detectors is well above the level of the dark count (but well below hundred thousand counts).

Q11 Describe what you observe and explain why this time we're seeing a photon bunching effect. Record the histograms for several values of rotation speed, which you can estimate using the tachometer. From your measurements, plot the evolution of the value of $g^{(2)}(0)$ and the correlation time as a function of the rotation speed of the ground glass.

Q12 Are your correlation measurements on photon arrival times compatible with those obtained on the photocurrent signal from a photodiode?

Q13 To conclude this section, qualitatively plot on the same graph the expected shape of the $g^{(2)}(0)$ functions for different values of the screen's rotation speed.

4.3 Single photon source

In this second part of the tutorial, we focus on the study of single-photon sources in the solid state.

A single photon is **unseparable**: at the input of an HBT interferometer, it is either transmitted or reflected by the splitter. A single-photon source is defined experimentally by the impossibility of observing zero-delay coincidences between the two HBT detectors[4]: while the arrival time of two consecutive photons remains governed by a random process, there is a characteristic time between several detection events which tends to unbunch the photons: this is known as *anti-bunching*.

The characteristic time in question is linked to the lifetime of the excited level, which intrinsically limits the speed at which absorption and emission cycles can succeed one another. It can be estimated by the width of the function $g^{(2)}(\tau)$.

These various definitions make it easy to calculate that, in the case of an ideal single-photon source, we obtain $g^{(2)}(0) = 0$, and that $g^{(2)}(\tau) = 1$ for $tau \gg \tau_c$ where τ_c is the characteristic time associated with the emission process cycle. It is typically in the range of few **nanoseconds**.

NV centers

In this tutorial, we focus on one of the most commonly studied types of solid-state single-photon source: NV centers. Diamond is a crystal composed of a lattice of carbon atoms. An NV center is one of diamond's crystalline defects: it consists in the substitution of one of these atoms by a nitrogen atom, directly adjacent to a gap (*vacancy* in English). (see Figure 7.7).

[4]More formally, a single photon source generates light whose quantum state is a pure one-photon Fock state: $|1\rangle$. The statistical distribution of the number of photons contained in the probed mode therefore reduces to a distribution of zero variance: a probability peak centered on $n = 1$.

An NV center locally disturbs the diamond crystal lattice, confining the wave function of certain electrons to the defect. The energy levels associated with these confined electrons are consequently discretized: in practice, an NV center can be considered here as a two-level quantum system, hosted in a crystalline, and therefore solid, matrix. Radiative decay between the upper and lower levels takes place by emission of a single photon. NV centers are sometimes referred to as "artificial atoms". The identification of NV centers as single-photon emitters, their characterization and now their advanced manipulation has been the subject of much scientific work, pioneered by Jörg Wrachtrup's team at Stuttgart University and Philippe Grangier's at the Institut d'Optique.

Unlike a single atom, there's no need to trap it in an ultra-high vacuum chamber, for example, using optical tweezers. This advantage comes at the price of a few drawbacks: an NV center is inserted into the crystal lattice, and is therefore particularly influenced by the crystal's phonons. Its spectral and coherence properties are much poorer than those of an atom - it should be pointed out that all atoms corresponding to the same isotope are identical and indistinguishable particles in quantum physics. This is not the case with NV centers.

In the lab, samples consisting of microscope coverslips coated with nanodiamond powder are used: i.e. a set of nanometer-sized diamond crystals that may contain NV centers in very small numbers, typically between 0 and 5 centers. Some nanodiamonds therefore host a single NV center, and their fluorescence can be excited and collected to obtain a single-photon source.

Scanning confocal microscopy

The setup used in this section is a scanning confocal microscope. Its purpose is to collect the fluorescence of single nanodiamonds. A single emitter emits extremely little light compared with extended meso- or macroscopic sources. Filtering out all other stray light sources is imperative to correctly observe the statistical properties of the light flux to be studied.

The microscope features an excitation laser diode at 532 nm (Oxxius), whose flux can be reduced by means of the combination of a half-wave plate and a polarization splitter cube. The excitation beam is focused on the sample using a microscope objective with a high numerical aperture (X100, NA=0.95). As the NV centers are located in the fluorescent excitation volume, part of their emitted flux is collected by the microscope objective and sent back towards infinity through a dichroic mirror filtering most of the pump photons.

The fluorescence channel features an afocal relay at the focus of which is a confocal pinhole, which gives the instrument its name. This iris is conjugated with the sample plane. When its size is chosen to be slightly larger than that of the excitation focal spot, the iris only lets through the fluorescence emitted by objects present in the plane of focus, and conjugated with the iris aperture.

At the relay output, fluorescence is directed to the HBT assembly of the previous section. The LynXea correlator first measures the number of fluorescence pulses received.

At this stage, no image is formed. All we have is a signal received on a photodiode. A 2D image is formed by scanning the sample surface : for each position of the sample stage, the fluorescence signal is recorded, and measurements are eventually combined to plot a 2D photoluminescent map.

In our setup, the LynXea is connected to a National Instruments acquisition card capable of counting the detection strokes received and controlling the position of three piezoelectric wedges in X, Y, Z. Software is used to program the voltage setpoints to be applied to the three wedges so that the sample is excited point by point by the green laser.

By using a removable mirror and a white-light illumination channel, it is possible to obtain a wide-field image on a camera. This imaging capability enables the excitation laser beam to be aligned, the plane of focus of the lens to be identified more easily, and the size of the confocal pinhole to be adjusted.

$\rightsquigarrow$ Start by checking the position of the microscope objective, and if it is very close to the surface, move it back sharply. Its working distance is very small, and focusing the set-up will require you to carefully approach the objective to the surface.
$\rightsquigarrow$ Turn the key and switch on the laser diode, remembering to connect the fan to regulate the diode temperature. Using the half-wave plate,set the laser power at its minimum.

$\rightsquigarrow$ Check that the laser reflects off the dichroic mirror, and is correctly sent to the back pupil of the microscope objective.

$\rightsquigarrow$ Turn on the white light source and check that the light reaches the sample surface.

$\rightsquigarrow$ Remove any filters or diaphragms from the confocal channel. Position the removable mirror towards the camera.

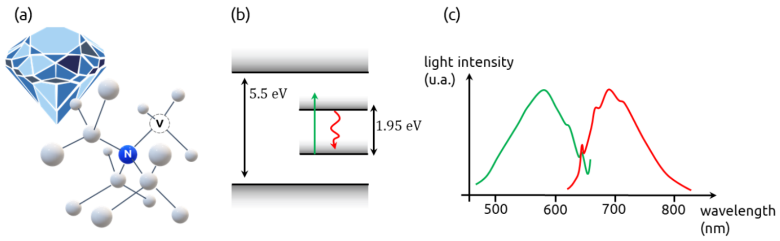

Figure 7.7: (a) Schematic representation of an NV center, with a nitrogen atom (N) next to a vacancy (V).(b) Energy levels of diamond. Diamond is a wide-gap semiconductor. The presence of an NV center creates a sublevel within this gap.(c) Absorption spectrum (green) and fluorescence spectrum (red). The main fluorescence transition, called the zero phonon line, of the NV center is at 635 nm (or $1.95, \mathrm{eV}$).spectra are strongly broadened by interaction with phonons.

$\rightsquigarrow$ On the computer, open the camera software. By adjusting the intensity of the white source and the integration time, start by obtaining an image of the sample surface.

$\rightsquigarrow$ If necessary, increase or decrease the laser power to observe the reflection of the weak laser beam towards the camera. Gently move the microscope objective closer to the surface, until you see the laser focus point.

$\rightsquigarrow$ Lower the laser power and observe the focusing plane in white light. You can confirm your focus position by moving the sample sideways using the micrometric translation screws: the surface of the slide usually has small defects which follow the movement of the stage in the field of view of the camera.

$\rightsquigarrow$ When the laser is correctly aligned, its focusing spot remains roughly rotationally symmetrical when moving slightly across the focal point. If necessary, slightly re-align the green laser to improve the quality of the spot observed.

Q14 Using the microscope's numerical aperture, estimate the diameter of the laser spot focused in the plane of the sample.

Q15 Confirm this estimate by direct measurement: the camera pixels have a lateral size of 10 x 10 $\mu\mathrm{m}$. The X100 microscope objective is an Olympus objective is infinity corrected, and designed for use with a 150 mm focal length

tube lens. The afocal relay consists of two 50 mm focal length lenses. The camera lens, set to infinity, has focal length $f = 100\,\mathrm{mm}$.

Q16 Based on your previous measurements, suggest a size of confocal hole to be placed in the afocal relay that will enable confocality to be adequately achieved.

$\rightsquigarrow$ Place the 50 μm pinhole in the middle of the afocal relay. Use the camera to observe the sample surface through the pinhole. Adjust the lateral position of the pinhole so that it overlaps the laser spot and is in the same plane of focus as the sample: the microscope is now confocal!

We'll now make sure that the HBT interferometer is aligned well enough to collect the fluorescence photons that emerge from the confocal pinhole.

$\rightsquigarrow$ **Make sure you switch off the LynXea!**

$\rightsquigarrow$ Remove the removable mirror from the bench. Disconnect one of the LynXea's fiber inputs, connect it to a fiber checker and switch it on. A strong red light now runs through the assembly in reverse propagation.

$\rightsquigarrow$ Check the path followed by the red light, which must reflect off several mirrors, pass through the afocal relay and its confocal pinhole, be reflected by the dichroic mirror and then be focused by the microscope objective onto the sample surface. Use the two mirrors between the confocal pinhole and the entrance to the HBT stage to adjust your alignment.

$\rightsquigarrow$ Once aligned, remove the fiber checker, reconnect the Lynxea fiber, and place the high-pass filter in the beam path - in addition to the dichroic mirror, it cuts off any remaining pump photons while allowing fluorescence to pass through.

$\rightsquigarrow$Turn on the LynXea again, and run the **Qudi** software on the computer to obtain photoluminescence maps.

$\rightsquigarrow$ First, start the **counter-gui** module. Observe the number of counts displayed by the interface, and compare it with the number of dark counts expected for the detectors. Cut the beam with a screen to deduce whether photons are actually being collected by the HBT stage; if necessary, increase the laser power from the minimum to obtain a signal on which to optimize your alignment.

$\rightsquigarrow$ With all filters in place and for an unambiguous fluorescence signal above the dark level, do your best to optimize the signal level using the alignment mirrors and the position of the confocal hole.

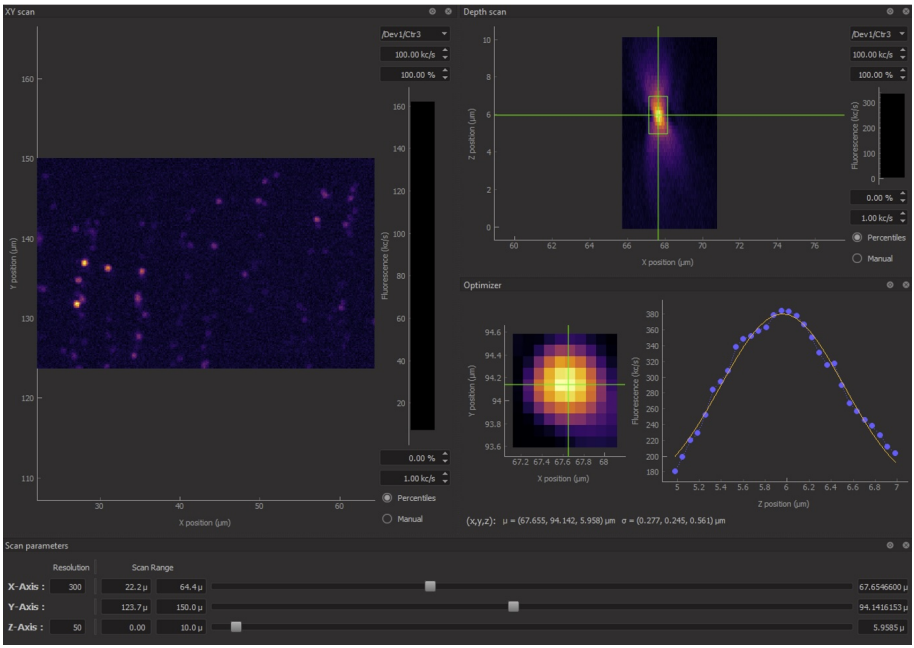

Figure 7.8: Software window for the confocal-gyu module of Qudi. The XY confocal map is displayed on the left panel ; the XZ confocal map is displayed on the top right ; the position optimizer on the bottom right. The sliders at the bottom of the screen or the cursor on the map can be used after the scan to drive the piezo stage and adjust manually the stage position

⇝Close the counting module, then start the confocal mapping module (confocal-gui, see Figure 7.8). Set up a surface scan of at least 20 x 20 microns, with a resolution of around 50 points per line.

⇝ Observe the average flux level and any fluorescent areas a few pixels wide that deviate significantly from this level.

Q17 Nanodiamonds are at most a few tens of nanometers on a side. What is the typical size of the fluorescent pattern seen on the photoluminescence map?

⇝ If the map turns out to be very uniform in terms of the number of shots, move very slightly over the sample, and restart a sufficiently spatially resolved

acquisition. If, after a few attempts, you observe nothing, remove the confocal hole and resume your search.

The nanodiamond powder forms a constellation of similar fluorescent spots, a few microns apart.

⇝ Once you've located all the nanodiamonds, use Qudi's zoom tools to successively zoom in closer and closer around a single nanodiamond.

⇝ Complete your setup using the stage position optimization module, which searches for the maximum fluorescence intensity based on a 2D Gaussian fit of the fluorescence profile of a nanodiamond you've isolated.

Q18 Once the center has been isolated, use Qudi's counting module to plot the curve showing the number of fluorescence counts detected as a function of excitation laser power. Comment on the possible presence of a saturation regime. As a reminder, the number of pulses in this experiment is expected to be less than one million pulses per second.

⇝ Close Qudi's counting module and confirm that LynXea's counting module gives you compatible values.

⇝Next, open the Lynxea correlation module.

This time, we use the **Time-Tagging** acquisition mode[5]. Here the exact, absolute date of photon detection on each of the module's two channels. This makes it possible to trace a complete histogram of delays between detection challenge, similarly to the previous experiments.

⇝ In the LynXea counting module, change the detector synchronization frequency to 1.25 MHz or 2.5 MHz. In the correlation module, select "**Time Tagging**" mode. Choose the location for saving the file.

⇝ Check that the number of counts on the two correlator channels is roughly balanced. Optimize the signal level by slightly adjusting the position of the piezo stages (use the sliders on the confocal module directly).

[5]The cross-correlation mode only recovered information on the delay times between detections on each channel. In practice, the LynXea's histogram acquisition mode eliminates a significant number of events from its processing, in order to retain a partial quantity of data that can be processed in real time. Data truncation is of no consequence when the signal-to-noise ratio is sufficient, which was the case in the first part of the session, but is not valid anymore now.

Q19 Note the value of the average detection rate on each channel. For a coincidence window at the LynXea's resolution limit (13 ps), estimate the acquisition time required to obtain an average count of 100 accidental coincidences. Knowing that it is possible to process the time tagging information to perform temporal binnning (i.e. concatenate several 13 ps windows to count more hits at the expense of temporal resolution), explain which acquisition time value you have chosen.

$\rightsquigarrow$ Perform your *time tagging* measurement by running the acquisition over typically several minutes. During this time, make sure that the number of strokes on the counters varies only slightly and remains close to its maximum: open the **Qudi** counting module, **counter-gui**, and constantly monitor the strokes, whose number may decrease if the piezo wedge drifts.

$\rightsquigarrow$ Correct the position of the wedge from time to time, if necessary, by moving the cursor on the confocal map displayed on the module.

Q20 Retrieve the time-tagging file generated by the acquisition. Use the python file provided (time-tagging-processing.py) to trace the histogram of delay times.

Q21 What are the different experimental signatures deviating from the level of observable accidental coincidences? Comment on the histogram obtained.

Q22 Confirm or not the presence of a drop in coincidences at short times, less than a few nanoseconds.Why do we speak of photon antibunching ?

Q23 Estimate the value of the parameter $g^{(2)}(0)$ with its associated uncertainties. Does the flux of emitted photons make the nanodiamond a source of non-classical radiation? A source of single photons?

Appendix : Semi-classical and quantum theory of photodetection

Semi-Classical photodetection theory and correlation functions

Semi-classical photodetection theory represents an intermediate approach between classical and quantum optics. In this framework, the incident electromagnetic field is treated as a classical quantity, while the detector (e.g., an atom) is modeled quantically, by a discrete distribution of levels. The detection process is then described by the transition from the atom's ground state

to its excited state. This approach can be used to describe a large number of phenomena observed experimentally, particularly in the case of coherent or thermal light.

In this theory, the probability that a detector will record a photon in an interval $\mathrm{d}t$ at time t is assumed to be proportional to the instantaneous intensity of the electromagnetic field, i.e. $I(t) = |E(t)|^2$, where $E(t)$ is the complex amplitude of the electric field.

$$P(t)\mathrm{d}t \propto I(t)\mathrm{d}t$$

First-order correlation function

The first-order correlation function is defined by the expression :

$$g^{(1)}(\tau) = \frac{\langle E^*(t)E(t+\tau)\rangle}{\langle |E(t)|^2\rangle},$$

where the operator $\langle\cdot\rangle$ denotes an ensemble or time average. This function measures the temporal coherence of the field, i.e. the ability of two field values separated by a τ interval to interfere. The modulus of $g^{(1)}(\tau)$ defines the degree of temporal coherence of the source in the classical sense of the term. Normalized to 1, it equals the visibility of interference at the interferometer output.

The function $g^{(1)}(\tau)$ defines the notion of coherence in the sense of classical optics: it is the ability of a field to generate interference. Its characteristic width is related to the coherence length of the source. However, the measurement of $g^{(1)}(\tau)$ is not always able to distinguish between fields of very different natures: it is well known that a laser and a spectral lamp are two sources capable of generating extremely contrasting interference close to the optical contact of a Michelson. However, the field of a spectral lamp exhibits phase and intensity fluctuations that justify describing it very differently from that of a laser. It is therefore necessary to explore the notion of higher-order coherence.

Second-order correlation function

On the same principle as above, we can define joint probabilities of detection. The joint probability of recording a first detection event at time t, followed by a second at time $t+\tau$ over time intervals $\mathrm{d}t$ is written :

$$P(t+\tau,t)(\mathrm{d}t)^2 \propto I(t)I(t+\tau)(\mathrm{d}t)^2$$

This probability is directly related to the second-order correlation function, defined by :

$$g^{(2)}(\tau) = \frac{\langle |E(t)|^2\,|E(t+\tau)|^2\rangle}{\langle |E(t)|^2\rangle^2} = \frac{\langle I(t)I(t+\tau)\rangle}{\langle I(t)\rangle^2}.$$

This function is exactly what is measured in the HBT experiment. It measures the correlation between two detections at times separated by τ. Since the numerator is a joint probability of detection, and the denominator a simple probability, $g^{(2)}(\tau)$ can be interpreted as a conditional (normalized) probability of detection:

$$g^{(2)}(\tau) = \frac{P(t+\tau|t)}{P(t)}$$

i.e. the probability of measuring a detection event at date $t+\tau$ after a first event detected at date t.

Specific properties of this function can be expected for $\tau = 0$. We can write :

$$g^{(2)}(0) = \frac{\langle I^2(t)\rangle}{\langle I(t)\rangle^2} \geq 1$$

the inequality being that of Cauchy-Schwarz.

It is also useful to highlight the very simple link between $g^{(2)}(\tau)$ and the intensity fluctuations of the source. If the variance in the measured field intensity is given by:

$$\sigma_I^2 = <I^2(t)><I(t)>^2$$

then

$$g(2)(0) = 1 + \frac{\sigma_I^2}{\langle I(t)\rangle^2}$$

which is another way of recovering the properties of the Cauchy-Schwarz inequality.

These results predict positive correlations in the intensity signal of a source, and between the two detectors in an HBT experiment, as it was first carried out in the radio domain (using "*square law detectors*", measuring an electric current). This is exactly what was observed, but let us emphasize that, at this stage, behind the formalism, this result is almost self-evident: light being a wave, it is simply split in two by the beamsplitter in an HBT interferometer. The intensity signal received on two symmetrically placed detectors is correlated, simply because it is the same ! The loss of correlation observed when moving one detector forward or backward is related to the timescales of intensity fluctuations, that is, to the temporal coherence length of the source.

The function $g^{(2)}(\tau)$ thus allows us to analyze the statistical nature of the detected light: and one can easily show that, depending on whether the light originates from a so-called “coherent” or thermal source, $g^{(2)}(\tau)$ will take on different characteristic values.

Relationship between $g^{(1)}$ and $g^{(2)}$ for thermal light (Gaussian field)

At this point, the exact expected value of the $g^{(2)}$ function has not yet been discussed.

In the particular case where the field $E(t)$ is a complex Gaussian random process, which is a reasonable assumption for thermal or pseudo-thermal light[6], one can apply the **Wick's theorem** to express fourth-order moments in terms of second-order moments. This leads to the remarkable relation:

$$g^{(2)}(\tau) = 1 + g^{(1)}(\tau)^2.$$

This relation is one of the central results of the semi-classical theory of photodetection. It predicts, in particular, that $g^{(2)}(0) = 2$ for a thermal field, since $|g^{(1)}(0)| = 1$.

$g^{(2)}$ for laser light.

The invention of the laser by Maiman quickly aroused tremendous interest due to its coherence properties, which were initially poorly understood. The hypothesis of Mandel and Wolf was that the difference between laser and thermal sources lay essentially in the coherence length—that is, the width of the function—and not in the value of $g^{(2)}(0)$.

An ideal laser results from a stimulated emission process, which precludes describing the field as a sum of independent random variables. Its field is defined by the absence of intensity fluctuations, $\sigma_I^2 = 0$. Therefore, the relation (**??**) predicts $g^{(2)}_{\text{laser}}(0) = 1$.

Conversely, the previous expressions thus show that if a pseudo-thermal source exhibits a value of $g^{(2)}(0)$ as high as 2, it is because it exhibits intensity fluctuations, whose temporal dynamics in turn define a coherence time (see Figure 7.9).

Limits of the Semi-Classical Theory

To a large extent, the semi-classical theory—describing light as a wave—accurately accounts for experimental results as long as the measured quantities are continuous variables, remaining compatible with the wave-like nature of light.

[6]"Thermal" light is modeled by a mode field resulting from the excitation of the mode by a multitude of independent sources, each generating a field described as a random process. The field of a thermal source is therefore the result of a sum of random variables, and the central limit theorem can be used to justify that the total field is described by a Gaussian random process.

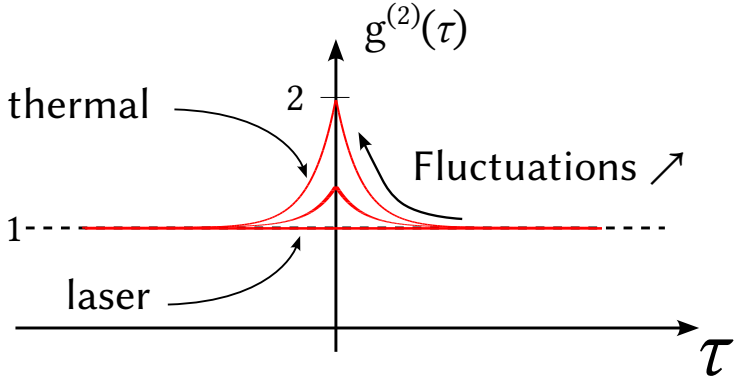

Figure 7.9: Relationship between $g^{(2)}(\tau)$ for a laser and a thermal source.Starting from $g^{(2)}(0) = 1$ for coherent light, such as that emitted by a laser, the presence of intensity fluctuations in a thermal source increases the value of $g^{(2)}(0)$. This also results in the emergence of a coherence time τ_c, which characterizes the width of the function.

The simple implementation of the HBT experiment with photodetectors shed new light on the positive correlations between detector pairs from a particle-like perspective: it reflects the tendency of photons from a thermal source to be detected in pairs, a phenomenon known as **bunching**.

The semi-classical theory, as it does not incorporate field quantization and thus the concept of photons, cannot account for bunching, nor for purely quantum effects in general—particularly those associated with single-photon sources. This is the domain of Glauber's theory of coherence.

Glauber's Theory of Coherence and Intensity Fluctuations

Glauber's theory of coherence forms the foundational framework of quantum optics. It provides a complete description of the electromagnetic field as a quantum system, notably introducing field operators and correlation functions. One of the major contributions of this theory is that it allows for the characterization of light states, in connection with photon statistics and intensity fluctuations as observed with photodetectors.

Field Operators and the Number Operator

The quantized electric field in a mode (e.g., for a monochromatic field in a cavity or a vacuum mode) is expressed as a superposition of creation and annihilation operators:

$$\hat{E}^{(+)}(t) \propto \hat{a}e^{-i\omega t}, \quad \hat{E}^{(-)}(t) = \left[\hat{E}^{(+)}(t)\right]^{\dagger} \propto \hat{a}^{\dagger}e^{i\omega t}.$$

L'intensité du champ, liée à l'énergie transportée, est alors reliée à l'opérateur nombre :

$$\hat{n} = \hat{a}^{\dagger}\hat{a}.$$

La moyenne de cet opérateur donne le nombre moyen de photons dans le mode : $\langle\hat{n}\rangle$, et sa variance décrit les fluctuations de photon :

$$(\Delta n)^2 = \langle\hat{n}^2\rangle - \langle\hat{n}\rangle^2.$$

Quantum theory of photodetection

Detecting a photon means absorbing it. The detection process is therefore intrinsically linked to the annihilation operator. For a situation involving a detector illuminated by a light field initially in the state $|i\rangle$ and potentially transitioning to a final state $|f\rangle$ after a photon is absorbed by the detector, the relevant matrix element is:

$$\langle f|\hat{E}^{(+)}(t)|i\rangle$$

The transition probability is related to the squared modulus of this term, $|\langle f|\hat{E}^{(+)}(t)|i\rangle|^2 = \langle i|\hat{E}^{(-)}(t)|f\rangle\langle f|\hat{E}^{(+)}(t)|i\rangle$, and the total detection probability is obtained by summing over all possible transitions, so that

$$P(t) \propto \langle\hat{E}^{(-)}(t)\hat{E}^{(+)}(t)\rangle = \langle\hat{n}(t)\rangle$$

while the coincidence probability between two detectors (or two clicks at different times) is:

$$P(t, t+\tau) \propto \langle\hat{E}^{(-)}(t)\hat{E}^{(-)}(t+\tau)\hat{E}^{(+)}(t+\tau)\hat{E}^{(+)}(t)\rangle$$

While these expressions appear formally similar to the classical case—involving products of complex fields and photon numbers—it is important to stress the non-commuting nature of the annihilation and creation operators: in other words, **the order of the operators is crucial**. This fundamental point is not captured by the semi-classical theory.

On this basis, Glauber introduced quantum correlation functions that fully describe the observable statistics obtained through photodetectors sensitive to individual photons.

Correlation functions in Glauber's framework

The coherence of the field is characterized by several time correlation functions.

1. First order : phase coherence

$$G^{(1)}(t,t+\tau) = \langle \hat{E}^{(-)}(t)\hat{E}^{(+)}(t+\tau)\rangle.$$

This function is linked to the classical time coherence of the field (resulting in amplitude interference. It can be normalized to get :

$$g^{(1)}(\tau) = \frac{G^{(1)}(t,t+\tau)}{\sqrt{\langle \hat{E}^{(-)}(t)\hat{E}^{(+)}(t)\rangle \langle \hat{E}^{(-)}(t+\tau)\hat{E}^{(+)}(t+\tau)\rangle}}.$$

2. Second order : intensity flucturations

$$G^{(2)}(t,t+\tau) = \langle \hat{E}^{(-)}(t)\hat{E}^{(-)}(t+\tau)\hat{E}^{(+)}(t+\tau)\hat{E}^{(+)}(t)\rangle.$$

The normalized function writes :

$$g^{(2)}(\tau) = \frac{G^{(2)}(t,t+\tau)}{G^{(1)}(t,t)G^{(1)}(t+\tau,t+\tau)},$$

and describes the ntensity fluctuations that can be measured by detecting coindicences. It contains advanced information on the statistical properties of light.

For $\tau = 0$, one getw :

$$g^{(2)}(0) = \frac{\langle \hat{a}^\dagger \hat{a}^\dagger \hat{a}\hat{a}\rangle}{\langle \hat{a}^\dagger \hat{a}\rangle^2}.$$

Using algebra for the quantum bosonic operators, one finally gets :

$$g^{(2)}(0) = \frac{\langle \hat{n}(\hat{n}-1)\rangle}{\langle \hat{n}\rangle^2} = 1 - \frac{1}{\langle \hat{n}\rangle} + \frac{(\Delta n)^2}{\langle \hat{n}\rangle^2}.$$

This explicit link between $g^{(2)}(0)$ and photon number fluctuations shows that light can be characterized through its variance.

Origin of Super-Poissonian Fluctuations in Thermal Light

Let us now consider a mode $\mathbf{k}$ at frequency ω within the cavity field. The component of the total field corresponding to this mode is itself a superposition of

contributions: the various excitations of this mode by N independent sources, where N is a very large number representing the atoms mentioned above.

$$\mathcal{E}_{\mathbf{k}}^{\mathrm{tot}} = \sum_{j=1}^{N} \mathcal{E}_{\mathbf{k}}^{j}$$

The fields $\mathcal{E}_{\mathbf{k}}^{i}$ represent the various excitations of the same mode by the N sources. They differ only by the complex excitation amplitude of this mode:

$$\mathcal{E}_{\mathbf{k}}^{j} = \mathcal{E}_0 e^{i\phi_j(t)}$$

The energy density of a field $\mathcal{E}$ is proportional to the squared modulus of the field, $|\mathcal{E}|^2$. The instantaneous energy density of the sum of waves is given by:

$$|\mathcal{E}|^2 = |\mathcal{E}_0|^2 \left(\sum_{j=1}^{N} e^{i\phi_j(t)} \right) \left(\sum_{k=1}^{N} e^{-i\phi_j} \right) = |\mathcal{E}_0|^2 \left(N + \sum_{j \neq k} e^{i(\phi_k - \phi_j)} \right)$$

Since the phases are randomly drawn between 0 and 2π, the statistical average of the second term in the parentheses tends toward zero:

$$|\overline{\mathcal{E}}|^2 \approx N |\mathcal{E}_0|^2$$

By modeling the field as resulting from a random process—specifically, the summation of a large number N of independent fields—we find that the energy density of a mode is (as expected) an incoherent sum: it corresponds to the energy density of each of the N fields radiated by the different sources.

We now turn to the energy fluctuations of a mode by computing the mean square of the energy:

$$\begin{aligned} ||\mathcal{E}|^2|^2 &= |\mathcal{E}_0|^4 \left| \left(N + \sum_{j \neq k} e^{i(\phi_k - \phi_j)} \right) \right|^2 \\ &= |\mathcal{E}_0|^4 \left(N^2 + 2N \sum_{j \neq k} e^{i(\phi_k - \phi_j)} + \sum_{j \neq k} e^{-i(\phi_k - \phi_j)} \sum_{l \neq m} e^{i(\phi_m - \phi_l)} \right) \end{aligned}$$

The second term, preceded by the factor $2N$, also has a statistical average equal to zero when the phases are randomly drawn between 0 and 2π.

In the third term, which represents a product between sums, many terms involve exponentials with differences of random variables, whose statistical average will also be zero. Only the terms for which the phases cancel out will

remain—specifically, those for which the indices match: $j = l$ and $k = m$. There is a total of N^2 such terms in the expansion of the product of sums. We then obtain:

$$\overline{||\mathcal{E}|^2|^2} = |\mathcal{E}_0|^4(N^2 + 0 + N^2) = 2|\mathcal{E}_0|^4 N^2$$

The variance of energy fluctuations is therefore :

$$\sigma_E^2 = \overline{||\mathcal{E}|^2|^2} - \overline{|\mathcal{E}^2|}^2 = 2|\mathcal{E}_0|^4 N^2 - (|\mathcal{E}_0|^2 N)^2 = N^2|\mathcal{E}_0|^4$$

And relative fluctuations are :

$$\frac{\sigma_E^2}{E^2} = \frac{N^2|\mathcal{E}_0|^4}{N^2|\mathcal{E}_0|^4} = 1$$

We arrive at a key result of wave mechanics: **the energy fluctuations of a single mode of the electromagnetic field are on the same order of magnitude as its total energy.**

And this is completely natural: this thermodynamic property is consistent with the phenomena of interference and diffraction. A field interfering with itself — that is, two-wave interference — exhibits fringes that show its energy density can drop to zero (perfectly dark fringes) or rise to twice the average energy density (bright fringes). In our case, the average energy is proportional to the number N of emitters, and due to interference, local values can reach up to N^2.

Wave and Particle Views of Intensity Fluctuations

The image of a photon as a particle imposes many limitations on physical interpretations. A photon is first and foremost an electromagnetic field excited once — in the sense of quantized harmonic oscillators. The quantities that define this field are purely wave-like in nature. The very nature of a wave implies a certain delocalization.

It is therefore not very meaningful to speak of the "position" of a photon, or to describe a light beam as a succession of photons[7].

That said, one can qualitatively represent a photon as a wave packet, consisting of a superposition of the system's various modes. The phenomena of

[7]The "position" of a photon is not a well-defined quantity. However, in simple cases, one can associate the distribution of the electromagnetic field with a probability density for detecting a photon with a detector. This is the case, for example, in a closed cavity supporting well-defined Hermitian modes. The antinodes of the field correspond to regions where the detection probability is higher — which can be interpreted as regions in space where a photon is more likely to be found. In the general case, however, this connection cannot be rigorously established, as the problem becomes strongly multi-mode.

photon bunching or anti-bunching, observable via coincidence measurements, as well as intensity fluctuations measurable through photocurrent, can then be interpreted in terms of different interference scenarios and phase relationships between wave packets.

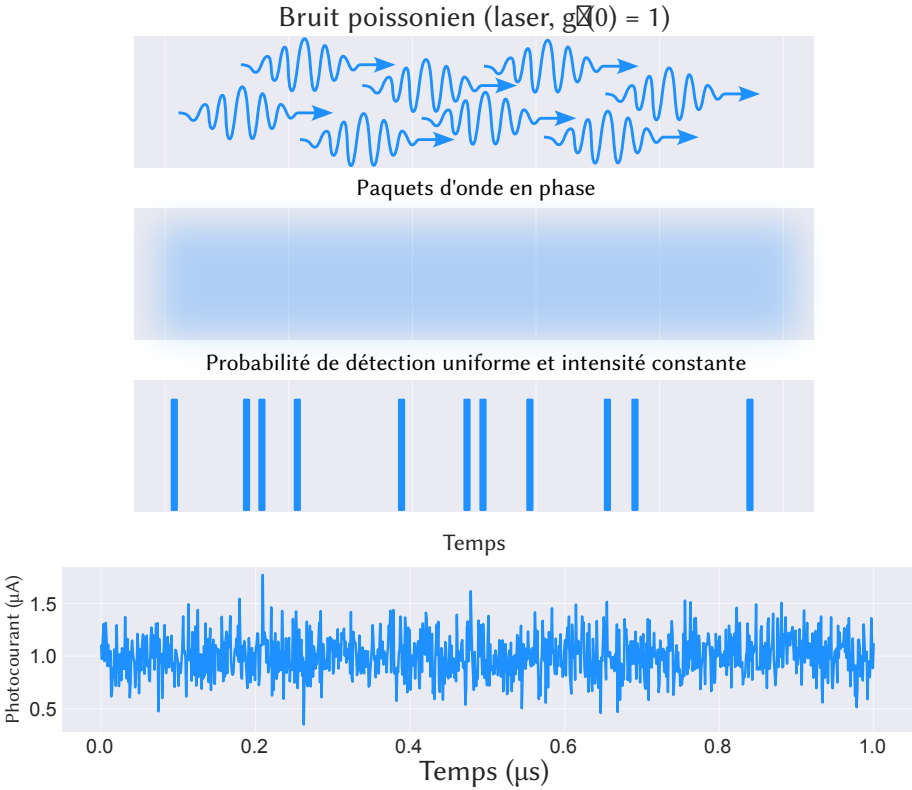

Figure 7.10: Interpretation of different photon statistics in terms of photocurrent or detection event statistics. (a) The Poissonian distribution, typical of lasers, corresponds to overlapping wave packets with no phase fluctuation. This results in a uniform and constant detection probability over time, which is macroscopically interpreted as the laser's constant intensity. The consequence is Poissonian noise — commonly referred to as shot noise — which is frequently encountered.

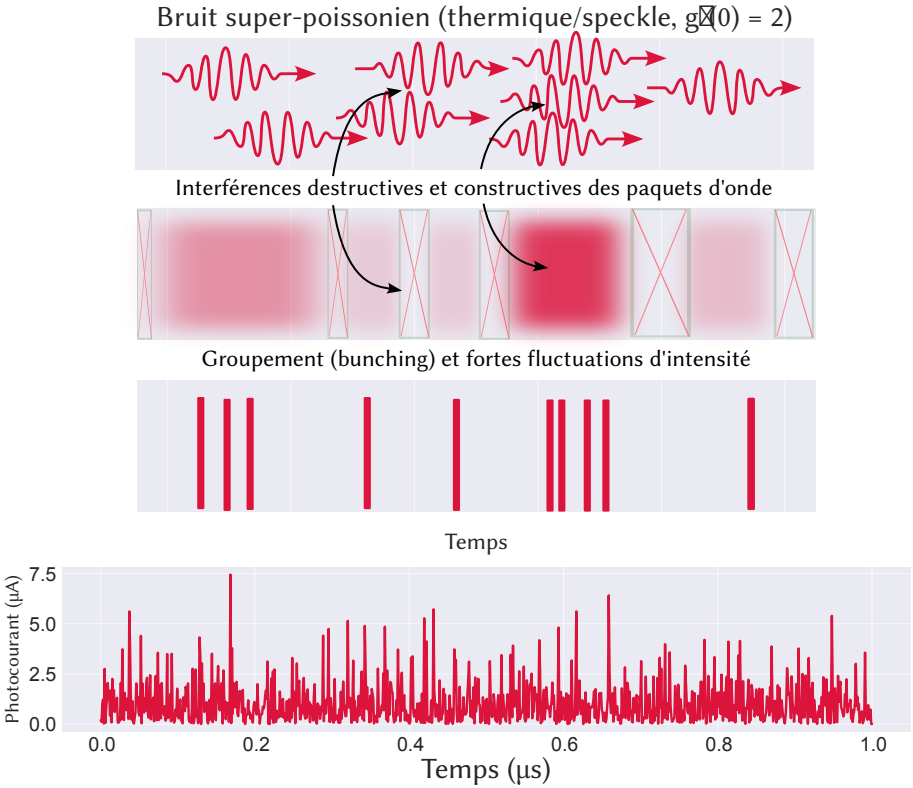

Figure 7.11: Interpretation of different photon statistics in terms of photocurrent or detection event statistics. (b) The random phase fluctuations between wave packets in a thermal source lead to significant fluctuations in the probability of presence, resulting in large intensity fluctuations and a bunching phenomenon, when the probability wave packets interfere constructively.

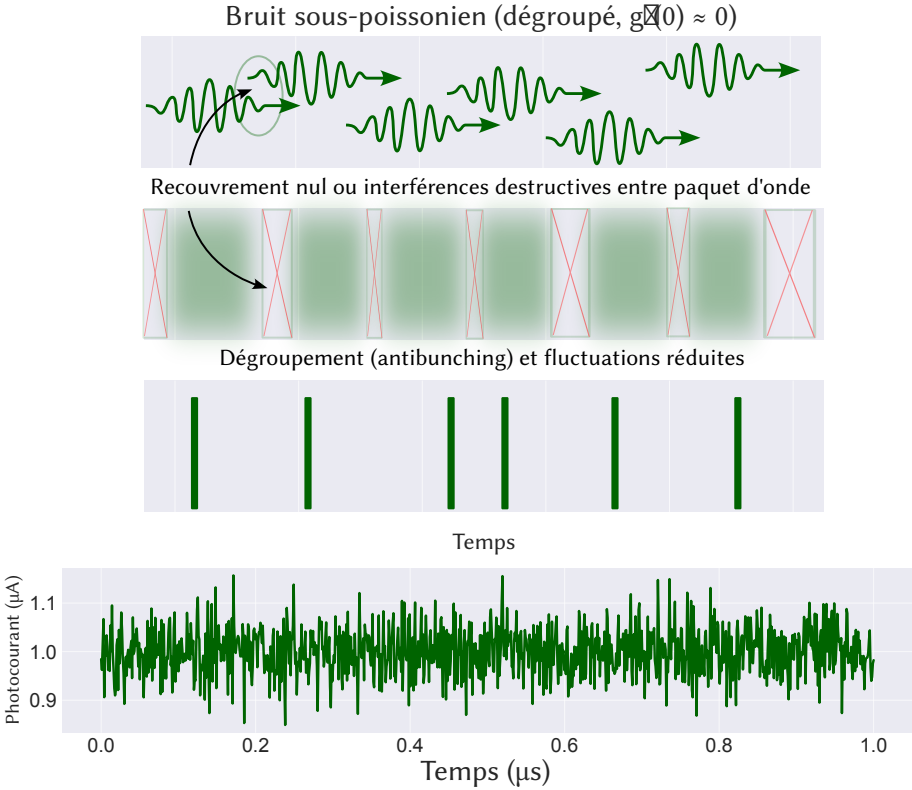

Figure 7.12: Interpretation of different photon statistics in terms of photocurrent or detection event statistics. (c) A single-photon source emits well-separated wave packets with minimal overlap. As a result, there is a vanishing probability of presence at regular intervals between each wave packet corresponding to a single photon. Intensity fluctuations are greatly reduced.